Spin-Polarized Transport in Single-Electron Spin-Valve Transistors

Von der Fakultät für Physik
der Universität Duisburg-Essen

zur Erlangung des akademischen Grades eines

„Doktors der Naturwissenschaften (Dr. rer. nat.)"

genehmigte Dissertation

von

Dipl.-Phys. Stephan Lindebaum
aus Gronau (Westfalen)

UNIVERSITÄT DUISBURG ESSEN

Referent:	Prof. Dr. J. König
Korreferent:	Prof. Dr. W. Belzig
Tag der mündlichen Prüfung:	11.07.2012

Contents

Deutsche Zusammenfassung

Die vorliegende Dissertation untersucht den elektronischen Transport durch mesoskopische Bauelemente aus dem Bereich der Spintronik. Dies ist von besonderem Interesse, da derartige Strukturen bereits erfolgreich industriell produziert und genutzt werden und darüber hinaus verspricht man sich von ihnen neuartige informationstechnologische Anwendungen. Hervorgerufen durch den andauernden Trend der Miniaturisierung elektrischer Komponenten haben spinelektronische Bauteile mittlerweile Strukturbreiten im Nanometerbereich erreicht. Allerdings kann man diese Verkleinerung nicht unbegrenzt fortsetzen, da auf den schon heutzutage erreichten Längenskalen die Gesetze der Quantenmechanik die momentane Funktionsweise der Bauelemente mehr und mehr beeinflussen. Daher wird es notwendig sein konzeptionell neuartige Strukturen einzuführen, die Quantenphänomene zu ihrem Vorteil nutzen.

Diesbezüglich bedeutende Beispiele sind ferromagnetische Einzelelektronentransistoren. Sie beruhen auf dem Tunneleffekt, nutzen die Eigenschaften des Elektronenspins und ermöglichen das Schalten sowie Verstärken elektrischer Signale. Das elektronische Transportverhalten dieser Bauelemente wird durch Einzelelektroneneffekte wie die Coulombblockade oder Coulomboszillationen bestimmt, wobei zusätzliche spinelektronische Phänomene wie die Spinakkumulation und der Tunnelmagnetwiderstand durch strukturinterne magnetische Materialen hervorgerufen werden.

Diese Arbeit behandelt eine spezielle Realisierung ferromagnetischer Einzelelektronentransistoren, nämlich den sogenannten *Einzelelektronenspinventiltransistor*. Dieser besteht aus einer metallischen Insel die über Tunnelkontakte mit zwei ferromagnetischen Zuleitungen verbunden ist. Zusätzlich ist die Insel kapazitiv an eine Gateelektrode gekoppelt. Basierend auf einem diagrammatischen Realzeit Formalismus entwickeln wir eine sequentielles Tunneln beschreibende Theorie, unter nichtstörungstheoretischer Betrachtung der Coulombwechselwirkung auf der Insel. Im Gegensatz zum Großteil der Arbeiten, die sich mit ferromagnetischer Einzelelektronentransistoren beschäftigen, betrachten wir den allgemeinen Fall nichtkollinearer Magnetisierungsrichtungen der beiden Zuleitungen. Dies bewirkt das Auftauchen neuartiger Transporteigenschaften, die im kollinearen Grenzfall nicht zu Tage treten. Beispielsweise existiert im betrachteten System ein wechselwirkungsinduziertes Austauschfeld, welches den elektrischen Transport nur im Falle nichtkollinearer Magnetisierungen messbar beeinflusst.

Im Einzelnen analysieren wir das Verhalten des auf der Insel akkumulierten Spins, den elektrischen Strom durch das Bauteil sowie die zugehörigen Stromfluktuationen. Dabei beobachten wir ein anspruchsvolles Transportverhalten des Systems hervorgerufen durch das Zusammenspiel von Ladungseffekten und Spinpolarisation. Wir finden eine hohe Empfindlichkeit des Inselspins auf eine Variation der Gatespannung, was die elektrische Steuerung der induzierten Magnetisierung ermöglicht. Desweiteren identifizieren wir die zweite Ableitung des Stroms nach der angelegten Transportspannung als ein mögliches Instrument zur Bestimmung des Grades der Zuleitungspolarisierung. Abschließend sei ausdrücklich betont, dass in unserer Analyse ein wesentliches Augenmerk auf den Auswirkungen des oben erwähnten Austauschfeldes liegt.

English Abstract

In the present thesis electronic transport through mesoscopic spintronic devices is investigated. This is particularly interesting since such structures have already proven industrial relevance and they additionally give rise to future information technology applications. As a result of the continuing trend of miniaturization in electronics modern spintronic structures have already reached the nanometer scale. However, a further size reduction may soon be prevented by the laws of quantum mechanics. Hence conceptually new kinds of devices that take advantage of the possibilities of quantum phenomena may need to be adopted.

Prominent examples of such spintronic structures are ferromagnetic single-electron transistors (fm SETs). They rely on quantum tunneling, exploit the intrinsic electron spin, and allow for the switching and amplification of electronic signals in response to a variation of a gate voltage. Their transport behavior is governed by single-charging effects as Coulomb blockade or Coulomb oscillations. Whereas fundamental spintronic effects as spin accumulation or tunnel magnetoresistance are introduced to the structure by the embedded ferromagnetic materials.

This work focuses on a special realization of a fm SET, the so called *single-electron spin-valve transistor*. It consists of a metallic island that is tunnel coupled to two adjacent ferromagnetic leads and capacitively coupled to a gate electrode. Based on a diagrammatic real-time approach a theory is derived that describes sequential tunneling through this system. The Coulomb interaction on the island is taken into account nonperturbatively. In contrast to most previous works studying fm SETs we consider the general setup with *noncollinear* angles between the lead magnetization directions. This causes new transport properties that differ from the collinear case. For instance, there is an interaction-induced exchange field present which does not affect the flow of electric charges in the parallel and antiparallel setup. However, for noncollinear lead magnetizations it acts on the spin that is accumulated on the central island resulting in notable variations of the transport properties of the considered system.

We analyze in detail the dynamics of the accumulated island spin, the electric current, as well as the current fluctuations of the single-electron spin-valve transistor. A remarkable transport behavior evoked by the interplay of charging effects and finite spin polarization is observed. For instance, we find a high sensitivity of the accumulated island spin on the variation of the applied gate voltage allowing for controlled electrical manipulation of a macroscopic spin. Furthermore, the second derivative of the current with respect to the bias voltage is demonstrated to be a convenient tool to determine the degree of polarization of the ferromagnetic leads. Finally, we note that in our analysis an emphasis is put on the influence of the interaction-induced exchange field on the system's transport properties.

1 Introduction

"Only the fact that I knew nothing about computers enabled me to break new paths..."

Prof. Dr. Konrad E. O. Zuse

Konrad E. O. Zuse was a German civil engineer of the 20th century. Driven by his desire to automatize monotonic static calculations, he invented the *Z3* (in 1941), which was the first fully automated and freely programmable computer in the world. Its calculation unit that was based on telephone relays was able to perform a single multiplication of two floating-point numbers in about five seconds. However, during the past 70 years, the efficiency of electric computers has drastically increased by exploiting and advancing different electronic subunits as vacuum tubes and transistors. The former were successfully integrated into computers just a few years after the initial operation of the *Z3*. They allowed for a few thousand floating-point operations per second (FLOPS). But nowadays, even standard processors that are used in ordinary home computers exhibit a FLOPS number of more than 10^9. Transistors embedded in integrated circuits are the fundamental building blocks of these modern processors.

Since their first realization in 1947 by J. Bardeen and W. H. Bratain, transistors enabled the continuous growth of computer efficiency simultaneously accompanied by a drastic size reduction. Currently, it is possible to create computer chips in mass production that contain more than one billion transistors. This corresponds to a device density that exceeds one million transistors per mm^2. Even on these length scales, the field effect transistor, which is the most common transistor, still relies on the movement of a huge number of electrons in bulk matter. However, a further miniaturization may soon be prevented by the laws of quantum mechanics since the dimensions have reached the nanometer scale. Hence in order to continue the size reduction of the circuit elements, conceptually new kinds of transistors that take advantage of the possibilities of quantum mechanics may need to be adopted.

A prominent example of such nanoelectronic devices is the so called *single-electron transistor* (SET). It consists of a mesoscopic central island placed between source and drain electrodes while the components are separated by insulators. The name SET stems from the fact that the current state can be switched from on to off in response to a variation of charge on a capacitively coupled gate electrode that corresponds to one single elementary charge or less. In contrast to the currently used field effect transistors, the motion of electrons through SETs relies on a fundamental quantum-mechanical effect, the quantum tunneling. It allows for the classically forbidden electron movement through the insulator junctions. Additionally, due to the small

size of the central region, the electrons passing it strongly interact via Coulomb interaction. As a consequence single-charging effects as *Coulomb blockade* and *Coulomb oscillations* govern the electronic transport characteristics of SETs. The architecture of the device evokes electrons to be transferred one by one through the central region. Sequential tunneling is dominant and higher order processes are suppressed due to the weak tunnel coupling. However, the subsequent uncorrelated tunneling processes are blocked if the charging energy of the central region, that is tunable by gate voltage, exceeds the energy given by temperature and applied bias voltage, i.e., the system is Coulomb blockaded. In this regime coherent simultaneous cotunneling processes have to be taken into account.

Over the years, besides computer chips also magnetic storage media as hard-disc drives experienced a continuous miniaturization. More and more data can be stored in increasingly smaller memory devices. Since the dimension of the single bits decreases the indicated magnetic fields become weaker and hence they are harder to detect. In 1988, an important discovery that enabled a further reduction in size was made by P. Grünberg and A. Fert. At the same time, they independently investigated Fe/Cr multilayer structures and observed a strong dependence of the electrical resistance on the relative orientation of the layers magnetization directions. This effect is called *giant magnetoresistance* (GMR). It has already proven great industrial relevance as it is exploited in modern highly sensitive hard-disk drive read heads. Consequently, for their work concerning the GMR Grünberg and Fert were awarded the Nobel Prize in Physics in 2007. By the discovery of the GMR a broad interest in nanoelectronic devices using the spin degree of freedom was stimulated. A new area in mesoscopic physics arose, the so called *spintronics*. In this field, besides the electron charge also the spin degrees of freedom are used for current and future applications in information technology.

By using ferromagnetic components, spintronic effects can be introduced to SETs. New phenomena arise that are caused by an interplay of the finite spin polarization and the strong electron-electron interaction on the central mesoscopic island. Recently, several experimental works were published considering various versions of ferromagnetic SETs. In the considered devices ferromagnetic or normal metallic electrodes are coupled two either ferromagnetic or nonmagnetic central parts and even superconducting materials were applied. The measurements address current-voltage characteristics, spin accumulation, magneto-Coulomb effects, as well as *tunnel magnetoresistance* (TMR). The latter is related to the GMR but describes electron tunneling through a potential barrier. It can be observed in ferromagnet/insulator hybrid structures if the spacer between two ferromagnetic layers is chosen in such a way that the ferromagnets are tunnel coupled to each other. Analog to the GMR the electrical resistance of TMR devices is maximal for antiparallel alignment of the layer magnetizations.

In the present thesis, electronic transport through a *single-electron spin-valve transistor* is theoretically investigated. This special realization of a ferromagnetic SET represents a convenient model system to study the interplay of Coulomb interaction and spin degrees of freedom. It consists of a metallic island that is tunnel coupled to two adjacent ferromagnetic leads and capacitively coupled to a gate electrode. Here, metallic means that the island energy spectrum can be assumed to be continuous,

i.e., the level spacing is small compared to the other relevant energy scales. By an applied bias voltage an electric current can be driven through the system. Based on a diagrammatic real-time approach a theory is derived that describes sequential tunneling through the single-electron spin-valve transistor. The Coulomb interaction on the island is taken into account nonperturbatively. In contrast to most previous works studying ferromagnetic SETs, the angle between the lead magnetization directions is not restricted to multiples of π, i.e., the general *noncollinear* setup is considered. This causes new transport properties that differ from the collinear case. For instance, there is an interaction-induced *exchange field* present in the single-electron spin-valve transistor which does not affect the flow of electric charges in the parallel and antiparallel setup. However, for noncollinear lead magnetizations it acts on the spin that is accumulated on the central island resulting in notable variations of the transport properties of the system.

The used technique enables the investigation of not just the mean charge current and related transport properties (as the TMR) but also allows for the analysis of the *current fluctuations* of the single-electron spin-valve transistor. This is especially important since the current-to-noise ratio is crucial for possible applications in the field of nanoelectronic devices. Furthermore, the fluctuations of the current can reveal additional information that is not contained in the average current.

This thesis is structured as follows. In the second chapter the underlying principles that have to be understood for an appropriate investigation of the electronic transport through the single-electron spin-valve transistor are presented. The chapter is divided into four main parts discussing the different "main ingredients" of the system and its experimental realizations. After a brief introduction to transistors in general, single-charging effects caused by Coulomb interaction are discussed in a general context and in detail for single-electron transistors. In the latter section the considerations are especially focused on the influence of the energy spectrum of the central part which can be either discrete (quantum dots) or continuous (metallic islands). Afterwards, fundamental spintronic devices and phenomena are introduced as the spin-valve, the GMR, the TMR, as well as the exchange field existent between the central part of the single-electron spin-valve transistor and the ferromagnetic leads.

In the third chapter the theoretical framework of this work, a real-time transport theory, is presented in detail. At the beginning, the Hamiltonian and the respective model that we use to describe the system are introduced. Afterwards, a generalized master equation describing the time evolution of the elements of a reduced density matrix, that only contains the island degrees of freedom, is derived. Subsequently, the calculation of occurring transition rates by means of a diagrammatic representation that relies on a presented Keldysh formalism is discussed. Finally, it is discussed how the mean-current formula is derived.

Based on the introduced theory, kinetic equations describing the island charge and spin degrees of freedom are derived in chapter 4. To this end, a perturbation expan-

sion of the master equation is performed up to the first order in the tunnel-coupling strength, i.e., sequential-tunneling processes are described within this framework. Furthermore, the long-time limit is considered where the elements of the reduced density matrix are stationary. The resulting equations are the basis for investigations of the transport properties of the noncollinear single-electron spin-valve transistor which are considered in the following two chapters.

Mean current and spin dynamics in both the linear (small bias voltages) and the nonlinear (large bias voltages) transport regimes are analyzed in chapter 5. Quantities as spin accumulation, conductance, TMR, and current-voltage characteristics are considered in detail. In the discussion, an explicit focus is put on the influence of the interaction-induced exchange field.

Current fluctuations are investigated in chapter 6 since they reveal additional information concerning electronic-transport processes through mesoscopic conductors. First, a brief introduction into the field of current noise is given. Afterwards, the already derived theoretical formalism is extended to additionally enable the calculation of the frequency-dependent current noise of the single-electron spin-valve transistor. In the last section of the chapter, the obtained results are presented. Sequently, the zero-frequency and finite-frequency limits are considered.

The conclusions in chapter 7 finish the present thesis.

2 Basic Principles of Single-Electron Spin-Valve Transistors

In this work we investigate the electronic transport properties of a single-electron spin-valve transistor, i.e. a single-electron transistor (SET) composed of two ferromagnetic leads which are tunnel coupled to a metallic island. This system contains three main ingredients. At first it represents a transistor, which is one of the most important electronic devices invented in the 20th century. Secondly, the magnetized components brake the spin symmetry and therefore spintronics play an important role. And at last, due to the small size of the island also Coulomb-interaction effects have to be taken into account. Hence in this chapter we will start by giving a brief introduction to every three parts, transistors in general, single-charge tunneling, and spintronics.

The central electrode of the considered single-electron spin-valve transistor exhibits a continuous electron density of states. By using quantum dots (discrete energy spectrum) instead of metallic islands SETs with similar transport characteristics can be realized. However, there are differences between discrete and continuous spectra which are explained in a separated section of the present chapter. Furthermore, in the closing paragraph, we will briefly review some fundamental theoretical and experimental works concerning SETs, to give an overview of the transport characteristics and the different realization techniques of such devices.

A part of subsection 2.4.5 has already been published in Ref. [1].

2.1 Transistor

A transistor is an electronic device that can switch and amplify an electronic signal. It is used as a fundamental building block of products of the modern electronic industry and hence it is omnipresent in todays society. The general idea is to control the current in an output circuit by tuning a small input current or voltage. There are a lot of different kinds of transistors, and all of them contain at least three electrodes including input and output terminals. The majority of transistor types are based on semiconducting materials, but by exploiting single-charging effects, as our work proposes, it is also possible to create transistors out of normal metals or even ferromagnets. The first working transistor was a point-contact transistor constructed in the Bell Laboratories. After years of underlying work J. Bardeen and W. H. Bratain finally build it in 1947.[2] They were working together with W. B. Shockley and every three of them were awarded the Nobel Prize in Physics in 1956 for their joint researches concerning transistors and semiconductors.

Since nowadays the field-effect transistor (FET) is the most common transistor, we want to discuss the functionality of this device in detail. More precisely we consider an

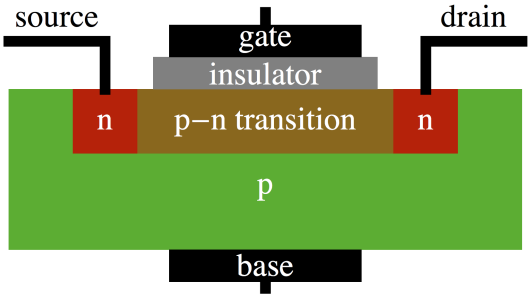

Figure 2.1: Cross section of n-channel metal-oxide semiconductor field-effect transistor.

n-channel metal-oxide semiconductor field-effect transistor (nMOSFET), but the basic concept stays the same for all FETs. A scheme of the nMOSFET is shown in *Fig. 2.1*. The source and drain electrodes are connected to highly doped n-type semiconductor regions embedded in a weakly p-doped Si crystal. Isolated from the semiconductor by an oxide layer, the gate electrode enables to control the current between source and drain. In combination with the base electrode a capacitor is realized that can modulate the charge concentration between the n-regions by tuning the potential difference of gate and base. For gate voltages larger than a given threshold ($V_{\text{gate}} > V_{\text{th}}$) n-channels open in the p-n transition area of the p-substrate. By applying a voltage between source and drain one can then drive a current from the left to the right n-doped region. By a further increase of the gate voltage also the current from source to drain increases due to a higher electron density in the transition region. But there is also a saturation gate voltage V_{sat} due to the fact that for $V_{\text{gate}} > V_{\text{sat}}$ all the lead electrons in the transport relevant energy window defined by source-drain voltage find an open n-channel to pass the device. Hence in this limit the current no longer depends on V_{gate}. In conclusion, it is possible to switch the transistor from the off-state into the conducting state by applying a gate voltage that exceeds V_{th}.

Following the trend of miniaturization in electronics also transistors have continuously reduced in size since their first realization in 1947. Nowadays, by using photolithography it is possible to build computer chips with a transistor density larger than 10^6 transistors per mm^2 in mass production. This enables that transistors, as a basic component of integrated electronic circuits, are present in nearly all modern electronic devices. As the device dimensions approach the nanometer scale quantum mechanics and Coulomb-interaction effects become important. Hence conceptually new kinds of a transistor are demanded. An exemplary transistor structure that relies on quantum mechanics and Coulomb-interaction effects is the so called *single-electron transistor* (SET). In this system the continuous movement of electrons like in common transistors is replaced by a discrete charging and discharging of a central electrode with single electrons. In the following paragraphs, we will introduce in detail to the field of SETs due to the fact that the structure considered in this thesis (single-electron spin-valve transistor) is a particular realization of a SET.

2.2 Single-Charge Tunneling

As mentioned in the previous paragraph, the proceeding reduction of the size of electronic devices using transistors evokes that quantum mechanics and Coulomb-interaction effects will be crucial for the understanding of the future transistor structures like SETs. The behavior of these devices is governed by the electrostatic energy and their functionality is based on transport of single charges.[3] We exemplarily consider charge transport through a small metallic island that is tunnel coupled to metallic source and drain leads, see *Fig. 2.2*. With an additional gate capacitively coupled to

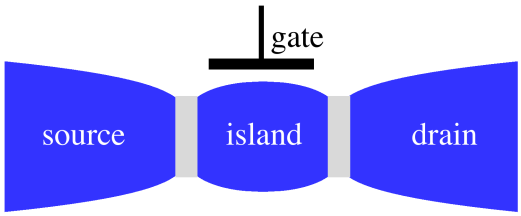

Figure 2.2: SET as model system of single-charge tunneling. Source and drain leads are connected to a small central electrode (island) via tunnel junctions. A gate is capacitively coupled to the island.

the island, the system represents a SET. A net current through the system can be generated by applying a finite bias voltage. Transport takes place by subsequent tunneling of electrons from the source through the island into the drain. To observe single-charging effects, quantum fluctuations of the number of electrons occupying the island must be negligible. The wave functions of island electrons have to be localized. Therefore, the resistances of the tunnel barriers must be large in comparison to the inverse conductance quantum $2e^2/h$. Naturally, the most important energy scale in the context of single-charge phenomena is the Coulomb-repulsion energy of electrons. Excess electrons tunneling onto the island have to overcome the energy difference between the charging states before and after the tunneling event. If the island is occupied by N electrons, the charging energy is given by

$$E_{\mathrm{ch}} = \frac{e^2}{2C_\Sigma}(N - N_{\mathrm{ext}})^2, \tag{2.1}$$

with $C_\Sigma = C_{\mathrm{source}} + C_{\mathrm{drain}} + C_{\mathrm{gate}}$ being the sum of the junction capacitances and the capacitance of an eventually applied gate voltage. Typical values of C_Σ in realized systems are about fF down to aF. The applied voltages induce an external charge $Q_{\mathrm{ext}} = eN_{\mathrm{ext}} = C_{\mathrm{source}}V_{\mathrm{source}} + C_{\mathrm{drain}}V_{\mathrm{drain}} + C_{\mathrm{gate}}V_{\mathrm{gate}}$. In *Fig. 2.3* the charging energy is plotted against the external charge. We see, that the energy which is necessary to change the charging state of the island is maximal for Q_{ext} being equal to multiples of the elementary charge and even vanishes for half-integer values of e. In the latter case, electron transport is possible independent of temperature or bias voltage. In conclusion, the bias voltage, that has to be applied to change the island charging state, strongly depends on the applied gate voltage, see also *Fig. 2.4* (a). The diamonds, which are called *Coulomb diamonds*, mark the regimes where the number of island electrons N is fixed. In their parameter range the current is blocked and the system is in the *Coulomb blockade* regime. Due to asymmetric capacitances $C_{\mathrm{source}} \neq C_{\mathrm{drain}}$ the upper and lower corner of the diamonds are slightly shifted. As discussed above

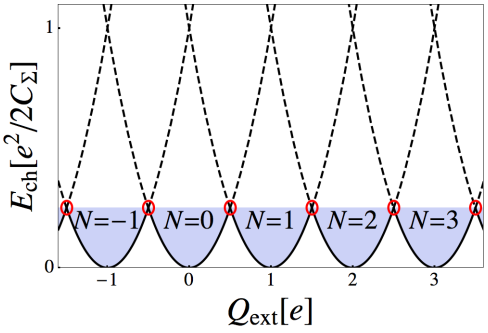

Figure 2.3: Coulomb energy of the island for different charging states N over external charge Q_{ext}. Red circles mark the degeneracy points between two adjacent charging states.

a variation of Q_{ext} by tuning the gate voltage can switch the transistor from the blocking into the conducting state. In the limit $V_{\text{bias}}, k_BT \ll e^2/(2C_\Sigma)$ this results in conductance peaks as illustrated in *Fig. 2.4* (b). The peaks of these *Coulomb oscillations* appear periodically at the degeneracy points of E_{ch} between two adjacent charging states. The width of the peaks is governed by temperature. This fact is related to a general requirement to observe single charging phenomena. To ensure that thermal fluctuations do not smear out charging effects it is necessary that the condition $E_{\text{ch}} \gg k_BT$ is fulfilled.

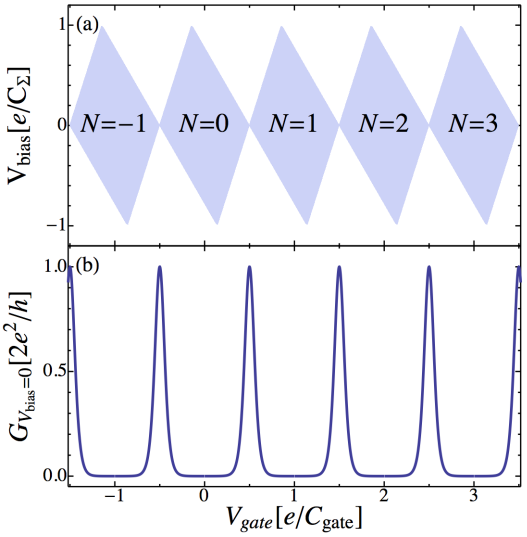

Figure 2.4: SET transport properties. (a) *Coulomb diamonds* mark the regime of *Coulomb blockade*. (b) *Coulomb oscillations* are periodic peaks in the conductance ($V_{\text{bias}} = 0$). For both plots the parameters $V_{\text{source/drain}} = \pm V_{\text{bias}}/2$ and $2C_{\text{source}} = C_{\text{drain}} = 4C_{\text{gate}}$ were chosen.

2.3 Metallic-Island and Quantum-Dot Single-Electron Transistor

As mentioned before, in this thesis the electronic transport through a single-electron spin-valve transistor is studied. This system is a particular realization of a SET with a metallic island (hosting a continuum of single-particle energy levels) being the mesoscopic central part of the device. It is also possible to realize SETs by replacing the island by a quantum dot with a discrete excitation spectrum. Both kinds of SETs

exhibit the same basic transport properties as presented in section 2.2. However, there are detailed features in the transport characteristics that depend on the present energy-level spectrum. Hence in this paragraph we will consider both metallic island and quantum dot coupled via tunnel junctions to two normal metallic leads in order to indicate their differences in transport.

A SET composed of a metallic island / quantum dot tunnel coupled to normal source and drain leads is modeled by the total Hamiltonian

$$H = H_{\text{island/dot}} + H_{\text{Coulomb}} + H_{\text{source}} + H_{\text{drain}} + H_{\text{tunnel}} \,. \tag{2.2}$$

The first part,

$$H_{\text{island}} = \sum_{l\sigma\nu} \varepsilon_{l,\text{island}}\, c^{\dagger}_{l\sigma\nu} c_{l\sigma\nu} \,, \tag{2.3}$$

$$H_{\text{dot}} = \sum_{l\sigma} \varepsilon_{l,\text{dot}}\, c^{\dagger}_{l\sigma} c_{l\sigma} \,, \tag{2.4}$$

describes the metallic island / quantum dot whose energy spectrum $\varepsilon_{l,\text{island/dot}}$ is continuous or discrete, respectively. A continuous spectrum is existent if the level spacing is small compared to the other relevant energy scales like temperature or bias voltage ($\Delta\varepsilon \ll k_B T, eV_{\text{bias}}$). The annihilation and creation operators of island/dot electrons in the state $l\sigma(\nu)$ are denoted by $c_{l\sigma(\nu)}$ and $c^{\dagger}_{l\sigma(\nu)}$, respectively. The index l labels the energy levels of the central region, $\sigma \in \{\uparrow, \downarrow\}$ the spin, and $\nu = 1, \ldots, N_c$ is the transverse channel index. In the case of a quantum dot, due to the geometry of the system, multiple transverse channels do not exist. The Coulomb interaction of the electrons occupying the central region is accounted for by the charging-energy term

$$H_{\text{Coulomb}} = \frac{e^2}{2C_{\Sigma}} (N - N_{\text{ext}})^2 \,, \tag{2.5}$$

where N is the number of electrons on the island/dot and $C_{\Sigma} = C_{\text{source}} + C_{\text{drain}} + C_{\text{gate}}$ the total capacitance. For equal capacitances of the two tunnel junctions and a symmetrically applied transport voltage, the external charge $e\,N_{\text{ext}} = C_G V_G$ depends on the gate voltage V_G only. Each of the normal leads is described as a reservoir of noninteracting fermions

$$H_{\text{source/drain}} = \sum_{k\sigma(\nu)} \epsilon_k^{\text{source/drain}}\, a^{\text{source/drain}\,\dagger}_{k\sigma(\nu)} a^{\text{source/drain}}_{k\sigma(\nu)} \,, \tag{2.6}$$

with indices for momentum k and $a^{\text{source/drain}\,(\dagger)}_{k\sigma\nu}$ being the annihilation (creation) operator of the respective lead. The leads are macroscopic objects, hence their energy spectrum $\epsilon_k^{\text{source/drain}}$ is continuous. We emphasize that the transverse channel index ν only appears for SETs containing a metallic island. The tunneling Hamiltonian $H_{\text{tunnel}} = H_{\text{tunnel, source}} + H_{\text{tunnel, drain}}$ describes tunneling of electrons between the central part of the SET and the leads, and the two contributions are defined as:

$$H_{\text{tunnel, source/drain}} = \sum_{kl\sigma(\nu)} T_{\text{source/drain}}\, a^{\text{source/drain}\,\dagger}_{k\sigma(\nu)} c_{l\sigma(\nu)} + \text{H.c.} \,. \tag{2.7}$$

Both the spin and for the island system also the transverse channel index ν are conserved during tunneling. This is obvious from the fact that the tunneling Hamiltonian is diagonal in σ and ν. The tunneling-matrix elements $T_{\text{source/drain}}$ are assumed to be independent of momentum k, spin σ, and transverse channel index ν. The tunneling rate for electrons from source/drain into the central part is quantified by $\Gamma_{\text{source/drain}}/\hbar = 2\pi\rho^{\text{source/drain}} \left|T_{\text{source/drain}}\right|^2/\hbar$, with the lead densities of states $\rho^{\text{source/drain}}$. In addition, we define $\Gamma = \Gamma_{\text{source}} + \Gamma_{\text{drain}}$.

After the presentation of the model, we now want to examine the transport processes through metallic-island and quantum-dot SETs. First, the system containing a quantum dot is considered. In the limit of zero temperature, two possible transport situations are illustrated in *Fig. 2.5* (a)-(b) by means of energy diagrams. The

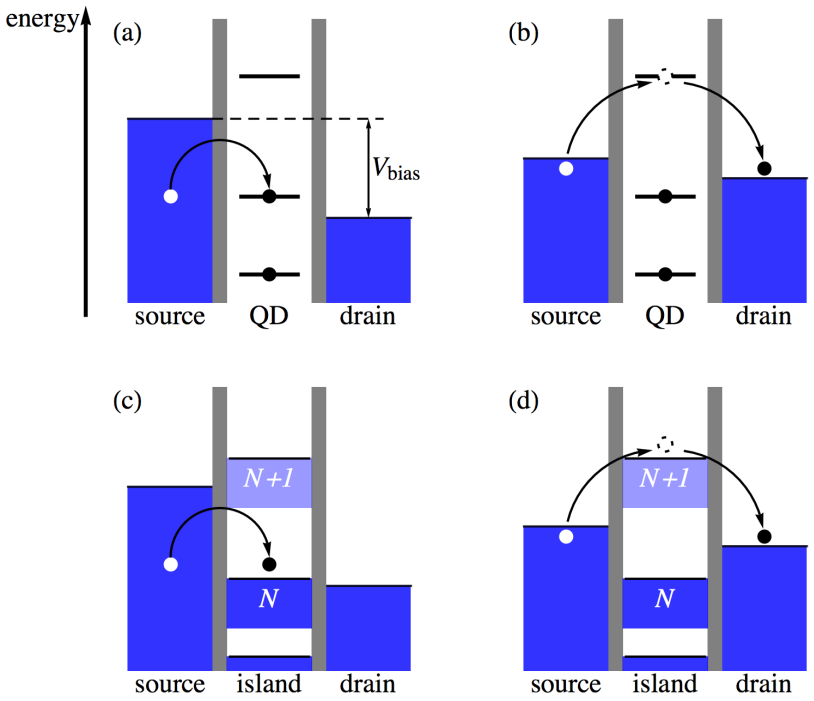

Figure 2.5: Energy scheme of tunneling through SETs. (a) Sequential tunneling through discrete level structure of a quantum dot, (b) QD cotunneling, (c) sequential tunneling through continuous spectrum of a metallic island, and (d) island cotunneling.

filled rectangles on the left and right-hand side of the scheme illustrate the levels of the continuous density of states of the leads that are filled up to the Fermi level. A temperature unequal to zero evokes a finite probability for occupation of higher levels. In the central part the discrete energy spectrum of the dot is represented by horizontal lines, the black disks mark electrons occupying the states, and the white ones represent holes excited in the leads due to tunneling. The positions of the lines include both the dot level spacing and the charging energy that is necessary to occupy the respective charging state of the dot. A variation of the gate voltage evokes a change of the external charge eN_{ext} and results in a shift (up or downwards) of the whole central

level structure. By applying a bias voltage V_{bias} the Fermi levels of source and drain are adjusted and the resulting transport window determines the relevant transport processes. Sequential-tunneling processes are dominant if the dot level lies within the transport window. These processes, which are of first order in tunnel-coupling strength Γ, are illustrated in *Fig. 2.5* (a). The electrons with the respective energy can tunnel into the dot and out of the dot one at a time, i.e., electrons tunnel through the dot in two uncorrelated processes. In *Fig. 2.5* (b) the transport window does not enclose any quantum dot level. The system is in the Coulomb-blockade regime. Sequential tunneling through the system is impossible ($T = 0$) and, therefore, cotunneling processes are dominant. Due to the fact that Heisenberg's uncertainty principle allows a short violation of energy conservation electrons can coherently tunnel through the dot in the depicted mode. The additional energy to occupy the dot level with a source electron for a short time is regained by subsequent tunneling into the drain. The dot state is virtually occupied (dashed circle). For the whole process, which is of second order in the tunnel-coupling strength Γ, energy is conserved.

Sequential tunneling and cotunneling processes through a metallic island enclosed by two normal leads can be visualized by energy schemes in an analog way, see *Fig. 2.5* (c)-(d). The discrete levels (black lines) in the central part of the quantum dot diagram are replaced by a continuum of states (blue rectangles). In contrast to the macroscopic leads, the charging energy is the dominant energy scale. Hence for different island occupation numbers N the whole spectrum is energetically shifted. This behavior is visualized by different rectangles each representing the density of states in a given charge state. Although the rectangles are confined at the bottom all the levels below the Fermi energy are occupied. We choose this kind of illustration due to the fact that different charge states have to be shown in a single scheme. To fill the island with an additional electron a level above the Fermi energy has to be occupied. In both diagrams, describing sequential tunneling (*Fig. 2.5* (c)) and cotunneling (*Fig. 2.5* (d)), after the transport process the island is occupied by N electrons. Concerning the latter, during the process the central electrode is virtually occupied by $N + 1$ electrons.

In this work, we consider a metallic island that is weakly tunnel coupled to the leads, hence sequential tunneling is dominant. Higher order processes like cotunneling are suppressed and not included in the used formalism. But already in the sequential-tunneling limit quantum-dot and metallic-island SETs exhibit different current-voltage characteristics. Again, we start with the consideration of the quantum-dot SET. The transport voltage V_{bias} is symmetrically applied to both leads and the discrete energy spectrum of the dot is chosen in such a way that only one level, that can be occupied by a single electron or doubly occupied by two electrons with different spins, contributes to transport. The respective current-voltage characteristics is shown in *Fig. 2.6* (a) for different ratios of the leads' tunnel-coupling strengths. At low positive and negative V_{bias} the quantum-dot level lies outside the transport window and the initial dot charge state, defined as N_0, does not change, i. e., the system is in the Coulomb blockade regime. The current increases stepwise whenever an energy level enters the transport window while the sign of V_{bias} determines the transport direction. This variation of current in a steplike manner results in peaks in the conductance ($G = \mathrm{d}I/\mathrm{d}V$) of the quantum-dot SET, see *Fig. 2.6* (b). There are two steps / peaks for positive

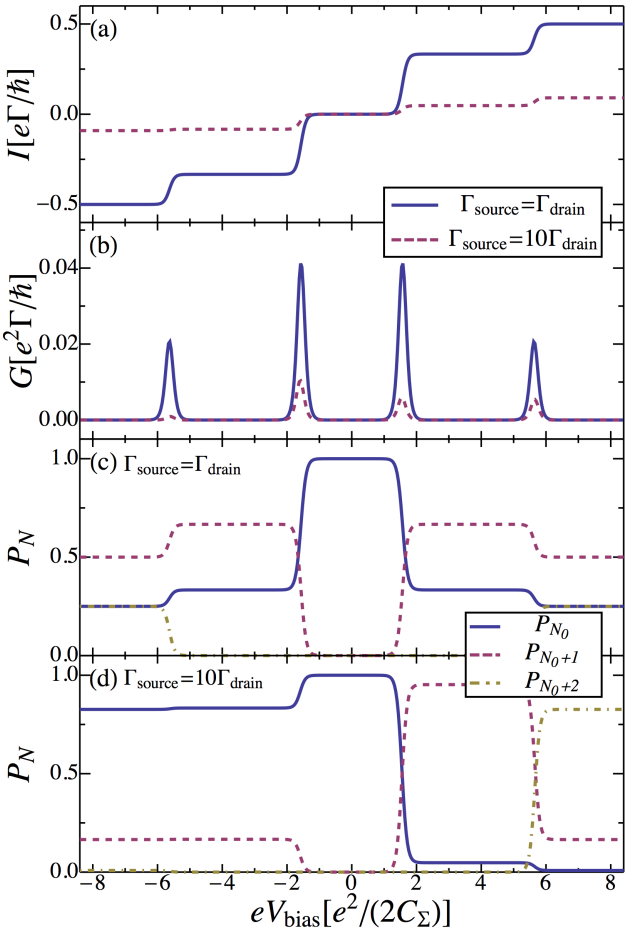

Figure 2.6: Transport characteristics of quantum-dot tunnel coupled to two normal leads in sequential tunneling limit. (a) Current (over applied bias voltage V_{bias}) increases stepwise due to the discrete dot energy spectrum. (b) The peaks in the conductance represent the excitation energies of higher dot charge states. (c)-(d) Corresponding occupation probabilities of the relevant charge states for symmetric and asymmetric tunnel couplings, respectively. The bias voltage symmetry of the system is broken by asymmetric couplings.

and negative bias due to the two different charging states ($N_0 + 1$ and $N_0 + 2$), that can additionally be occupied. In *Fig. 2.6* (c)-(d) the occupation probabilities of the relevant charge states are plotted over transport voltage for symmetric and asymmetric couplings to the leads, respectively. It is obvious that an asymmetric coupling to source and drain breaks the bias voltage symmetry of the system. In this case, the direction of transport is important since depletion and filling probabilities of the dot depend on the involved tunnel junction. This can be seen in *Fig. 2.6* (d), for positive bias voltage electrons tunnel from source into the dot with a relatively high probability defined by Γ_{source}, but depletion of the dot via tunneling to drain is suppressed due to the small coupling Γ_{drain}. As a result, if the transport voltage is large enough the system tends to occupy the higher charge states. This behavior changes for negative V_{bias} as filling (Γ_{drain}) is suppressed and depletion (Γ_{source}) is enhanced. In this situation, the probability to find the quantum dot in the lowest possible charge state N_0 is dominant.

A SET composed of a metallic island tunnel coupled to two normal leads exhibits transport characteristics similar to those of a quantum-dot SET, see *Fig. 2.7*. The current through the island SET as a function of bias voltage is plotted in *Fig. 2.7* (a).

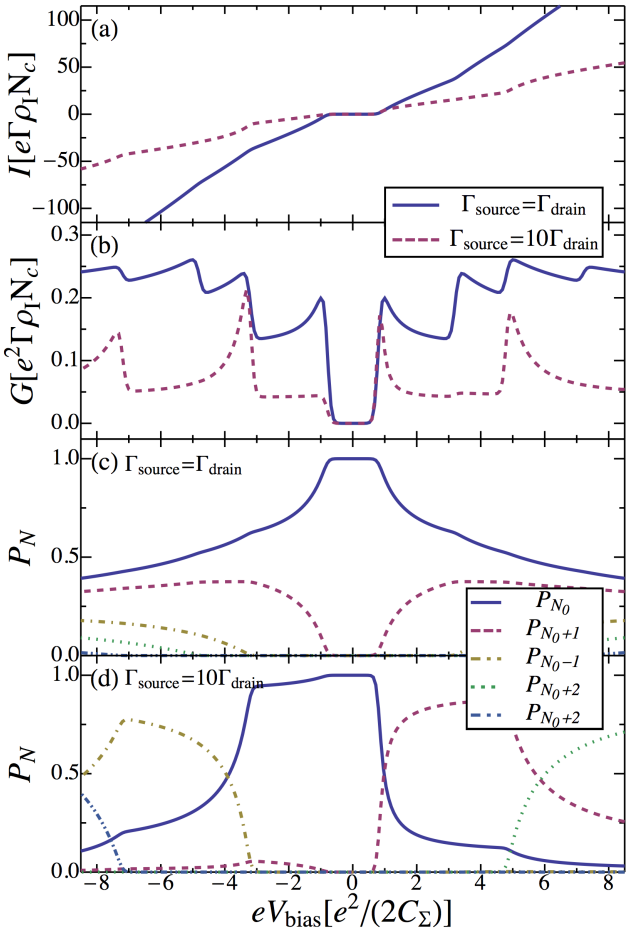

Figure 2.7: Transport characteristics of metallic-island tunnel coupled to two normal leads in sequential tunneling limit. (a) Current (over applied bias voltage V_{bias}) increases continuously. Coulomb steps are strongly suppressed for symmetric coupling to leads. The island density of states is denoted by ρ_I. (b) The peaks in the conductance represent the excitation energies of island charge states. (c)-(d) Corresponding occupation probabilities of the relevant charge states for symmetric and asymmetric tunnel couplings, respectively. The bias voltage symmetry of the system is broken by asymmetric couplings.

As in the quantum-dot case, the asymmetric lead coupling leads to a reduction of the current and an asymmetric bias dependance. The latter can better be seen in the conductance (*Fig. 2.7* (b)) and in the respective plot of the occupation probabilities (*Fig. 2.7* (d)). Analog to the quantum-dot SET, the bias asymmetry is caused by the different depletion and filling probabilities defined by the couplings Γ_{source} and Γ_{drain}. For negative transport voltage depletion of the island is favored and for positive V_{bias} the island is primarily filled up with additional electrons. Now, we want to discuss the differences in transport characteristics compared to the dot system. At low bias voltages, the transport through both systems is blocked until eV_{bias} exceeds the Coulomb blockade threshold and the next charging state $N_0 + 1$ enters the transport window. By further increasing of the bias applied to the island SET, more and more levels of the continuous spectrum contribute to transport, and after each charging step the current increases continuously in contrast to the discrete dot spectrum. An asymmetric choice of tunnel couplings pronounces the Coulomb steps of the charge states entering the transport window which are strongly suppressed in the symmetric island case, see *Fig. 2.7* (a).[4,5] The discussed replacement of the constant plateaus

between the Coulomb steps in the quantum-dot SET by the continuous increase of the island system, naturally leads to a non-vanishing conductance between the peaks marking the charge-state excitation energies, see *Fig. 2.7* (b).

To conclude, in this paragraph we considered a quantum dot and a metallic island tunnel coupled to two normal leads. Both systems are basic representations of SETs. We discussed their transport properties and illustrated sequential tunneling and co-tunneling processes. The current-voltage characteristics of the systems are similar but exhibiting a few differences that are addressed to the different energy spectra of the central parts of the SETs.

2.4 Spintronics

It is obvious that the replacement of the central region (metallic island or quantum dot) is not the only possibility to change transport properties of SETs. To control not just the charge but also the spin degrees of freedom of transport electrons ferromagnetic components can be integrated into the device, e. g., by using ferromagnetic leads. Due to the magnetism spintronic effects will appear in such structures. In the past decades, the field of spintronics was intensively investigated and corresponding devices already play an important role in todays information technologies.[6–9] The discoverers of the giant-magnetoresistance effect (GMR effect), which is one of the major advancements concerning spintronics, received the Nobel Prize in Physics in 2007. At the same time, but independently P. Grünberg and A. Fert investigated Fe/Cr multilayer structures and discovered the GMR.[10,11] In this paragraph we will introduce the reader to the field of spintronics. To this end, we will discuss the spin valve, the GMR, and the related tunnel-magnetoresistance effect (TMR effect). For SETs containing ferromagnetic and nonmagnetic materials spin accumulation in normal metals and, depending on the explicit setup, an interaction induced exchange field are of great importance. Hence we will also present the fundamentals concerning these spintronic effects.

2.4.1 Spin Valve

Typical examples of spintronic devices are spin valves, see *Fig. 2.8*. The polarization directions of at least two ferromagnetic layers enclose an arbitrary angle ϕ. The coercive fields of the ferromagnets differ, hence the angle ϕ is tunable by an outer magnetic field. By applying a finite bias voltage a charge current I can be driven through the system. There are two different typical choices of sample geometry. On the one hand the current flows parallel to the multilayer planes and on the other hand normal to the interfaces. In both cases, due to the finite polarization of the layers the magnitude of I strongly depends on ϕ. The underlying phenomenas causing this behavior (GMR and TMR) are explained in detail in the following two paragraphs 2.4.2 and 2.4.3, respectively.

Since the polarization angle and hence the current is very sensitive to an outer magnetic field, spin valves are of great technological interest. In industry spin valves used as magnetic-field sensors are suitable especially in the context of modern storage devices, e. g. as read heads in hard-disc drives.

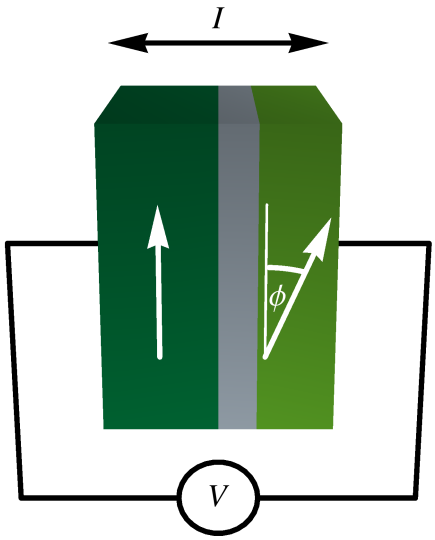

Figure 2.8: Scheme of a spin valve. The polarization directions of two ferromagnets enclose an angle ϕ. A bias voltage V can be applied to drive a current I (perpendicular to the layers) through the system. The magnitude of I strongly depends on ϕ and the angle is tunable by an outer magnetic field.

2.4.2 GMR Effect

In 1988 P. Grünberg and A. Fert independently observed a strong dependence of the electrical resistance of ferromagnetic/nonmagnetic multilayer structures on the relative orientation of the magnetization directions (GMR effect). In the following, to introduce the GMR we want to discuss the Grünberg experiment[10] in detail.

The considered sample is a Fe/Cr/Fe-sandwich structure consisting of two 12 nm thick Fe stripes and a 1 nm thick non-ferromagnetic Cr spacer in between. Due to the thin Cr layer the two Fe films are antiferromagneticaly coupled and the magnetizations point along the stripes (easy axis), but even relatively small magnetic fields ($\propto 10^{-2}$ T) can force the magnetizations to align parallel. The electrical resistance is measured at room temperature with the four-point method, while the current flows parallel to the layers. During the measurements a time dependent magnetic field is applied to the probe. The resistance is measured while a complete hysteresis loop is scanned through. Grünberg *et al.* consider two different cases, on the one hand the outer magnetic field is applied along the easy axis of the ferromagnets and on the other hand parallel to the hard axis. In the former case the current always flows along the film magnetization, hence the resistivity is not influenced by the magnetoresistivity-anisotropy effect and the resistivity variation exclusively originates from the change of the relative Fe magnetization. The respective original measurement of hysteresis and resistivity is shown in *Fig. 2.9*, the former was measured via the magneto-optic Kerr effect (MOKE). In the lower diagram the relative resistivity $\Delta R = R - R_{||}$ normalized to $R_{||}$ is plotted over the applied magnetic field B_0. Here, $R_{||}$ is the saturated resistivity of the probe along the easy axis. At the points 1 and 3 the magnetization switches from antiparallel to the parallel state and the points 2 and 4 mark the contrary magnetization reversals. When the transitions between the different magnetization alignments take place the

resistivity of the system experiences a change of about 1,5 %. In comparison to the resistivity change of a single 25 nm thick Fe film (caused by anisotrope magnetoresistivity) this corresponds to an increase by the factor 10. A further enhancement of the GMR effect to 10 % is realized by using a multilayer with 3 Fe strips and cooling the system to about 5 K.

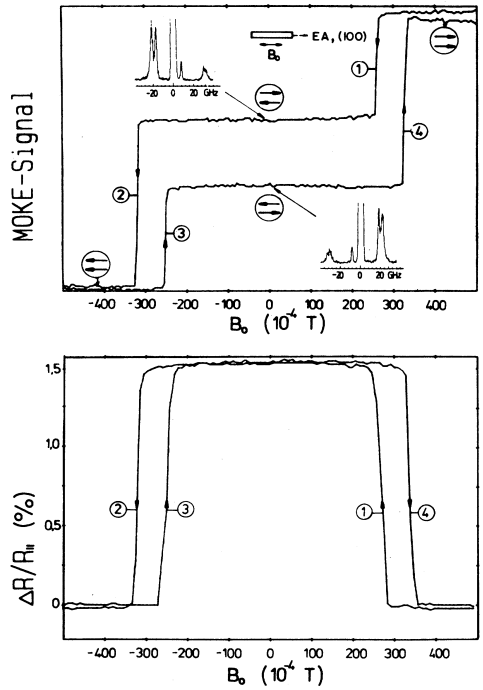

Figure 2.9: Original measurements of the GMR experiment performed by P. Grünberg *et al.*[10] The upper plot shows the hysteresis of the Fe/Cr/Fe-sandwich structure with a magnetic field applied along the easy axis of the sample. The arrows indicate the magnetization state of the two Fe layers. In the lower diagram the normalized relative electrical resistance is plotted over the magnetic field. The decrease of the resistivity is about 1,5 % if the probe switches from the antiparallel into the parallel state.

Now, we will explain the existence of the GMR effect by considering the transport of electrons through the model system of a collinear spin valve, see *Fig. 2.10*. The bias voltage is applied perpendicular to the layers. If the spin quantization axis of the transport electrons is chosen to point in the direction of the layers magnetization, then the current is composed of spin up and spin down electrons, whose magnetic moments are aligned along this axis. The two spin channels of the current are considered to be independent, i.e., spin-flip processes are neglected. Electrons with a given spin are transported through the spin valve, their path is visualized by the dashed lines in *Fig. 2.10*. The probability to be scattered (crosses on dashed lines) in a ferromagnetic layer is enhanced if the electron spin differs from the layer magnetization. Equivalent-circuit diagrams are shown below the parallel and antiparallel alignment sketches of the spin valve. The two independent spin channels and the associated resistances are illustrated. Calculations of the total resistances R_p and R_ap of the parallel and antiparallel circuit, respectively, yield

$$R_\mathrm{p} = \frac{2R_\mathrm{small}R_\mathrm{large}}{R_\mathrm{small}+R_\mathrm{large}}\,, \tag{2.8}$$

$$R_\mathrm{ap} = \frac{1}{2}(R_\mathrm{small}+R_\mathrm{large})\,. \tag{2.9}$$

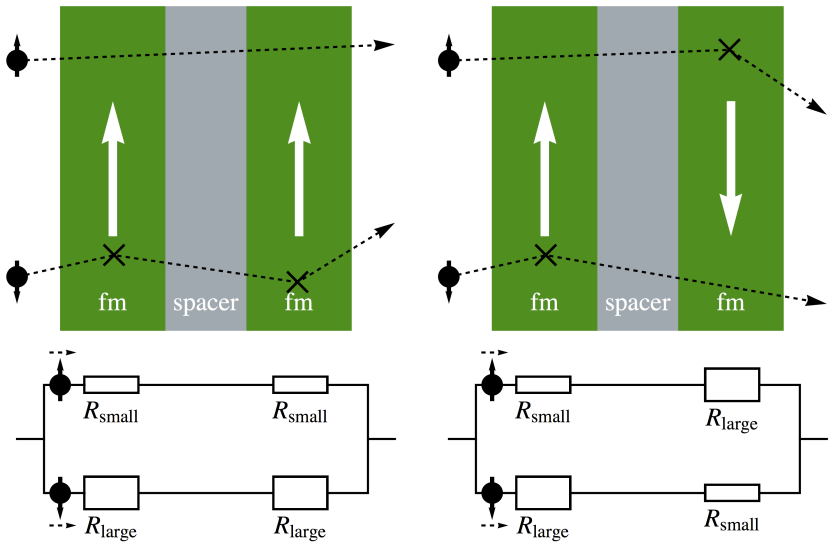

Figure 2.10: GMR effect. Transport of spin up and spin down electrons through a collinear spin valve is illustrated. Depending on the polarization of the ferromagnets (fm) the spin channels experience a different resistance. The total resistance is, as it can be seen in the lower equivalent-circuit diagrams, larger in the antiparallel setup.

A comparison of Eq. (2.8)-(2.9) reveals $R_\mathrm{p} \leq R_\mathrm{ap}$, while the equality of the total resistances is only reached in the negligible limit $R_\mathrm{small} = R_\mathrm{large}$. Hence by means of the considered model it is shown that the antiparallel setup of the spin valve has a larger resistance than the parallel one.

2.4.3 TMR Effect

The tunnel-magnetoresistance (TMR) effect is related to the GMR but requires electrons tunneling through a potential barrier. It can be observed in spin-valve structures (see *Fig. 2.8*) if the spacer between two ferromagnetic layers is chosen in such a way that the ferromagnets are tunnel coupled to each other. Analog to the GMR the electrical resistance of TMR devices is maximal for antiparallel alignment of the layer magnetizations. The first description of the TMR effect was published in 1975 by Jullière[12] and a theoretical treatment followed by Maekawa and Gäfvert.[13] A subsequent generalization of the previous works in the context of band theory by Slonczewski[14] also allows for noncollinear magnetizations.

First, we consider the collinear case and define the TMR as $\mathrm{TMR} = (G_\mathrm{p} - G_\mathrm{ap})/G_\mathrm{p}$ with G_p and G_ap being the conductances of the parallel and antiparallel situations, respectively. We emphasize that in literature there are some other definitions of the TMR which slightly deviate from the definition above. In the parallel setup in both ferromagnets the spin up electrons are chosen to represent the majority electrons and the spin quantization axis points in the direction of the layer polarization. While for antiparallel aligned magnetizations in one layer the spin down electrons are the ma-

jority electrons. Still the quantization axes of both layers point in the same direction. With this choice of the spin quantization axes the following proportionalities are valid for the conductances

$$G_{\mathrm{p}} \propto \rho_1^+(\varepsilon_{\mathrm{F}})\rho_2^+(\varepsilon_{\mathrm{F}}) + \rho_1^-(\varepsilon_{\mathrm{F}})\rho_2^-(\varepsilon_{\mathrm{F}}) \,, \tag{2.10}$$

$$G_{\mathrm{ap}} \propto \rho_1^+(\varepsilon_{\mathrm{F}})\rho_2^-(\varepsilon_{\mathrm{F}}) + \rho_1^-(\varepsilon_{\mathrm{F}})\rho_2^+(\varepsilon_{\mathrm{F}}) \,. \tag{2.11}$$

In the parallel (antiparallel) setup majority electrons tunnel into majority (minority) states of the other layer, which are characterized by their densities of states $\rho_i^{+(-)}$ at the Fermi energy ε_{F}. The two summands in Eq. (2.10)-(2.11) describe the independent spin channels, i.e., spin-flip processes are neglected. Jullière deduces a notation of the TMR which only depends on the polarizations of the two ferromagnets:

$$\mathrm{TMR} = \frac{2p_1p_2}{1+p_1p_2} \,, \tag{2.12}$$

with $p_i = [\rho_i^+(\varepsilon_{\mathrm{F}}) - \rho_i^-(\varepsilon_{\mathrm{F}})]/[\rho_i^+(\varepsilon_{\mathrm{F}}) + \rho_i^-(\varepsilon_{\mathrm{F}})]$. The layer polarization p_i describes the asymmetry of the majority and minority densities of states and takes values from 0 to 1. A perfect polarization ($p_i = 1$) represents a half metal, while $p_i = 0$ is equivalent to an unpolarized material. An analysis of Eq. (2.12) yields that the TMR vanishes if the polarization of at least one layer is equal to zero. By using materials with higher polarization the TMR increases and becomes one in the case of two half metals ($p_1 = p_2 = 1$).

If the polarization directions of two tunnel-coupled ferromagnets enclose an arbitrary angle ϕ, then the conductance of the system is given by $G(\phi) = G_0\,(1 + p_{1,\mathrm{B}}p_{2,\mathrm{B}}\cos\phi)$. The factors $p_{i,\mathrm{B}}$ are called effective spin polarizations. They are defined as the product of the polarization p_i and a factor $A_{i,\mathrm{B}}$ which describes the momentum dependence of the wave-function penetration into the tunnel barrier, with $-1 < A_{i,\mathrm{B}} < 1$.[14] The cosine dependence of the conductance on the angle ϕ results from the overlap of the spinor wave functions of the two ferromagnets. There are already several experimental papers verifying the predicted electronic transport behavior through a spin valve.[15–17] It is possible to define a generalized tunnel magnetoresistance to treat the noncollinear situation:

$$\mathrm{TMR}(\phi) = \frac{G(0) - G(\phi)}{G(0)} \tag{2.13}$$

$$= \frac{p_{1,\mathrm{B}}p_{2,\mathrm{B}}}{1+p_{1,\mathrm{B}}p_{2,\mathrm{B}}}\,(1-\cos\phi) \,. \tag{2.14}$$

The lower equation is similar to the collinear situation, see Eq. (2.12), while the factor $(1-\cos\phi)$ describes a reduction of the TMR by a deviation from the antiparallel setup. By definition the angle dependent TMR vanishes in the parallel case.

In conclusion, the TMR results from the spin polarization of the ferromagnets at the Fermi energy, while it decreases if the angle between the layer magnetization directions deviates from the antiparallel alignment.

2.4.4 Spin Accumulation

A fundamental spintronic effect, that is crucial in the context of ferromagnetic SETs, is the so called *spin accumulation*. It arrises in ferromagnetic/normal metal heterostructures. During transport of electrons from a ferromagnet into a normal metal one spin type is dominant. Hence spin angular momentum is transferred to the normal conductor and a finite magnetization builds up. First experimental observations of spin accumulation at ferromagnetic/paramagnetic interfaces were performed by M. Johnson and R. H. Silsbee in the 1980s.[18,19] There are a lot of subsequent works observing spin accumulation in different systems containing mesoscopic islands,[20,21] spin valves,[22–25] and even graphene.[26–30]

To introduce spin accumulation in more detail we consider a simple model system, see *Fig. 2.11*, that consists of a large metallic region enclosed by antiparallel aligned ferromagnetic source and drain leads.[31] The related densities of states (Stoner model)

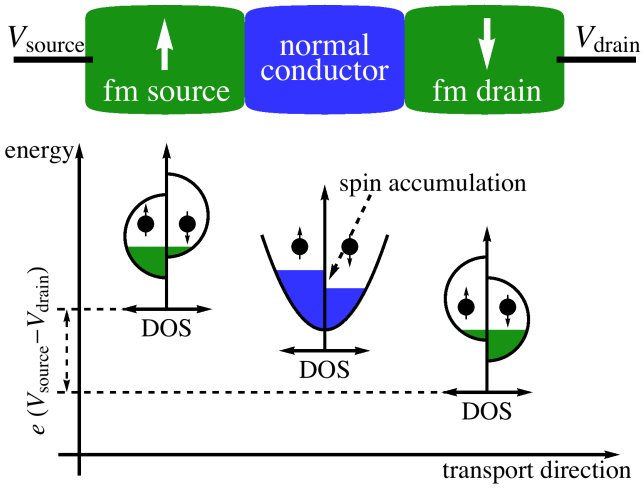

Figure 2.11: Spin-accumulation model system.[31] Two antiparallel polarized ferromagnets enclose a normal metal. The spin dependent interface resistances lead to a splitting of the Fermi energies on the central electrode.

are shown below the three regions. A non-equilibrium situation is created by applying a bias voltage $V_{source} - V_{drain}$ that drives a current from source to drain through the system. We choose the spin quantization axis to point in the magnetization direction of the left ferromagnet and treat the two spin sorts as independent electron channels. Caused by the finite spin polarization of the source lead at the Fermi surface mainly up electrons enter the central region. But for these electrons transmission from the normal metal into the drain is suppressed because there are just a few spin-up states available. The chemical potential of the central region adjusts in such a way that a constant current flow through the system is guaranteed and spin accumulation is described by the resulting spin splitting of the chemical potential of the normal conductor. In the considerations above we assumed that the ratio between charge-variation and spin-relaxation time is small. Otherwise the spin imbalance will decay between two tunneling events, and no spin will accumulate.

2.4.5 Exchange Field

The system that we are considering in this work is the single-electron spin-valve transistor, i. e., a metallic island tunnel coupled to ferromagnetic source and drain leads. This device is conceptually similar to a quantum-dot spin valve. In the latter, the central island hosting a continuum of single-particle energy levels is replaced by a quantum dot with a discrete level spectrum. This can be realized by either shrinking the central island in size or by using semiconductors or carbon nanotubes instead of metals. Quantum-dot spin valves have been studied extensively both theoretically[32–51] and experimentally.[52–60] One intriguing prediction[33–35] for the quantum-dot spin valve was the existence of an interaction-induced exchange field that acts on the spins of the quantum-dot electrons as a consequence of the tunnel coupling to spin-polarized leads. This exchange field, that is tunable by gate- and bias voltage, leads to a precession of an accumulated dot spin[33,34] or a splitting in the Kondo resonance.[35] The latter has been experimentally confirmed recently.[54,57,58] The origin of the exchange field is a level renormalization that is spin dependent as a consequence of spin-dependent tunnel couplings. This idea has later been transferred to describe gate-dependent tunneling-induced level shifts in carbon nanotubes with orbital-dependent tunnel couplings to normal leads[61] and to molecular systems with different tunnel couplings of degenerate molecular states to two normal leads.[62] Despite its different origin the exchange field acts like an outer magnetic field. This was shown in the context of carbon nanotubes attached to nickel leads by applying a magnetic field that compensates the exchange field.[58]

Now, we want to discuss the theoretical description of the exchange field existent in a quantum-dot spin valve by means of the work of Braun *et al.*.[34] In this work kinetic equations for the quantum-dot occupation and its accumulated spin are derived in the sequential-tunneling limit within a diagrammatic real-time transport formalism. The exchange field emerges in the kinetic equation that describes the time evolution of the accumulated spin $\mathbf{S}$ on the quantum dot

$$\frac{\mathrm{d}\mathbf{S}}{\mathrm{d}t} = \left(\frac{\mathrm{d}\mathbf{S}}{\mathrm{d}t}\right)_{\mathrm{acc}} + \left(\frac{\mathrm{d}\mathbf{S}}{\mathrm{d}t}\right)_{\mathrm{rel}} + \left(\frac{\mathrm{d}\mathbf{S}}{\mathrm{d}t}\right)_{\mathrm{rot}}. \tag{2.15}$$

The first two terms on the right-hand side describe the accumulation and relaxation of the spin via tunneling from and to the spin-polarized electrodes and the third one

$$\left(\frac{\mathrm{d}\mathbf{S}}{\mathrm{d}t}\right)_{\mathrm{rot}} = \mathbf{S} \times \sum_{r=L,R} \mathbf{B}_r \tag{2.16}$$

includes the exchange field between lead r and quantum dot defined as

$$\mathbf{B}_r = \frac{p_r \Gamma_r \hat{\mathbf{n}}_r}{\pi\hbar} \int' \mathrm{d}\omega \left(\frac{f_r(\omega)}{\omega - \epsilon - U} + \frac{1 - f_r(\omega)}{\omega - \epsilon}\right), \tag{2.17}$$

with lead polarization p_r, lead magnetization direction $\hat{\mathbf{n}}_r$, tunneling rates Γ_r, energy of the single quantum-dot level ϵ, Coulomb-repulsion energy U and Fermi function of the leads f_r. Furthermore, the prime at the integral denotes Cauchy's principal value.

The exchange-field contributions lead to a rotation of the accumulated spin around the total field $\mathbf{B}_L + \mathbf{B}_R$, see Eq. (2.16). While in the case of collinear configurations of the lead magnetizations the field does not influence the transport behavior because it is parallel aligned to $\mathbf{S}$. The integral in Eq. (2.17) vanishes for $U = 0$ or $p_r = 0$, i.e., the exchange field is only present in interacting quantum-dot spin valves with finite lead polarizations. A change of gate voltage varies the level energy ϵ and the Fermi functions f_r introduce a bias-voltage sensitivity. Thus, an electrical control of the exchange field is possible. In *Fig. 2.12* the bias dependence of the exchange field between left lead and quantum dot is plotted. The extrema are located at voltages where the energy

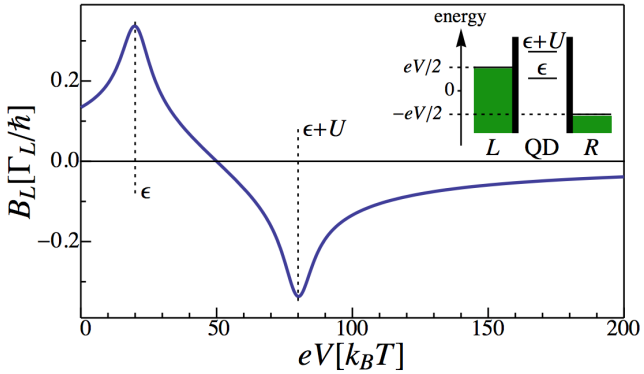

Figure 2.12: Magnitude of the exchange field $\mathbf{B}_L$ over applied bias voltage. The inset shows the energy-level scheme of the considered quantum-dot spin valve. The chosen parameters are $p_L = 0.3$, $\epsilon = 10k_BT$, and $U = 30k_BT$.

levels of the quantum dot enter the transport window ($eV/2 \in \{\epsilon, \epsilon + U\}$). While at the particle-hole symmetry point ($eV/2 = \epsilon + U/2$) the exchange field vanishes. In the discussed paper, Braun *et al.* show that the precession of the accumulated spin evoked by the exchange field results in an increase of the current flowing through the system and additionally weakens the spin-valve effect by rotating the spin out of its blocking position.

It is quite natural to expect the existence of a similar exchange field for a single-electron spin-valve transistor. The implications of such an exchange field on the linear conductance has already been theoretically discussed in the Coulomb regime by applying a rate-equation approach.[63,64] In the present work, we consider the same system and derive kinetic equations for the island charge and spin within a diagrammatic real-time transport formalism up to lowest order in the tunnel-coupling strength (sequential-tunneling limit). We will not restrict to the linear response but also consider the nonlinear-response regime. In the present thesis, we will demonstrate that the exchange field of the single-electron spin-valve transistor automatically emerges in the kinetic equations as a result of the considered Hamiltonian. Furthermore, its implications on electronic transport will be discussed in this thesis.

2.5 Realizations of Single-Electron Transistors

In general, SETs consist of a small central region that is tunnel coupled to source and drain leads and a gate electrode is coupled electrostatically to the central part. Many different realizations of SETs are possible by using different materials and setups.

As central part metallic islands or quantum dots can be used exhibiting continuous or discrete energy spectra, respectively. Furthermore, additional properties can be introduced to the system by employing ferromagnetic or superconducting structures. In the present section, we consider basic SET experiments to introduce the reader to the transport characteristics and the methods to produce SETs.

2.5.1 Island Coupled to Normal Metallic Leads

The first realized SET structures were composed of two normal metallic leads and a metallic island in between. They were produced in the late 80s of the last century. We consider a pioneering experiment performed by T. A. Fulton and G. J. Dolan in the Bell Laboratories.[65] They measured the current-voltage characteristics of a small capacitance C formed by an Al electrode ($0.05 \times 0.8\ \mu m^2$) that is contacted to three adjacent leads. In *Fig. 2.13* the original scanning-electron micrograph, a respective sketch of the used sample geometry, and a measured I-V curve is shown. In the micrograph the three Al-Al tunnel junctions are labeled by a, b, and c. The

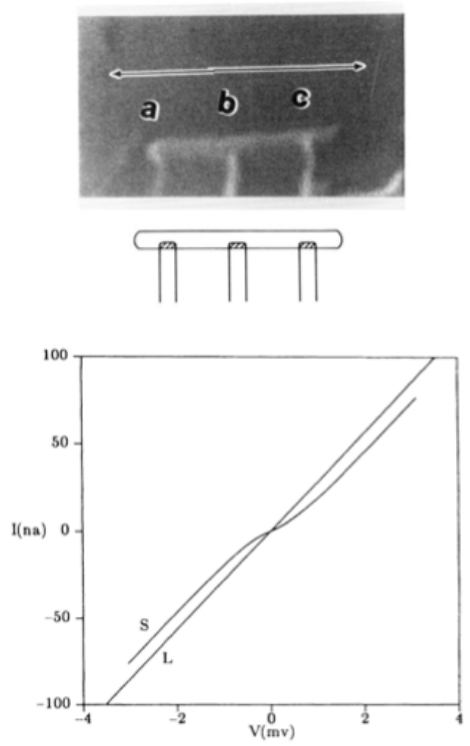

Figure 2.13: Scanning-electron micrograph, sketch, and original I-V curve of a experimental realization of a SET.[65] Three electrodes are contacted to a small central electrode via tunnel junctions a-c. The double arrow indicates the length of 1 μm. The measured current flows through the junctions a and b and the third junction was used to monitor the voltage of the central electrode. Due to single charging a region of reduced current arises in the I-V curve S. The curve L represents the Ohmic limit and was measured by means of an island exhibiting a large capacitance.

measured current flows through the junctions a and b while the third junction c was used to monitor the voltage of the central electrode. An electric field can be applied to the central electrode by an Au-Cr film on the back side of the oxidized silicon-wafer substrate. The measurements were performed in a temperature range of 4.2 K down to 1.1 K. This even allows the observation of superconducting effects due to the fact that for low temperatures of about 1.1 K the electrodes are superconducting.

The shown I-V curve labeled S was measured at 1.7 K and depicts the characteristic enhanced resistance (Coulomb gap) around zero bias, which is evoked by tunneling of single electrons to and from the central electrode. Due to the small capacitance C of the central electrode the charging energy $e^2/(2C)$ is large enough to suppress tunneling and hence to decrease the current for lower bias voltages. As a reference a curve labeled L that represents the Ohmic limit is also plotted. To obtain the data of L a similar cofabricated sample having a large capacitance was used. The measurements of T. A. Fulton and G. J. Dolan correspond closely to the previous theoretical predictions of single-electron charging effects.[66–69] Their experiment was followed by several subsequent experimental works also considering SETs composed of two normal leads enclosing a small central region.[70–75] Among these, there are groups using an alternative method to fabricate SETs by employing a scanning tunneling microscope (STM) to probe a metal particle deposited on an oxide layer on top of a substrate, see *Fig. 2.14*.[71–73,75] This kind of technique enables to measure the current through particles having very small capacitances of about 1 aF. Additionally, in these systems it is possible to vary the junction parameters of the sample by moving the tip to different metal particles or by tuning the distance between tip and particle. The

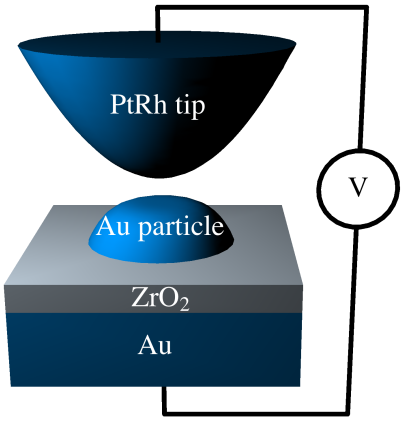

Figure 2.14: Sketch of experimental realization of a SET.[75] The PtRh STM tip is positioned above an Au nanoparticle and the resistance of the junction is tunable via changing the distance between tip and particle. The tunnel barrier between particle and Au(111) surface is build by a ZrO_2 layer.

first experiments that considered systems containing a central electrode that exhibits a discrete density of states instead of metallic nanostructures were realized by using semiconductors.[76,77] In these works a two-dimensional electron gas is formed in GaAs-AlGaAs heterostructures. By applying an electric field to deposited split gates narrow regions of electron gas are defined that represent the leads and the central part of the SET.

2.5.2 Island Coupled to Ferromagnetic Leads

To observe spintronic effects like the aforementioned spin accumulation or tunnel magnetoresistance in SETs ferromagnetic components have to be added to the charge-based electronic devices discussed in the previous paragraph. This can be achieved by employing ferromagnetic leads or ferromagnetic central electrodes. We divide the present paragraph into two parts discussing both metallic and ferromagnetic islands tunnel

coupled to two adjacent ferromagnetic leads. Due to the spin degrees of freedom besides charging effects the devices of the presented experiments also exhibit spintronic phenomena.

Ferromagnetic Island

The first SETs containing ferromagnetic components were realized in the late 90s of the last century.[78–82] The fabricated devices were composed of two ferromagnetic leads enclosing a small ferromagnetic electrode and an adjacent gate electrode that can tune the energy states of the island. Exemplarily, we consider the experiment performed by K. Ono, H. Shimada, and Y. Ootuka.[79] They used a sample consisting of two Ni/NiO/Co junctions in series, see *Fig. 2.15*. The Ni electrodes are located on a Si

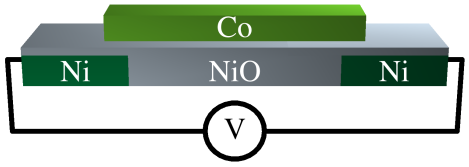

Figure 2.15: Sketch of experimental realization of SET with ferromagnetic island and leads.[79] Source and drain Ni electrodes are tunnel coupled to a central Co island.

substrate and covered by an NiO layer that tunnel couples the electrodes below to an upper Co island ($0.014 \times 0.150 \times 2.5\ \mu m^3$). The gate electrode is positioned on the back side of the substrate. A magnetic field that was applied to the long axis of the electrodes enables to measure not only the current-voltage characteristics but also the magnetoresistance of the sample for various gate voltages. By tuning the magnetic field from large enough negative to positive values the sample passes through different magnetic configurations. Due to the different coercivity fields of the electrodes the lead magnetizations can be align parallel or antiparallel to the island magnetization. In the antiparallel setup the spin-valve effect leads to an increase of the resistance. In *Fig. 2.16* the original plot of the magnetoresistance over applied magnetic field is shown. The measurement was performed at 20 mK in a high bias voltage regime

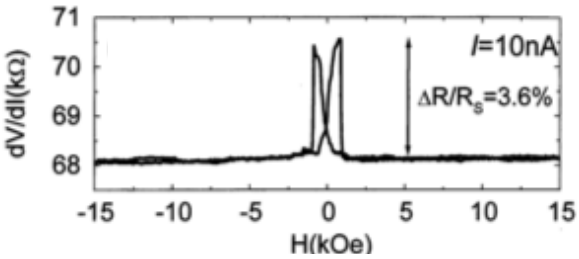

Figure 2.16: Measurement of magnetoresistance over applied magnetic field that switches the configuration of a ferromagnetic SET between the parallel and antiparallel state.[79]

(0.8 mV). For high positive and negative magnetic fields the magnetizations of the electrodes are aligned parallel. Since the field is driven from -15 kOe to 15 kOe and back again two peaks are visible in the magnetoresistance representing the switching into the antiparallel setup. As illustrated in the figure the magnetoresistance ratio normalized to the saturation resistance at high fields R_S is 3,6 %. The obtained value is significantly smaller than 15 %, which is the value predicted by the TMR formula of

Jullière, see Eq. (2.12), using the experimentally determined polarizations $p_1 = 23\%$ and $p_2 = 35\%$ for Ni and Co, respectively. The authors address the reduction of magnetoresistance to the fact that the multidomain Ni electrodes and the Co island are not completely antiparallel polarized due to pinning of magnetizations at surface by oxide or due to dipole interactions between electrodes. Furthermore, they point out that spin scattering processes and the low height of the tunnel barriers can also provoke the reduction of magnetoresistance.

Single-electron transistors whose components are all ferromagnetic still attract extensive interest and hence continuously experimental papers dealing with them are published.[23,83–87]

Metallic Island

In the present paragraph, we will consider experimental realizations of collinear (parallel or antiparallel) single-electron spin-valve transistors. As mentioned before, these systems consist of a central metallic island that is tunnel coupled to two ferromagnetic leads and capacitively coupled to a gate electrode. The respective experiments use single metallic nanoparticles as central part of the transistor and address current-voltage characteristics as well as the magnetoresistance of the devices.[88–91] Now, we consider the experiment of R. S. Liu, D. Suyatin, H. Petterson, and L. Samuelson performed in 2006 in detail.[90] A sketch of their system is drawn in *Fig. 2.17*. Two Ni electrodes

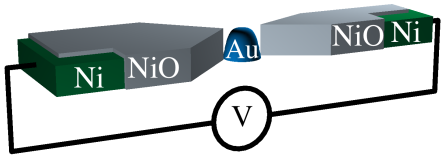

Figure 2.17: Experimental realization of a single-electron spin-valve transistor.[90] Two Ni leads covered by a NiO layer are tunnel coupled to an Au particle.

sandwich a 30 nm high Au-nanoparticle disc with 30 nm diameter. The tunnel contacts are realized by covering the Ni electrodes with a NiO. Next to these three parts a Ni side gate is fabricated. The whole device is placed on top of a SiO_2 layer grown on a Si substrate. Source (30×220 nm^2) and drain (30×80 nm^2) cross sections are different in size and hence the electrodes exhibit unequal coercivity fields which enables to switch between parallel and antiparallel magnetization alignment by variation of an outer magnetic field. Additionally, the authors were able to tune the tunnel-coupling strength to source and drain by using an atomic-force-microscope manipulation technique that enables to move the Au nanoparticle between the electrodes with angstrom precision.[92] In their work, the authors presented measurements of the current through the transistor performed at 4.2 K and compared the cases of symmetric and asymmetric tunnel couplings. In *Fig. 2.18* the original measurements of the differential conductances ($\mathrm{d}I/\mathrm{d}V$) as a function of bias V_d and gate voltage V_g are shown. The upper plot represents the symmetrically coupled single-electron spin-valve transistor and the lower one the asymmetric device. Both plots show the typical Coulomb diamonds at low bias. However, in the symmetric case the current remains finite in the

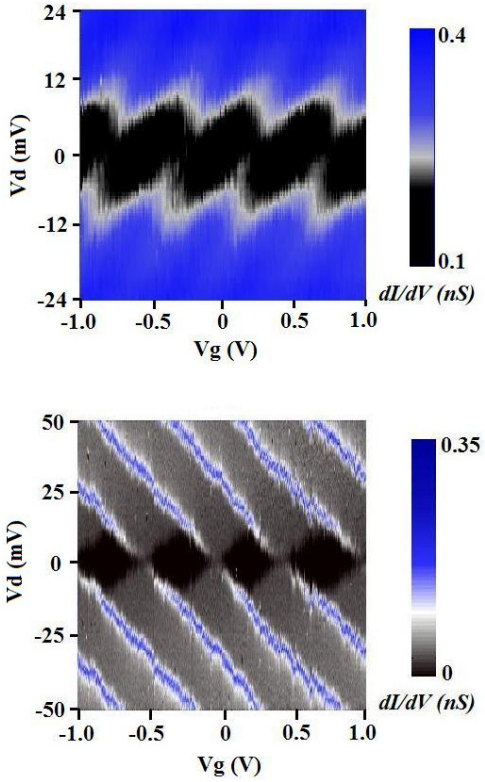

Figure 2.18: Measured differential conductance $\mathrm{d}I/\mathrm{d}V$ of a single-electron spin-valve transistor as a function of applied bias V_d and gate voltage V_g.[90] The upper plot represents the case of a symmetric tunnel coupling of the island to the electrodes and the lower one a strongly asymmetric coupling. Both plots show the characteristic Coulomb diamonds. However, for the device with a symmetric coupling the conductance in the Coulomb-blockade regime remains finite due to cotunneling processes.

Coulomb-blockade regime due to cotunneling processes. A finite background charge evokes a shift of the diamonds with respect to vanishing gate voltage $V_\mathrm{g} = 0$. The high-conductance strips in the figure of the asymmetric device reflect the pronounced Coulomb steps in the respective current-voltage characteristics of the device. Magnetoresistance measurements were not presented in the discussed paper but in the other above cited experimental works.[88,89,91]

3 Real-Time Transport Theory

In the previous chapter, we introduced to the basic principles of the single-electron spin-valve transistor. Besides fundamental properties and phenomena also experimental realizations of the system and similar spintronic devices were discussed. In the present chapter, the theoretical framework we use to describe electronic transport through the single-electron spin-valve transistor is being discussed in detail. We derive a master equation, that describes the dynamics of the transistor. Its solution, that is obtained by using a diagrammatic real-time formalism, represents the basis for the discussion of the spin accumulation and its implication on transport in linear and nonlinear response, which will be presented in chapters 5 and 6.

The present chapter is organized as follows. In the first section, we discuss the used model of the single-electron spin-valve transistor. Afterwards, the reduced density matrix, which only describes the island degrees of freedom, is introduced. We derive the master equation of the system that determines the time evolution of the matrix elements. Subsequently, the diagrammatic calculation of occurring transition rates is considered. As a last point, we present the charge-current formula of the system.

Parts of section 3.1 have already been published in Ref. [1].

3.1 Model

At the beginning of section 2.3, we briefly introduced a model which describes quantum dots or metallic islands that are tunnel coupled to two normal leads. This framework already contains parts of the model that we want to discuss now. However, for the sake of completeness, we present the full model of the single-electron spin-valve transistor, even though there will be repeating definitions.

The system under consideration is shown in *Fig. 3.1*. It is modeled by the total Hamiltonian $H = H_I + H_C + H_L + H_R + H_T$. The first part,

$$H_I = \sum_{l\sigma\nu} \varepsilon_l \, c^\dagger_{l\sigma\nu} c_{l\sigma\nu} \,, \tag{3.1}$$

describes the metallic island whose energy spectrum ε_l is characterized by a small level spacing $\Delta\varepsilon$. The index l labels the energy levels of the island, $\sigma \in \{\uparrow, \downarrow\}$ the spin, and

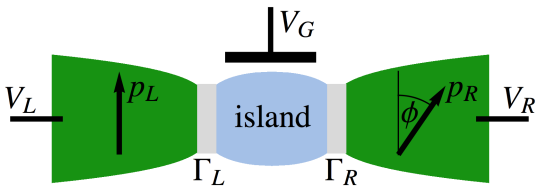

Figure 3.1: Noncollinear single-electron spin-valve transistor: a metallic island is tunnel coupled to ferromagnetic source and drain leads, whose polarizations directions enclose an angle ϕ.

$\nu = 1, \ldots, N_c$ is the transverse channel index. The annihilation (creation) operator of island electrons in the state $l\sigma\nu$ is denoted by $c^{(\dagger)}_{l\sigma\nu}$. We assume that the energy levels are independent of spin and transverse channel number. We will consider the limit of temperature and bias voltage being larger than the level spacing, $k_BT, eV \gg \Delta\varepsilon$, for which the energy spectrum can be viewed as continuous.

The Coulomb interaction of the island electrons is accounted for by the charging-energy term

$$H_C = E_C(N - N_{\text{ext}})^2\,, \tag{3.2}$$

where N is the number of electrons on the island. The charging energy scale $E_C = e^2/(2C_\Sigma)$ is determined by the total capacitance C_Σ, which is the sum of the capacitances of the two tunnel junctions, C_L, C_R, and the gate, C_G. For equal capacitances of the two tunnel junctions and a symmetrically applied transport voltage, the external charge $e\,N_{\text{ext}} = C_G V_G$ depends on the gate voltage V_G only. We emphasize that symmetric junction capacitances still allow for asymmetric tunnel-coupling strength between central electrode and leads. This is due to the fact that the tunnel couplings are much more sensitive to a variation of the junction geometry than the capacitances C_r. For later convenience, we define Δ_N as the difference of charging energies of $N+1$ and N electrons, i.e., $\Delta_N = E_C[2(N - N_{\text{ext}}) + 1]$.

Each of the leads is described as a reservoir of noninteracting electrons:

$$H_r = \sum_{ks\nu} \epsilon_{rks}\, a^\dagger_{rks\nu} a_{rks\nu}\,, \tag{3.3}$$

with $a^{(\dagger)}_{rks\nu}$ being the annihilation (creation) operator of lead $r \in \{L, R\}$ and momentum k. The index $s = +(-)$ denotes the majority (minority) spin states (along the magnetization direction $\hat{\mathbf{n}}_r$ of the respective lead) with the density of states ρ^r_s, which we assume to be energy independent. The lead's degree of spin polarization is characterized by $p_r = (\rho^r_+ - \rho^r_-)/(\rho^r_+ + \rho^r_-)$. The angle enclosed by $\hat{\mathbf{n}}_L$ and $\hat{\mathbf{n}}_R$ is denoted by ϕ.

The tunneling Hamiltonian $H_T = \sum_r H_{T,r}$, with

$$H_{T,r} = \sum_{kls\sigma\nu} V^r_{ks\sigma\nu}\, a^\dagger_{rks\nu} c_{l\sigma\nu} + \text{H.c.}\,, \tag{3.4}$$

describes tunneling between island and leads. Both the spin and the transverse channel index ν are conserved during tunneling. The latter is obvious from the fact that the tunneling Hamiltonian is diagonal in ν. In the following, we assume the tunneling matrix elements $V^r_{ks\sigma\nu} = V^r_{s\sigma}$ to be independent of momentum k and transverse channel index ν. Spin conservation is accounted for by expressing $V^r_{s\sigma}$ as a product of the (spin-independent) tunnel amplitudes t_r and the matrix elements of an SU(2) rotation that connects the (in general) different spin quantization axes for the two leads and the island. For the derivation of the kinetic equations, that is used in the presented thesis, it is convenient to choose the spin quantization axis of the island $\hat{\mathbf{n}}_S$ along the direction of the accumulated island spin $\mathbf{S}$. Its orientation relative to the lead's magnetization directions can be parametrized by two angles, as shown in *Fig. 3.2*: the

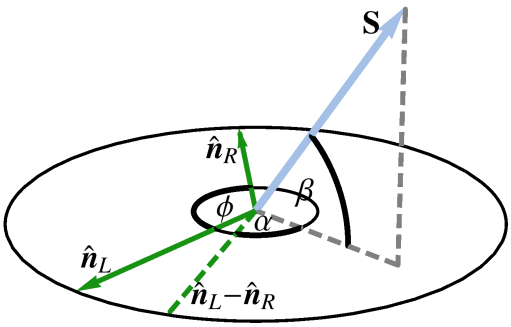

Figure 3.2: Scheme of relation between defined angles α, β, the polarization directions of the two leads $\hat{\mathbf{n}}_L, \hat{\mathbf{n}}_R$, and the accumulated spin on the island $\mathbf{S}$.

angle α enclosed by the $\hat{\mathbf{n}}_L - \hat{\mathbf{n}}_R$-axis and the projection of $\mathbf{S}$ onto the $(\hat{\mathbf{n}}_L, \hat{\mathbf{n}}_R)$-plane, and the angle β between $\mathbf{S}$ and the $(\hat{\mathbf{n}}_L, \hat{\mathbf{n}}_R)$-plane itself. Then, the tunnel-matrix elements $V^L_{s\sigma}$ for the left lead become

$$V^L_{\pm\uparrow} = \frac{t_L}{\sqrt{2}} \left[\pm e^{i\phi/2} \cos\left(\frac{\beta}{2} - \frac{\pi}{4}\right) - ie^{i\alpha} \sin\left(\frac{\beta}{2} - \frac{\pi}{4}\right) \right], \tag{3.5}$$

$$V^L_{\pm\downarrow} = \frac{t_L}{\sqrt{2}} \left[\pm e^{i\phi/2} \sin\left(\frac{\beta}{2} - \frac{\pi}{4}\right) + ie^{i\alpha} \cos\left(\frac{\beta}{2} - \frac{\pi}{4}\right) \right], \tag{3.6}$$

while the elements of the right lead are described by the same expressions but with the replacements $L \to R$ and $\phi \to -\phi$. The tunneling rate for electrons from lead r with spin s into the island spin state σ is quantified by $\Gamma^r_{s\sigma}/\hbar = 2\pi\rho^r_s |V^r_{s\sigma}|^2/\hbar$. In addition, we define $\Gamma^r_\sigma = \sum_s \Gamma^r_{s\sigma}$, $\Gamma_r = \sum_\sigma \Gamma^r_\sigma/2$, as well as $\Gamma = \sum_r \Gamma_r$.

3.2 Master Equation and Diagrammatic Technique

In the present section, we describe the formalism which enables us to investigate the electronic transport through the single-electron spin-valve transistor. Since we are not interested in the behavior of the lead degrees of freedom, we integrate them out and derive an effective description, which only contains the degrees of freedom of the metallic island. Based on the model presented in the previous section, a generalized master equation, that describes the time evolution of the density matrix of the system, is derived. To solve the master equation, a perturbative analysis of the transport properties up to first order in the tunnel-coupling strength (sequential-tunneling limit) is performed. This is reasonable due to the fact that source and drain are weakly coupled (tunnel contacts) to the island. Rates that occur in the master equation are calculated within a diagrammatic theory.[94–97] In the used formalism the Coulomb charging energy of the island electrons is taken into account nonperturbatively.

3.2.1 Density Matrix

The dynamics of a quantum-mechanical system is determined by the time evolution of its total density matrix $\hat{\rho}(t)$. Each physical observable of the system is characterized

by the expectation values of the respective operator. Formulated in the Heisenberg picture, the expectation value of operator A at time t is given by

$$\langle A\rangle(t) = \mathrm{tr}\left[e^{iH(t-t_0)}Ae^{-iH(t-t_0)}\hat{\rho}(t_0)\right] = \mathrm{tr}\left[A(t)_{\mathrm{Heis}}\hat{\rho}(t_0)\right], \tag{3.7}$$

with the initial time t_0 and the Hamiltonian of the system H. The assumption that the single-electron spin-valve transistor is decoupled before t_0, i. e., the tunneling Hamiltonian vanishes for $t \leq t_0$, causes a factorization of the initial density matrix:

$$\hat{\rho}_0 \equiv \hat{\rho}(t_0) = \hat{\rho}_0^{\mathrm{island}} \otimes \hat{\rho}_0^L \otimes \hat{\rho}_0^R. \tag{3.8}$$

The three parts represent the island and the two leads. As mentioned in the previous section, ferromagnetic source and drain are described as reservoirs of noninteracting electrons. Hence they are governed by the density matrix of the grand-canonical ensemble:

$$\hat{\rho}_0^r = \frac{1}{Z_0^r} e^{-\frac{H_r - \mu_r N_r}{k_B T}}. \tag{3.9}$$

Here, Z_0^r is the grand-canonical partition function, μ_r the chemical potential, and $N_r = \sum_{ks\nu} a^\dagger_{rks\nu} a_{rks\nu}$ the particle-number operator of the respective lead r. Boltzmann factor k_B and temperature T also appear.

In comparison to $\hat{\rho}_0^r$, the structure of the island density matrix is much more complex. An island state is characterized by the ket vector $|\chi\rangle = |\{n_{l\sigma\nu}\}\rangle$, where $n_{l\sigma\nu} \in \{0, 1\}$ counts if the corresponding island level l (transverse channel ν) is occupied by a spin-σ electron. In this notation, the elements of the reduced density matrix are defined as $P_{\chi_2}^{\chi_1} \equiv \langle\chi_1|\,\hat{\rho}_{\mathrm{red}}\,|\chi_2\rangle$. Diagonal elements $P_\chi^\chi \equiv P_\chi$ describe the probabilities to find the island in the corresponding state $|\chi\rangle$. The normalization condition $\sum_\chi P_\chi = 1$ is fulfilled. For later convenience, we introduce the notation $|(\bar{\chi}_{l\nu};\psi)\rangle = |\chi\rangle$, where $\bar{\chi}_{l\nu}$ describes the occupation of all island levels except for the orbital l and channel index ν, while $\psi \in \{0, \uparrow, \downarrow, \mathrm{d}\}$ explicitly shows the occupation of level l and channel ν. Due to the continuous level spectrum the dimension of the density matrix is huge. In general, all matrix elements of $\hat{\rho}_0^{\mathrm{island}}$ are relevant to describe the electronic transport through the single-electron spin-valve transistor. But in the context of the generalized master equation, we will demonstrate that due to physical properties and reasonable assumptions the number of elements $P_{\chi_2}^{\chi_1}$, that have to be taken into account, drastically reduces, see chapter 4.

3.2.2 Keldysh Contour and Reduced Propagator

In the following, we will write down the equations in the interaction picture. In this notation, the expectation value of a given operator A is given by:

$$\langle A\rangle(t) = \mathrm{tr}\left[A(t)_{\mathrm{Int}}\hat{\rho}(t)_{\mathrm{Int}}\right] = \mathrm{tr}\left[\hat{T}_{\mathrm{anti}} e^{-i\int_{t_0}^t \mathrm{d}t' H_T(t')_{\mathrm{Int}}} A(t)_{\mathrm{Int}} \hat{T} e^{i\int_{t_0}^t \mathrm{d}t' H_T(t')_{\mathrm{Int}}} \hat{\rho}_0\right], \tag{3.10}$$

with $\hat{T}$ being the time-ordering operator and $\hat{T}_{\mathrm{anti}}$ the anti-time-ordering operator. By using a formalism based on the Keldysh contour,[93] it is possible to transform Eq. (3.10)

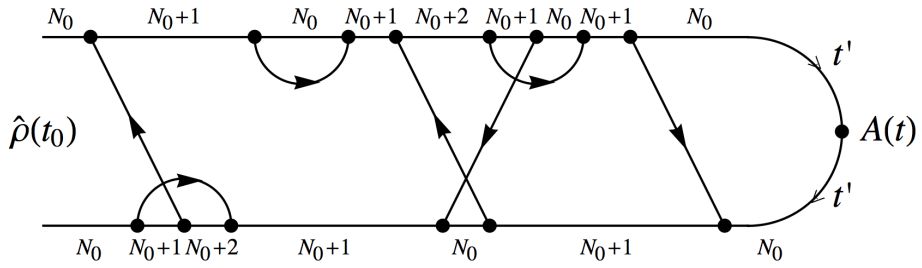

Figure 3.3: Scheme of Keldysh contour. Time t' propagates from t_0 to t and back to t_0. Tunneling of electrons into and out of the leads evokes a change of the island state. The number of electrons occupying the island in the respective state is written next to the contour.

into a simpler form:

$$\langle A \rangle (t) = \mathrm{tr}\left[\hat{T}_K e^{-i\int_K \mathrm{d}t' H_T(t')_{\mathrm{Int}}} A(t)_{\mathrm{Int}} \hat{\rho}_0\right]. \tag{3.11}$$

A scheme of a respective diagrammatic representation, incorporating the Keldysh contour, is plotted in *Fig. 3.3*. The main component of the figure is the Keldysh contour, which is represented by the curve on which the time t' runs from initial time t_0 to the considered time t and back to t_0. The terms of the tunneling Hamiltonian $V^r_{ks\sigma\nu}\, a^\dagger_{rks\nu} c_{l\sigma\nu}$ and $V^{r^*}_{ks\sigma\nu}\, c^\dagger_{l\sigma\nu} a_{rks\nu}$ are taken into account by outgoing and incoming vertices, respectively. Each vertex describes transport of one electron via tunneling from the island to lead r or vice versa. Tunneling lines between two of these Keldysh-contour vertices symbolize contractions of lead creation and annihilation operators by means of Wick's theorem. The time-ordering operator T_K appearing in Eq. (3.11) orders all following operators with respect to the Keldysh-contour time and the integration over t' also has to be performed along the contour. A more detailed discussion of the diagrammatic representation will be presented in the following subsections.

As already mentioned, we treat the leads as reservoirs of noninteracting electrons. Hence the trace over the leads can be performed and we obtain

$$\langle A \rangle (t) = \mathrm{tr}_{\mathrm{island}} \left[\mathbf{\Pi} A(t)_{\mathrm{Int}} \hat{\rho}_0\right], \tag{3.12}$$

with

$$\mathbf{\Pi} \equiv \mathrm{tr}_L \mathrm{tr}_R \left[\hat{T}_K e^{-i\int_K \mathrm{d}t' H_T(t')_{\mathrm{Int}}} \hat{\rho}_0^L \hat{\rho}_0^R\right], \tag{3.13}$$

being the reduced propagator. To obtain Eq. (3.12) we used that in the discussed system, for an arbitrary operator B, the relation $\mathrm{tr}\,[B] = \mathrm{tr}_{\mathrm{island}}\mathrm{tr}_L\mathrm{tr}_R\,[B]$ is valid. In the applied technique, the traces in Eq. (3.13) can be performed by means of Wick's theorem. This is due to the fact that the leads are described as noninteracting electron reservoirs.

3.2.3 Generalized Master Equation

In the present paragraph, a time-dependent master equation, that describes the time evolution of all density-matrix elements $P^{\chi_1}_{\chi_2}$, will be derived. This equation describes

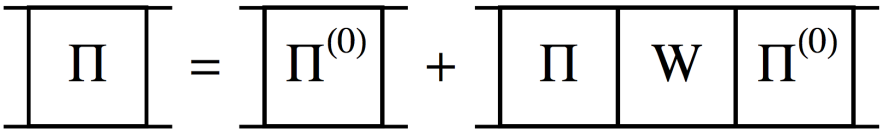

Figure 3.4: Visualization of the Dyson equation of the reduced propagator Π, see Eq. (3.15).

the matrix elements for all initial values at time t_0, as long as the whole set fulfills the probability-normalization condition. The elements $P^{\chi_1}_{\chi_2}(t)$ correspond to the quantum-statistical expectation values of the respective projectors and with Eq. (3.12) we obtain:

$$P^{\chi_1}_{\chi_2}(t) = \langle |\chi_2\rangle \langle \chi_1| \rangle (t) = \sum_{\chi_1'\chi_2'} \Pi^{\chi_1\,\chi_1'}_{\chi_2\,\chi_2'}(t,t') P^{\chi_1'}_{\chi_2'}(t'). \tag{3.14}$$

On the right-hand side, the term $\Pi^{\chi_1\,\chi_1'}_{\chi_2\,\chi_2'}(t,t')$ represents the elements of the already introduced reduced propagator, see Eq. (3.13). They describe the evolution of the reduced system (metallic island) in the Keldysh formalism from state $|\chi_1'\rangle$ at time t' forward to $|\chi_1\rangle$ at time t and the subsequent evolution from state $|\chi_2\rangle(t)$ back to $|\chi_2'\rangle(t')$. In the diagrammatic language $\Pi^{\chi_1\,\chi_1'}_{\chi_2\,\chi_2'}(t,t')$ is the sum of all diagrams with the given states at the beginnings and ends of the forward- and backward-Keldysh propagators. The reduced propagator fulfills the Dyson equation

$$\begin{aligned}\Pi^{\chi_1\,\chi_1'}_{\chi_2\,\chi_2'}(t,t') =& \Pi^{(0)\chi_1\,\chi_1'}_{\chi_2\,\chi_2'}(t,t') \\ &+ \sum_{\chi_1''\chi_2''} \int_{t'}^{t} \mathrm{d}t_1 \int_{t'}^{t_1} \mathrm{d}t_2 \Pi^{(0)\chi_1\chi_1}_{\chi_2\chi_2}(t,t_1) W^{\chi_1\,\chi_1''}_{\chi_2\,\chi_2''}(t_1,t_2) \Pi^{\chi_1''\,\chi_1'}_{\chi_2''\,\chi_2'}(t_2,t'),\end{aligned} \tag{3.15}$$

with $\Pi^{(0)\chi_1\chi_1'}_{\chi_2\chi_2'}(t,t') = \exp\left[i(E_{\chi_1} - E_{\chi_2})(t-t')\right]\delta_{\chi_1,\chi_1'}\delta_{\chi_2,\chi_2'}$ being the free propagator that only consists of a forward- and backward-Keldysh propagator. A visualization of the propagator's Dyson equation is shown in *Fig. 3.4*. In the last term of Eq. (3.15) the fourth order tensor $\mathbf{W}$, that corresponds to the self energy of the system, connects the reduced propagator to the free propagator. Starting from the Dyson equation, we obtain by performing the derivative with respect to time t, multiplying with $P^{\chi_1'}_{\chi_2'}(t')$, summation over χ_1' and χ_2', and using Eq. (3.14) the following general form of the master equation:

$$\frac{\mathrm{d}}{\mathrm{d}t} P^{\chi_1}_{\chi_2}(t) = -\frac{i}{\hbar}\left(E_{\chi_1} - E_{\chi_2}\right) P^{\chi_1}_{\chi_2}(t) + \int_{t_0}^{t} \mathrm{d}t_1 \sum_{\chi_1'\chi_2'} W^{\chi_1\,\chi_1'}_{\chi_2\,\chi_2'}(t,t_1) P^{\chi_1'}_{\chi_2'}(t_1)\,. \tag{3.16}$$

Here, the definition of the energies of the reduced system, $E_\chi \equiv \langle\chi|\left(H_I + H_C\right)|\chi\rangle$, is used. Due to the fact that Eq. (3.16) also enables the calculation of the time evolution of the off-diagonal density-matrix elements it is called *generalized master equation*. The kernel elements $W^{\chi_1\,\chi_1'}_{\chi_2\,\chi_2'}(t,t_1)$, that occurred for the first time in Eq. (3.15), now characterize transitions between the matrix elements $P^{\chi_1'}_{\chi_2'}(t_1)$ and $P^{\chi_1}_{\chi_2}(t)$ of the density matrix at the respective times.

In general, the obtained generalized master equation describes non-Markovian behavior, i. e., the time evolution of matrix element $P_{\chi_2}^{\chi_1}(t)$ depends on the reduced density matrix at previous times t_1. In the stationary limit, however, all matrix elements of $\hat{\rho}_{\mathrm{red}}$ become time independent ($P_{\chi_2}^{\chi_1}(t) = P_{\chi_2}^{\chi_1}(t_1) = P_{\chi_2}^{\chi_1}$), and with the additional definition $W_{\chi_2\,\chi_2'}^{\chi_1\,\chi_1'} = \int_{t_0}^{t} \mathrm{d}t_1\, W_{\chi_2\,\chi_2'}^{\chi_1\,\chi_1'}(t,t_1)$, Eq. (3.16) simplifies to

$$0 = \frac{\mathrm{d}}{\mathrm{d}t} P_{\chi_2}^{\chi_1} = -\frac{i}{\hbar}\left(E_{\chi_1} - E_{\chi_2}\right) P_{\chi_2}^{\chi_1} + \sum_{\chi_1'\chi_2'} W_{\chi_2\,\chi_2'}^{\chi_1\,\chi_1'} P_{\chi_2'}^{\chi_1'} \,. \tag{3.17}$$

This representation of the generalized master equation is the basis of all following considerations and calculations of the transport dynamics through the noncollinear single-electron spin-valve transistor. Starting from this equation we will derive kinetic equations for the island charge and spin which are fundamental for the investigation of the electronic properties. In the following two subsections, we will discuss in detail the procedure to obtain the kernel elements $W_{\chi_2\,\chi_2'}^{\chi_1\,\chi_1'}$. The used technique allows for a systematic perturbation expansion in the coupling strength Γ. In our work, we truncate the expansion at the lowest order Γ to describe the weak-coupling limit (sequential tunneling). However, the diagrammatic rules to obtain the kernel elements are generally formulated and not restricted to the sequential-tunneling limit.

3.2.4 Master Equation in Frequency Space

The introduced master equation (3.17) is written in time space. However, to solve it and to calculate transport quantities as the current or the current noise it is useful to switch into frequency space. The diagrammatic rules that enable to calculate the kernel $\mathbf{W}$ will be also formulated in the frequency space. We start by writing the Dyson equation (3.15) in matrix notation:

$$\mathbf{\Pi}(t,t') = \mathbf{\Pi}^{(0)}(t,t') + \int_{t'}^{t} \mathrm{d}t_1 \int_{t'}^{t_1} \mathrm{d}t_2\, \mathbf{\Pi}^{(0)}(t,t_1)\mathbf{W}(t_1,t_2)\mathbf{\Pi}(t_2,t'). \tag{3.18}$$

Here, it is already used that the considered system is invariant under translations in time, i.e., for all of the three fourth-rank tensors (kernel, free propagator, and reduced propagator) the equation $\mathbf{T}(t,t_0) = \mathbf{T}(t-t_0)$ is valid. The transition into frequency space is performed by the Laplace transform $\mathbf{T}(\omega) = \int_0^\infty \mathrm{d}t \exp\left[-i(\omega - i0^+)t\right]\mathbf{T}(t)$ and yields the following form of the Dyson equation

$$\mathbf{\Pi}(\omega) = \mathbf{\Pi}^{(0)}(\omega) + \mathbf{\Pi}^{(0)}(\omega)\mathbf{W}(\omega)\mathbf{\Pi}(\omega). \tag{3.19}$$

The diagrammatic visualization of the Dyson equation in frequency space corresponds to that of Eq. (3.15) with an additional bosonic line carrying the energy $\hbar\omega$ originating from the Laplace transformation, see *Fig. 3.5*. Simple calculations reveal that Eq. (3.19) is equivalent to

$$\left[\mathbf{\Pi}^{(0)}(\omega)^{-1} - \mathbf{W}(\omega)\right]\mathbf{\Pi}(\omega) = \mathbf{1}. \tag{3.20}$$

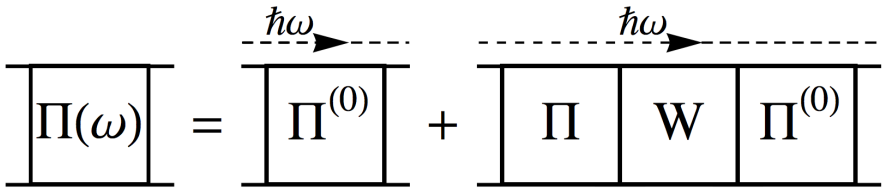

Figure 3.5: Visualization of the Dyson equation in frequency space, see Eq. (3.19).

By multiplication with frequency ω and applying the final value theorem $\lim_{\omega\to 0}(i\omega + 0^+)\mathbf{\Pi}(\omega) = \lim_{t\to\infty}\mathbf{\Pi}(t) = \hat{\rho}_{\mathrm{red}}$ we, eventually, obtain the master equation in the stationary state

$$0 = \left[\mathbf{\Pi}^{(0)}(\omega=0)^{-1} - \mathbf{W}(\omega=0)\right]\hat{\rho}_{\mathrm{red}}. \tag{3.21}$$

In the frequency space the elements of the free propagator are given by

$$\Pi^{(0)\chi_1\chi_1'}_{\chi_2\chi_2'}(\omega) = \frac{i\delta_{\chi_1,\chi_1'}\delta_{\chi_2,\chi_2'}}{E_{\chi_1} - E_{\chi_2} - \hbar\omega + i0^+}. \tag{3.22}$$

To obtain the elements $P^{\chi_1}_{\chi_2}$ of the reduced density matrix $\hat{\rho}_{\mathrm{red}}$, we still have to determine the kernel $\mathbf{W}(\omega)$ in the limit of vanishing frequency ω. The diagrammatic rules that enable to calculate it are being derived in the following subsection.

3.2.5 Kernel and Perturbation Expansion

To illustrate the procedure that yields the kernel elements $W^{\chi_1\,\chi_1'}_{\chi_2\,\chi_2'}$ up to a given order in the tunnel-coupling strength, we start by expanding the exponential that occurs in the definition of the reduced propagator, see Eq. (3.13), in powers of the tunneling Hamiltonian:

$$\begin{aligned}\hat{T}_K e^{-i\int_K \mathrm{d}t' H_T(t')_{\mathrm{Int}}} =& \sum_{m=0}^{\infty}(-i)^m \underbrace{\int_K \mathrm{d}t_1 \int_K \mathrm{d}t_2 ... \int_K \mathrm{d}t_m}_{t_1>t_2>...>t_m} \hat{T}_K \left[H_T(t_1)_{\mathrm{Int}} H_T(t_2)_{\mathrm{Int}} ... H_T(t_m)_{\mathrm{Int}}\right] \\ =& 1 - i\int_K \mathrm{d}t_1 \hat{T}_K \left[\sum_{kls\sigma\nu} V^r_{s\sigma}\, a^\dagger_{rks\nu}(t_1) c_{l\sigma\nu}(t_1) + \mathrm{H.c.}\right] + O({V^r_{s\sigma}}^2). \end{aligned} \tag{3.23}$$

Here, the equation is written in time space, having in mind that later on we will switch into frequency space to formulate the diagrammatic rules for the calculation of $\mathbf{W}(\omega = 0)$. The time ordering $t_1 > t_2 > ... > t_m$ is to be understood with respect to the Keldysh contour. The expansion in the tunnel-matrix elements $V^r_{s\sigma}$ can be visualized by irreducible blocks on the Keldysh contour, see *Fig. 3.6*. These are directly related to the kernel elements $W^{\chi_1\,\chi_1'}_{\chi_2\,\chi_2'}(t_1, t_2)$ that are diagrammatically symbolized by the sum of all irreducible diagram blocks with the respective states and times. Irreducible means that there is no possibility to place a vertical line that divides a diagram in two parts without cutting a tunneling line. The diagrammatic representation of the

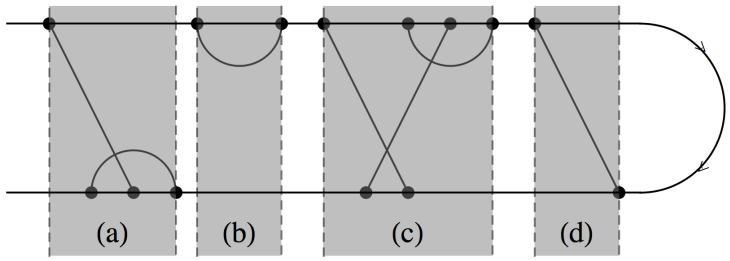

Figure 3.6: Irreducible blocks on the Keldysh contour. Diagrams of different order in the tunnel-coupling strength Γ, in the context of Eq. (3.23), are plotted. (a) Second order, (b) first order, (c) third order, and (d) first order.

self-energy element $W^{\chi_1\,\chi_1'}_{\chi_2\,\chi_2'}(t_1,t_2)$ is plotted in *Fig. 3.7*. On the upper Keldysh-contour segment the time propagates from t_2 to t_1 and vice versa on the lower segment. Analog, the island state evolves from $|\chi_1'\rangle$ to $|\chi_1\rangle$ and from $|\chi_2\rangle$ to $|\chi_2'\rangle$. As can be seen in Eq. (3.13), the terms of the perturbation expansion that are of odd order in $V^r_{s\sigma}$ vanish and only diagrams containing an even number of vertices exist. Each vertex describes electron tunneling into or out of the metallic island, i.e., the island-occupation number is changed by one electron. In diagrams, the number of tunneling lines that connect two vertices represents the order in the tunnel-coupling strength $\Gamma \propto |V^r_{s\sigma}|^2$. Furthermore, tunneling lines illustrate the contraction of lead creation and annihilation operators by means of Wick's theorem. They correspond to the expectation value of the product of the respective operators:

$$\left\langle a^\dagger_{rks\nu}(t)a_{r'k's'\nu'}(t')\right\rangle = \delta_{rr'}\delta_{kk'}\delta_{ss'}\delta_{\nu\nu'}e^{i\varepsilon_{rks\nu}(t-t')}f^+_r(\varepsilon_{rks\nu}), \tag{3.24}$$

$$\left\langle a_{rks\nu}(t)a^\dagger_{r'k's'\nu'}(t')\right\rangle = \delta_{rr'}\delta_{kk'}\delta_{ss'}\delta_{\nu\nu'}e^{-i\varepsilon_{rks\nu}(t-t')}f^-_r(\varepsilon_{rks\nu}). \tag{3.25}$$

Here, $f^+_r(\varepsilon) = 1/[\exp\left(\frac{\varepsilon-\mu_r}{k_BT}\right)+1]$ represents the Fermi function of lead r and we define $f^-_r(\varepsilon) = 1 - f^+_r(\varepsilon)$. For each vertex, the respective prefactors $V^r_{s\sigma}$, $V^r_{s\sigma'}$, $V^{r^*}_{s\sigma}$, or $V^{r^*}_{s\sigma'}$ of the relevant tunneling Hamiltonian summand have to be taken into account. The different quantum numbers σ and σ' appear due to the fact that the single summands of H_T do not conserve the spin although the total tunneling Hamiltonian does. Hence the initial spin σ of a tunneling line can differ from its final spin σ'. This variation of spin

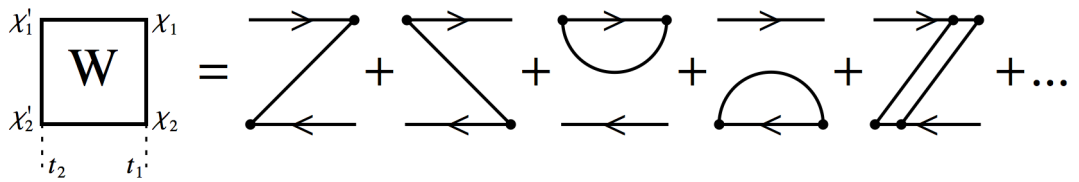

Figure 3.7: Diagrammatic representation of the self-energy element $W^{\chi_1\,\chi_1'}_{\chi_2\,\chi_2'}(t_1,t_2)$. It consists of all irreducible diagram blocks connecting the respective island states.

is caused by the noncollinear lead magnetization directions (chosen spin-quantization axes), see section 3.1, and not due to spin-flip processes during tunneling.

To formulate diagrammatic rules that enable to calculate the kernel $\mathbf{W}(\omega = 0)$ we again switch into the frequency space. The n vertices of a diagram are time ordered from the left to the right and denoted by $\tau_1, \tau_2, ..., \tau_n$. As a result, the Keldysh integrals $\int_K$ can be treated as common integrals, while an additional factor -1 has to be taken into account for every vertex placed on the backward propagator of the contour. Under the assumption of a diagonal initial density matrix $\hat{\rho}_0$ one obtains the following expressions:

$$\int_{-\infty}^{0} \mathrm{d}\tau_1 \int_{\tau_1}^{0} \mathrm{d}\tau_2 ... \int_{\tau_{n-2}}^{0} \mathrm{d}\tau_{n-1} e^{0^+\tau_1} e^{-i\Delta\varepsilon_1(\tau_1-\tau_2)} e^{-i\Delta\varepsilon_2(\tau_2-\tau_3)} ... e^{-i\Delta\varepsilon_{n-1}\tau_{n-1}}$$
$$= i^{n-1} \frac{1}{\Delta\varepsilon_1 + i0^+} \cdot \frac{1}{\Delta\varepsilon_2 + i0^+} \cdot ... \cdot \frac{1}{\Delta\varepsilon_{n-1} + i0^+} \,. \quad (3.26)$$

The quantities $\Delta\varepsilon_i$ represent the difference of left-going and right-going energies of the irreducible diagrams between τ_i and τ_{i+1}. We emphasize that in addition to the energies of the forward and backward propagators also the energies of the tunneling lines have to be taken into account.

Diagrammatic Rules

Finally, the considerations above enable us to formulate diagrammatic rules for the calculation of the self-energy elements $W^{\chi_1\,\chi_1'}_{\chi_2\,\chi_2'}$. The determination of these elements is necessary to solve the generalized master equation, see Eq. (3.17), that determines the dynamics of the single-electron spin-valve transistor.

1. Draw all topologically different irreducible diagrams with n directed tunneling lines for the n-th order in Γ. Assign the energies E_χ to the forward and backward propagator sections, the frequencies ω and a reservoir index r to the tunneling lines, and the island states $\chi_1, \chi_1', \chi_2, \chi_2'$ to the respective ends of the two propagators.

2. For each time segment between two adjacent vertices at times τ_j and τ_{j+1} (independent of whether they are positioned on the same or on opposite propagator) write a resolvent $1/(\Delta\varepsilon_j + i0^+)$. Here, $\Delta\varepsilon_j$ represents the difference of left-going and right-going energies, so that the right-going ones are counted negatively.

3. Multiply with the factor $\rho_s^r V_{s\sigma}^r V_{s\sigma'}^{r^*} f_r^+(\omega)$ or the factor $\rho_s^r V_{s\sigma}^r V_{s\sigma'}^{r^*} f_r^-(\omega)$ for each tunneling line that propagates backward or forward with respect to the Keldysh contour, respectively. The spin σ' corresponds to the electron spin that enters the metallic island from the lead and σ is the electron spin that leaves the island.

4. An overall factor is given by $-i(-1)^{b+c}$, with the number of vertices on the backward propagator b and c being the number of crossings of tunneling lines.

5. Each vertex contributes with a factor $\langle\chi'|\, c_{l\sigma\nu}^{(\dagger)} \,|\chi\rangle$, with χ (χ') being the state that enters (leaves) the vertex with respect to the Keldysh contour.

6. Integrate over all energies $\hbar\omega$ of the tunneling lines.

7. Sum over the leads $r \in \{L, R\}$, the lead minority and majority spin $s \in \{+, -\}$, and if possible over the island spin state $\sigma \in \{\uparrow, \downarrow\}$.

3.2.6 Current Formula

The charge current through lead r corresponds to the time evolution of the electron-number operator of the lead, i.e., $I_r = -e\frac{\mathrm{d}N_r}{\mathrm{d}t}$. In the context of the finite-frequency noise, see chapter 6, we will demonstrate that it is useful to consider the symmetrized current $I = (I_L - I_R)/2$. As we are interested in the stationary state, the charge on the island is conserved. Due to this fact, we are able to define the current flowing through the device as $I = I_L = -I_R$. Hence the symmetrization is not important for the current itself but we choose it for later convenience. By means of the quantum-mechanical equation of motion (Heisenberg picture) one obtains

$$I_r = -\frac{ie}{\hbar}[H, N_r] = -\frac{ie}{\hbar}\sum_{kls\sigma\nu} V^r_{s\sigma}\, a^\dagger_{rks\nu} c_{l\sigma\nu} + \text{H.c.}\,. \tag{3.27}$$

A comparison of this expression with the tunneling Hamiltonian of lead r, see Eq. (3.4), yields that I_r can directly be obtained from $H_{T,r}$ by performing the replacement $V^r_{s\sigma} \to -ieV^r_{s\sigma}/\hbar$. The constant complex prefactor can easily be incorporated in the diagrammatic technique. Eventually, the stationary charge current through lead r is given by

$$I_r = \sum_{\chi\,\chi_1'\chi_2'} \left(W^{I_r}\right)^{\chi\,\chi_1'}_{\chi\,\chi_2'} P^{\chi_1'}_{\chi_2'}\,, \tag{3.28}$$

where the matrix elements of the current transition rates $\mathbf{W}^{I_r}(\omega = 0)$ are directly obtained by multiplying the corresponding matrix elements of $\mathbf{W}(\omega = 0)$ with the net transported charge from lead r to the island. We note that minus signs originating from the complex prefactor and factors $1/2$ that appear due to the definition of the symmetrized current have to be taken into account appropriately. Due to completeness we write down the symmetrized mean current in matrix notation:

$$I = \mathrm{tr}\left[\mathbf{W}^I(\omega = 0)\hat{\rho}_{\mathrm{red}}\right]. \tag{3.29}$$

Here, we used the definition $\mathbf{W}^I(\omega = 0) = \mathbf{W}^{I_L}(\omega = 0) + \mathbf{W}^{I_R}(\omega = 0)$.

4 Kinetic Equations

In the present chapter, we derive kinetic equations for the island charge and spin up to lowest order in the tunnel-coupling strength. We emphasize that the obtained equations describe the noncollinear situation, which, in comparison to the parallel and antiparallel cases, drastically complicates the required theoretical framework. The resulting kinetic equations are the basis for the investigation of the transport properties of the single-electron spin-valve transistor. We note that the results presented in this chapter have already been published in Ref. [1].

As starting point of the discussion, we choose the following representation of the master equation:

$$0 = \frac{\mathrm{d}}{\mathrm{d}t} P_{\chi_2}^{\chi_1} = -\frac{i}{\hbar} \left(E_{\chi_1} - E_{\chi_2} \right) P_{\chi_2}^{\chi_1} + \sum_{\chi_1', \chi_2'} W_{\chi_2 \chi_2'}^{\chi_1 \chi_1'} P_{\chi_2'}^{\chi_1'} \; . \tag{4.1}$$

A detailed derivation of this formula and the corresponding diagrammatic rules that enable to calculate the kernel $\mathbf{W}(\omega = 0)$ were presented in chapter 3.

The single-electron spin-valve transistor contains a metallic island that exhibits a dense level spectrum. Hence the dimension of the reduced density matrix, that describes the island degrees of freedom, is huge. Therefore, there is also a large set of master equations determining the time evolution of the system. A drastic simplification of the problem is achieved by getting rid of the off-diagonal matrix elements of the reduced density matrix on the right-hand side of Eq. (4.1). Since the tunneling Hamiltonian conserves charge and is diagonal in the transverse channel index, only those matrix elements $P_{\chi'}^{\chi}$ of states $|\chi\rangle = |\{n_{l\sigma\nu}\}\rangle$ and $|\chi'\rangle = |\{n'_{l\sigma\nu}\}\rangle$ with the same number of island electrons in any channel ν need to be considered, $\sum_{l\sigma} n_{l\sigma\nu} = \sum_{l\sigma} n'_{l\sigma\nu}$. A further simplification relies on the assumption that there is a fast, spin-independent energy relaxation within the island, i.e., the time scale of energy-relaxation τ_{er} is smaller than the dwell time τ_{dw} (which, in turn, is smaller than the intrinsic spin-flip time τ_{sf} in order to sustain spin imbalance on the island). This is reasonable due to the fact that in contrast to quantum dots, metallic islands accommodate a large number of electrons and hence exhibit many relaxation channels. As a consequence, any coherent superpositions between states with different occupations of the orbital levels l are destroyed and only coherences between different spin states are kept. This leads to the more restrictive condition $\sum_{\sigma} n_{l\sigma\nu} = \sum_{\sigma} n'_{l\sigma\nu}$. Since the spectrum on the island is spin degenerate, energy differences $E_{\chi} - E_{\chi'}$, that would appear on the right-hand side of Eq. (4.1), vanish.

To remove the remaining coherent superpositions of different spin states we choose the spin quantization axis on the island along the direction of the accumulated spin and, furthermore, assume that the steady-state spin structure of the island is rotationally invariant about the quantization axis. The latter assumption neglects any

anisotropies of quadrupole and higher moments within the plane perpendicular to the dipole moment. Eventually, we conclude $n_{l\sigma\nu} = n'_{l\sigma\nu}$ for the proper choice of the spin quantization axis, i.e., only diagonal matrix elements $P_\chi \equiv P_\chi^\chi$ enter the right-hand side of the master equations in the stationary limit,

$$0 = \frac{\mathrm{d}}{\mathrm{d}t} P_{\chi_2}^{\chi_1} = \sum_\chi W_{\chi_2\,\chi}^{\chi_1\,\chi} P_\chi \,, \tag{4.2}$$

Analog, the current formula of the system, see Eq. (3.28), simplifies to

$$I_r = \sum_{\chi\,\chi'} \left(W^{I_r}\right)_{\chi\,\chi'}^{\chi\,\chi'} P_{\chi'}^{\chi'} . \tag{4.3}$$

The assumed fast, spin-independent energy relaxation within the island does not only destroy coherences of states with different occupations of the orbital levels l, it also leads to a thermal equilibrium among all states that are connected by this relaxation, i.e., states with given numbers $N_\uparrow$ and $N_\downarrow$ of spin $\uparrow$ and $\downarrow$ electrons on the island. The individual occupation for level l with spin σ and channel index ν under the condition that the island contains $N_\uparrow$ and $N_\downarrow$ electrons with spin $\uparrow$ and $\downarrow$, respectively, can be expressed by the conditional probabilities $F(l\sigma\nu|N_\uparrow, N_\downarrow)$. Beenakker first introduced these probability functions to discuss resonant tunneling through a quantum dot coupled to two electron reservoirs,[98] while Barnaś *et al.* used them in the context of collinear single-electron spin-valve transistors.[99] In thermal equilibrium, $F(l\sigma\nu|N_\uparrow, N_\downarrow)$ reduces to the Fermi function with a spin-dependent chemical potential, $f(\varepsilon_l - \mu_\sigma(N_\sigma))$ with $f(E) = 1/[\exp(\frac{E}{k_B T}) + 1]$. The spin-dependent chemical potential $\mu_\sigma(N_\sigma)$ is determined by the condition

$$N_\sigma = \sum_l f\left[\epsilon_l - \mu_\sigma(N_\sigma)\right] . \tag{4.4}$$

The kernels $W_{\chi_2\,\chi}^{\chi_1\,\chi}$ in Eq. (4.2) depend on the initial state χ. But most of the information about the individual occupations of the levels contained in χ are irrelevant for the evaluation of the kernel matrix element. What matters is the occupation and the energy of only those island levels that are involved in the tunneling processes that take place in the transition described by the considered kernel. In this thesis, we restrict ourselves to first order in the tunnel-coupling strength, due to the fact that we want to describe the sequential-tunneling limit. Each kernel is, then, a sum over contributions for which only one level l and transverse channel index ν is involved (we remind that coherent superpositions of different levels l or transverse channels ν do not appear). In the notation $|\chi\rangle = |(\bar{\chi}_{l\nu}; \psi)\rangle$, which makes the occupation of level l and channel index ν explicit, the non-vanishing kernel matrix elements can be written in the form $W_{(\bar{\chi}_{l\nu};\psi_2)\,(\bar{\chi}_{l\nu};\psi)}^{(\bar{\chi}_{l\nu};\psi_1)\,(\bar{\chi}_{l\nu};\psi)}$, i.e., the part $\bar{\chi}_{l\nu}$ is not changed during the transition. The value of the kernel depends on the total island charge $N \equiv N_\uparrow + N_\downarrow$ via the charging-energy contribution to the Hamiltonian and the occupation and energy of only the selected level l and transverse channel index ν. This occupation, however, is fully determined by the spin-dependent chemical potential $\mu_\sigma(N_\sigma)$, which, in turn, depends on $N_\uparrow$ and $N_\downarrow$.

For an island with a dense level spectrum, the dependence of the chemical potential $\mu_\sigma(N_\sigma)$ on N_σ is rather weak: the change for each added electron with spin σ is of the order of the mean level spacing $\Delta\varepsilon$ and, thus, much smaller than the energy scales k_BT, eV relevant for transport. Therefore, we use $\mu_\sigma(N_\sigma) \approx \mu_\sigma$ independent of N_σ in the following. This has the consequence that the value of the kernel matrix element $W^{\chi_1\,\chi}_{\chi_2\,\chi}$ depends only on the total island charge N (of state χ, i.e., $N = \sum_\sigma N^\sigma_\chi$ with $N^\sigma_\chi = \sum_{l\nu}\langle\chi|c^\dagger_{l\sigma\nu}c_{l\sigma\nu}|\chi\rangle$), the energy and occupation of the island level l with channel index ν that is involved in the transition. This dependence can be cast in the notation $W^{\psi_1\,\psi}_{\psi_2\,\psi}(l,\nu,N)$, where the occupation of the levels and channels different from l or ν does not appear explicitly. An energy scheme of the considered single-electron spin-valve transistor, that illustrates the executed assumptions, is drawn in *Fig. 4.1*.

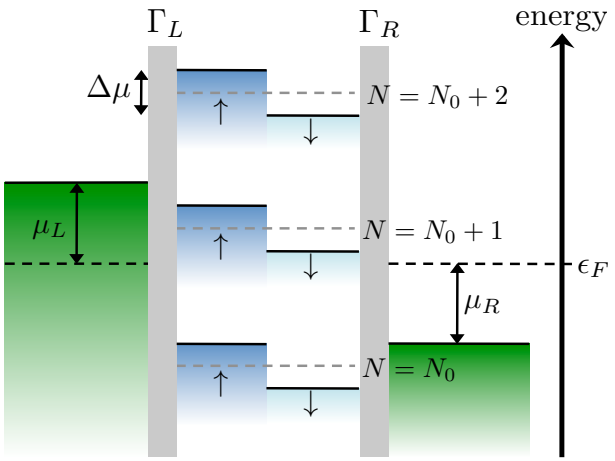

Figure 4.1: Energy scheme of single-electron spin-valve transistor. The island is described as two independent electron reservoirs related to the spin species $\sigma \in \{\uparrow,\downarrow\}$. The chemical potentials $\mu_{L,R}$ describe the applied bias voltage and $\Delta\mu = \mu_\uparrow - \mu_\downarrow$ determines the spin accumulation on the central electrode. The charge states N are tunable via gate voltage and ϵ_F denotes the Fermi energy.

The independent degrees of freedom governed by the master equations are the probabilities to find N electrons on the island,

$$P_N = \sum_\chi P_\chi \delta_{N,N_\chi}\,, \tag{4.5}$$

as well as the three components of the total island spin, or, equivalently, the magnitude and the direction of the island spin. The latter enter the right-hand side of the kinetic equations through the spin splitting $\Delta\mu \equiv \mu_\uparrow - \mu_\downarrow$ of the chemical potential, $S = \hbar\rho_I\Delta\mu/2$, and the angles α and β appearing in the tunnel matrix elements. We remark that, for a constant density of states on the island, the average chemical potential $\mu \equiv (\mu_\uparrow + \mu_\downarrow)/2$ does not depend on the amplitude of the accumulated spin S. For each independent degree of freedom we need one kinetic equation. These are provided by the master equations for the following operators A: the projector

$|N\rangle\langle N| = \sum_\chi |\chi\rangle\langle\chi|\delta_{N,N_\chi}$ on the state with total island charge N and the total island spin $\hat{\mathbf{S}} = (\hbar/2)\sum_{l\sigma\sigma'\nu} c^\dagger_{l\sigma\nu}\vec{\boldsymbol{\sigma}}_{\sigma\,\sigma'}c_{l\sigma'\nu}$, where $\vec{\boldsymbol{\sigma}}$ is the vector of Pauli spin matrices. The kinetic equations are given by

$$0 = \frac{\mathrm{d}}{\mathrm{d}t}P_N = \sum_{\chi\chi'}\delta_{N,N_\chi}W^{\chi\,\chi'}_{\chi\,\chi'}P_{\chi'} \tag{4.6}$$

$$0 = \frac{\mathrm{d}}{\mathrm{d}t}\langle\hat{\mathbf{S}}\rangle = \sum_{\chi_1\chi_2\chi'}\langle\chi_2|\,\hat{\mathbf{S}}\,|\chi_1\rangle\,W^{\chi_1\,\chi'}_{\chi_2\,\chi'}P_{\chi'}\,. \tag{4.7}$$

Introducing all the simplifications on the right-hand side, as discussed above, and making use of the notation $f^+_\sigma(\epsilon_l) = f(\epsilon_l - \mu_\sigma)$ and $f^-_\sigma(\epsilon_l) = 1 - f(\epsilon_l - \mu_\sigma)$ leads to

$$\begin{aligned}
0 = \frac{\mathrm{d}}{\mathrm{d}t}P_N &= \sum_{l\nu}W^{0\,0}_{0\,0}(l,\nu,N)f^-_\uparrow(\epsilon_l)f^-_\downarrow(\epsilon_l)P_N \\
&\quad+\sum_{l\nu\sigma}W^{\sigma\,0}_{\sigma\,0}(l,\nu,N-1)f^-_\uparrow(\epsilon_l)f^-_\downarrow(\epsilon_l)P_{N-1} \\
&\quad+\sum_{l\nu\sigma}W^{0\,\sigma}_{0\,\sigma}(l,\nu,N+1)f^+_\sigma(\epsilon_l)f^-_{\bar\sigma}(\epsilon_l)P_{N+1} \\
&\quad+\sum_{l\nu\sigma}W^{\sigma\,\sigma}_{\sigma\,\sigma}(l,\nu,N)f^+_\sigma(\epsilon_l)f^-_{\bar\sigma}(\epsilon_l)P_N \\
&\quad+\sum_{l\nu\sigma}W^{d\,\sigma}_{d\,\sigma}(l,\nu,N-1)f^+_\sigma(\epsilon_l)f^-_{\bar\sigma}(\epsilon_l)P_{N-1} \\
&\quad+\sum_{l\nu\sigma}W^{\sigma\,d}_{\sigma\,d}(l,\nu,N+1)f^+_\uparrow(\epsilon_l)f^+_\downarrow(\epsilon_l)P_{N+1} \\
&\quad+\sum_{l\nu}W^{d\,d}_{d\,d}(l,\nu,N)f^+_\uparrow(\epsilon_l)f^+_\downarrow(\epsilon_l)P_N\,,
\end{aligned} \tag{4.8}$$

for the probabilities P_N. For the z component of the island spin we obtain

$$\begin{aligned}
0 = \frac{\mathrm{d}}{\mathrm{d}t}\langle S_z\rangle &= \hbar\sum_{Nl\nu\sigma}\sigma W^{\sigma\,0}_{\sigma\,0}(l,\nu,N)f^-_\uparrow(\epsilon_l)f^-_\downarrow(\epsilon_l)P_N \\
&\quad+\hbar\sum_{Nl\nu\sigma}\sigma W^{\sigma\,\sigma}_{\sigma\,\sigma}(l,\nu,N)f^+_\sigma(\epsilon_l)f^-_{\bar\sigma}(\epsilon_l)P_N \\
&\quad+\hbar\sum_{Nl\nu\sigma}\sigma W^{\sigma\,d}_{\sigma\,d}(l,\nu,N)f^+_\uparrow(\epsilon_l)f^+_\downarrow(\epsilon_l)P_N,
\end{aligned} \tag{4.9}$$

where σ contributes to sums with a $+$ sign for $\sigma =\uparrow$ and a $-$ sign for $\sigma =\downarrow$. The kinetic equations for the $x-$ and y-components of the island spin, expressed by the raising and lowering operators $\langle\mathbf{S}^\pm\rangle = \langle\mathbf{S}_x \pm i\mathbf{S}_y\rangle$, are

$$\begin{aligned}
0 = \frac{\mathrm{d}}{\mathrm{d}t}\langle\mathbf{S}^+\rangle &= \hbar\sum_{Nl\nu}W^{\downarrow\,0}_{\uparrow\,0}(l,\nu,N)f^-_\uparrow(\epsilon_l)f^-_\downarrow(\epsilon_l)P_N \\
&+\hbar\sum_{Nl\nu\sigma}W^{\downarrow\,\sigma}_{\uparrow\,\sigma}(l,\nu,N)f^+_\sigma(\epsilon_l)f^-_{\bar\sigma}(\epsilon_l)P_N \\
&+\hbar\sum_{Nl\nu}W^{\downarrow\,d}_{\uparrow\,d}(l,\nu,N)f^+_\uparrow(\epsilon_l)f^+_\downarrow(\epsilon_l)P_N,
\end{aligned} \tag{4.10}$$

and the kinetic equation for $\langle \mathbf{S}^{-} \rangle$ is the same but with the replacement of $W^{\downarrow\psi}_{\uparrow\psi}(l,\nu,N)$ by $W^{\uparrow\psi}_{\downarrow\psi}(l,\nu,N)$ on the right-hand side.

The explicit values of $W^{\psi_1\psi}_{\psi_2\psi}(l,\nu,N)$ are given in Appendix A. We plug them in and replace the summation over the island levels l by an integration over an energy ω, multiplied by the island density of states of the given spin ρ_I^σ. In this thesis, we assume the central electrode of the single-electron spin-valve transistor to be nonmagnetic, hence the density of states is spin independent, $\rho_I^\sigma = \rho_I/2$. The occurring integrals can be carried out and we finally get the following master equations:

$$\begin{aligned} \frac{\mathrm{d}}{\mathrm{d}t}P_N &= \pi \sum_{r\sigma} \left[\alpha^{+}_{r\sigma}(\Delta_{N-1})P_{N-1} + \alpha^{-}_{r\sigma}(\Delta_N)P_{N+1}\right. \\ &\qquad \left. -\alpha^{+}_{r\sigma}(\Delta_N)P_N - \alpha^{-}_{r\sigma}(\Delta_{N-1})P_N\right], \qquad (4.11) \\ \frac{\mathrm{d}}{\mathrm{d}t}\langle S_z\rangle &= \pi\hbar \sum_{Nr\sigma} \sigma \left[\alpha^{+}_{r\sigma}(\Delta_N) - \alpha^{-}_{r\sigma}(\Delta_{N-1})\right] P_N. \qquad (4.12) \end{aligned}$$

Here, we used the definition of the island rate functions

$$\alpha^{\pm}_{r\sigma}(E) := \pm\alpha^0_{r\sigma}\, \frac{E-(\mu_r-\mu_\sigma)}{\exp\left[\pm\frac{E-(\mu_r-\mu_\sigma)}{k_BT}\right]-1}, \qquad (4.13)$$

where $\alpha^0_{r\sigma} = \frac{\rho_I N_c}{2\pi\hbar}\Gamma^r_\sigma$ is the dimensionless conductance of lead r for island spin σ, N_c the number of transverse channels, and E is the energy of the tunneling electron. The equations (4.11) are linearly dependent. Hence, to solve the kinetic equations we need an additional equation that is provided by the normalization condition $\sum_N P_N = 1$. For collinear single-electron spin-valve transistors ($\phi \in \{0,\pi\}$), the spin accumulation naturally points in a direction parallel to the lead magnetization directions $\hat{\mathbf{n}}_r$, this directly defines the angles α and β. Therefore, the Eqs. (4.11)-(4.12) are sufficient to describe such a system but not the noncollinear case.

In the derivation of Eqs. (4.9)-(4.12), we have used a specific coordinate system for the spin. In the chosen coordinate system, the x and y components of $\mathbf{S}$ vanish. The final version of the kinetic equations for the spin can, however, be written in a coordinate-free representation. First, we proceed in a manner analogous to the paragraph above, i.e., the kernels are plugged in and the summation over l is replaced by an integration over energy ω. Starting from the master equations of $\langle \mathbf{S}^{\pm}\rangle$, see Eq. (4.10), and by using the kinetic equation of $\langle S_z\rangle$, see Eq. (4.12), one finally obtains the following coordinate-free representation of the master equation for the island spin $\mathbf{S}$:

$$\frac{\mathrm{d}\langle\mathbf{S}\rangle}{\mathrm{d}t} = \left(\frac{\mathrm{d}\langle\mathbf{S}\rangle}{\mathrm{d}t}\right)_{\mathrm{acc}} + \left(\frac{\mathrm{d}\langle\mathbf{S}\rangle}{\mathrm{d}t}\right)_{\mathrm{rel}} + \left(\frac{\mathrm{d}\langle\mathbf{S}\rangle}{\mathrm{d}t}\right)_{\mathrm{rot}}. \qquad (4.14)$$

Accumulation, relaxation, and rotation processes determine the time evolution of $\mathbf{S}$. The contribution, which builds up an average spin, reads

$$\left(\frac{\mathrm{d}\,\langle\mathbf{S}\rangle}{\mathrm{d}t}\right)_{\mathrm{acc}} = \frac{\pi\hbar}{2}\sum_{Nr\sigma} p_r \frac{\Gamma_r}{\Gamma^r_\sigma}\left[\hat{\mathbf{n}}_r + (\hat{\mathbf{n}}_r\cdot\hat{\mathbf{n}}_S)\hat{\mathbf{n}}_S\right]\left[\alpha^{-}_{r\sigma}(\Delta_{N-1}) - \alpha^{+}_{r\sigma}(\Delta_N)\right]P_N. \qquad (4.15)$$

Transitions to a charge state N by tunneling of electrons from the leads onto the island and vice versa are described by this term and lead to a polarization of the island. On the one hand, tunneling processes of both leads r accumulate a spin in the direction of the respective polarization $\hat{\mathbf{n}}_r$. But on the other hand, due to the macroscopic spin of the central electrode, there is an additional accumulation contribution in the direction of $\mathbf{S}$. In equilibrium ($V = 0$), there is no current flowing through the central electrode and the equation above becomes $\left(\frac{\mathrm{d}\mathbf{S}}{\mathrm{d}t}\right)_{\mathrm{acc}} = 0$. Hence, without any applied bias voltage, there is no spin accumulated on the island, i.e. $\mathbf{S} = 0$. In contrast to the accumulation contribution, the relaxation term

$$\left(\frac{\mathrm{d}\langle\mathbf{S}\rangle}{\mathrm{d}t}\right)_{\mathrm{rel}} = -\sum_{Nr\nu} P_N \int \mathrm{d}\omega\, \Gamma_r\, \mathbf{s}(\omega) \left[f_r^-(\omega + \Delta_{N-1}) - f_r^+(\omega + \Delta_N)\right], \quad (4.16)$$

causes a decay of the island spin, which is characterized by $\mathbf{s}(\omega)$. The vector

$$\mathbf{s}(\omega) = \frac{\hbar\rho_I}{2}[f_\uparrow(\omega) - f_\downarrow(\omega)]\hat{\mathbf{n}}_S \quad (4.17)$$

corresponds to the energy-dependent spin density in the central electrode. The influence of the exchange field between ferromagnetic lead r and island is represented by the third contribution of Eq. (4.14):

$$\left(\frac{\mathrm{d}\langle\mathbf{S}\rangle}{\mathrm{d}t}\right)_{\mathrm{rot}} = -\frac{g\mu_B}{\hbar}\sum_r \int \mathrm{d}\omega\, \mathbf{s}(\omega) \times \mathbf{B}^r_{\mathrm{exc}}(\omega). \quad (4.18)$$

Here, we used the dimensionless magnetic moment of electrons g, the Bohr magneton μ_B, and the definition of the exchange field between island and lead r:

$$\mathbf{B}^r_{\mathrm{exc}}(\omega) = \frac{p_r\Gamma_r N_c}{2\pi g\mu_B}\,\hat{\mathbf{n}}_r \sum_N P_N \int' \mathrm{d}\omega' \left[\frac{f_r^-(\omega')}{\omega' - \omega - \Delta_N} + \frac{f_r^+(\omega')}{\omega' - \omega - \Delta_{N-1}}\right], \quad (4.19)$$

where the prime at the integral denotes a principal value integral. The exchange field can be interpreted as a many-body interaction effect. In the limit of noninteracting island electrons ($E_C = 0$) it vanishes independent of gate voltage. The contributions $\mathbf{B}^r_{\mathrm{exc}}(\omega)$ act on the spin like an applied external magnetic field, which points in the polarization direction of lead r. This results in a precession of the accumulated spin out of the ($\hat{\mathbf{n}}_L$,$\hat{\mathbf{n}}_R$) plane. Equation (4.19) is similar to the expression of an exchange field existent between a single-level quantum dot and ferromagnetic leads, which was first introduced by Braun *et al.* in the context of a quantum-dot spin valve, see Eq. (2.17) in subsection 2.4.5.[34] But in contrast to the quantum-dot spin valve, there is a net spin accumulated on the island in all possible charge states P_N. Hence the total exchange field is a composition of all charge-state contributions. Additionally, the integration over ω in Eq. (4.18) results from the continuous density of island states.

Having derived the kinetic equations for P_N and $\langle\mathbf{S}\rangle$, the stationary charge current through lead r may be calculated. We start from the already introduced current formula $I_r = \sum_{\chi\chi'} \left(W^{I_r}\right)^{\chi\,\chi'}_{\chi\,\chi'} P_{\chi'}$. This expression was derived in the context of the

diagrammatic real-time technique in subsection 3.2.6. Executing the same procedure as in the previous considerations of the master equations one gets

$$I_r = e\pi \sum_{N\sigma} \left[\alpha^+_{r\sigma}(\Delta_N) - \alpha^-_{r\sigma}(\Delta_{N-1})\right] P_N \,. \tag{4.20}$$

5 Current and Spin Dynamics

Based on the kinetic equations that were derived in chapter 4, we now investigate the transport of electrons through the single-electron spin valve transistor. For this, we calculate the accumulated spin $\mathbf{S}$ and the electric current I as a function of the system parameters such as gate voltage V_G, bias voltage V, angle ϕ between source and drain's magnetization direction, and the degree of polarization p. The present chapter is separated into two parts discussing both the linear and the nonlinear regimes. An explicit focus in the discussion is put on the influence of the exchange field on the transport characteristics. Most of the results presented in this chapter have previously been published in Ref. [1].

5.1 Linear-Response Regime

We start by considering the single-electron spin-valve transistor in the linear-response regime ($eV \ll k_BT, E_C$). All quantities are periodic in the gate voltage V_G with periodicity e/C_G. For low temperatures, at most two charge states N_0 and N_0+1 have a non-vanishing occupation probability. The presented analytic formulas for the linear-response regime are derived for this limit. With increasing temperature, more charge states may become occupied. The results plotted in the figures are always calculated taking into account all relevant charge states.

To describe the linear-response regime, the system of master equations, see Eqs. (4.11) and (4.14), is expanded up to first order in the transport voltage V. The term associated with rotation of the accumulated island spin simplifies to

$$\left(\frac{\mathrm{d}\langle\mathbf{S}\rangle}{\mathrm{d}t}\right)^{\mathrm{lin}}_{\mathrm{rot}} = \frac{g\mu_B}{\hbar}\langle\mathbf{S}\rangle \times \mathbf{B}^{\mathrm{lin}}_{\mathrm{exc}} \,, \tag{5.1}$$

where we used the expression of the exchange field in linear response

$$\mathbf{B}^{\mathrm{lin}}_{\mathrm{exc}} = \sum_r \int \mathrm{d}\omega \; f'(\omega)\; \mathbf{B}^r_{\mathrm{exc}}(\omega)|_{V=0} \;. \tag{5.2}$$

The magnitude $B^{\mathrm{lin}}_{\mathrm{exc}} = |\mathbf{B}^{\mathrm{lin}}_{\mathrm{exc}}|$ is plotted for different angles ϕ as a function of the gate voltage in *Fig. 5.1*. The exchange field vanishes at the symmetry point between two resonances (middle of Coulomb valley), i.e., at integer values of C_GV_G/e, in accordance to the case of the quantum-dot spin valve. At half-integer values of C_GV_G/e, where the two charge states N_0 and N_0+1 are degenerate ($\Delta_{N_0} = 0$), the exchange field vanishes due to a cancellation of the N_0 and N_0+1 contributions of $\mathbf{B}^r_{\mathrm{exc}}(\omega)$. This is in contrast to the case of a quantum-dot spin valve, where the exchange field is

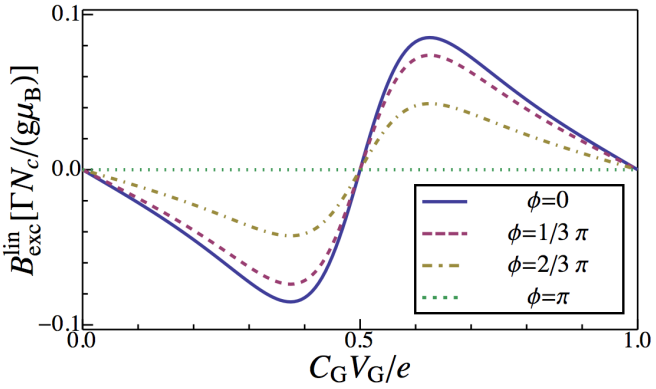

Figure 5.1: Magnitude of exchange field in linear response as a function of applied gate voltage for different angles between the lead polarization directions. Parameters $p_L = p_R = 0.3$, $\Gamma_L = \Gamma_R = \Gamma/2$, and $E_C = 10 k_B T$ were chosen.

maximal at the resonance position for transport. To understand this difference we consider the resonance between charge state 0 (empty dot) and 1 (singly occupied dot) of the single-level quantum dot. Here, the symmetry is broken due to the fact that on the one hand the state 1 can be virtually excited to the doubly-occupied state 2 but on the other hand there is no corresponding virtual excitation of the state 0 in a lower charge state. Hence the different contributions do not cancel each other.

In the following, we assume symmetric polarizations ($p_L = p_R = p$) and tunnel-coupling strengths ($\Gamma_L = \Gamma_R = \Gamma/2$). In this case, the total exchange field points in the $\hat{\mathbf{n}}_L + \hat{\mathbf{n}}_R$-direction and rotates the spin out of the ($\hat{\mathbf{n}}_L$,$\hat{\mathbf{n}}_R$) plane, see *Fig. 5.2*. The

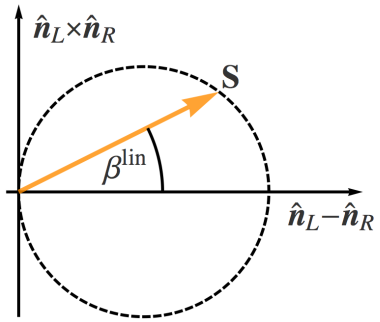

Figure 5.2: Scheme of accumulated spin **S** in linear-response regime. The spin precesses within a plane defined by $\hat{\mathbf{n}}_L - \hat{\mathbf{n}}_R$ and $\hat{\mathbf{n}}_L \times \hat{\mathbf{n}}_R$. The spin precession is accompanied by a decreased magnitude of accumulated spin.

island spin **S** acquires a component perpendicular to the ($\hat{\mathbf{n}}_L$,$\hat{\mathbf{n}}_R$) plane. We obtain $\alpha^{\rm lin} = 0$ and

$$\beta^{\rm lin}(\phi) = -\arctan\left(\frac{4 g \mu_B k_B T}{\Gamma N_c \Delta_{N_0}} B^{\rm lin}_{\rm exc}(\phi) \sinh\frac{\Delta_{N_0}}{k_B T}\right). \tag{5.3}$$

In *Fig. 5.3*(a), the rotation angle is plotted as a function of the gate voltage. Sign changes appear both at integer and at half-integer values of $C_G V_G/e$, which reflects the sign change of the exchange field at these positions. Away from these points, the angle $\beta^{\rm lin}$ is finite. Close to but not exactly at integer values of $C_G V_G/e$ and at low temperatures ($E_C \approx 10 k_B T$), the angle approaches $\pm\pi/2$. There, a small variation V_G induces a strong reorientation of the spin **S**, as illustrated by the insets of *Fig. 5.3*(a). This high sensitivity can be quantified by the slope of $\beta^{\rm lin}$ with respect to V_G. For low temperature ($k_B T \ll E_C$), we find that the slope is proportional to

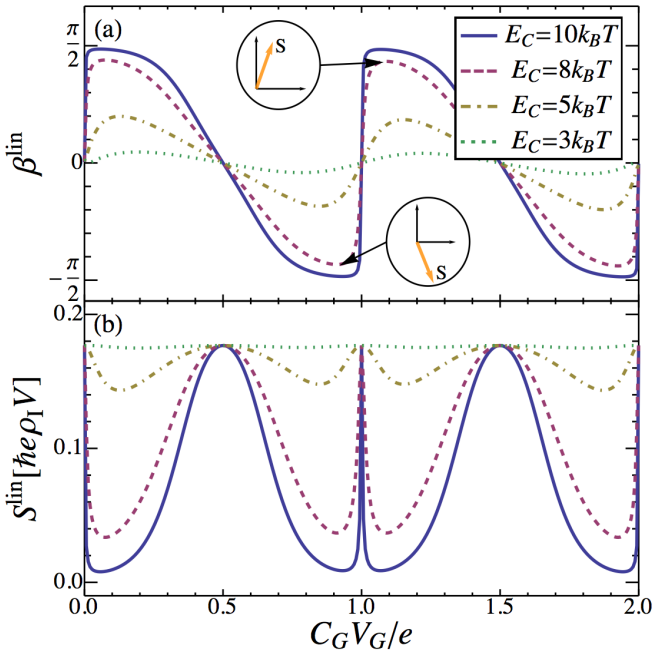

Figure 5.3: (a) Angle $\beta^{\rm lin}$ and (b) spin accumulation $S^{\rm lin}$ for different temperatures as a function of gate voltage. The chosen parameters are $p_L = p_R = 0.5$, $\Gamma_L = \Gamma_R = \Gamma/2$, and $\phi = \pi/2$.

$k_BTp\cos\frac{\phi}{2}\exp(E_C/k_BT)/E_C^2$, which increases exponentially with decreasing temperature. As a consequence, the gate-voltage range close to integer values of C_GV_G/e is ideal for manipulating the direction of the island spin.

The absolute value S, which is determined by the accumulation and relaxation term of the spin master equation reads

$$S^{\rm lin}(\phi) = \frac{\hbar\rho_I e}{2} Vp \sin\frac{\phi}{2}\cos\beta^{\rm lin}(\phi). \tag{5.4}$$

It is proportional to the cosine of $\beta^{\rm lin}$, hence the magnitude decreases with increasing angle $\beta^{\rm lin}$ and vanishes for $\beta^{\rm lin} = \pm\pi/2$, see Fig. 5.2. Thus, the effect of the exchange field is not just an rotation of $\mathbf{S}$ but also a reduction of its magnitude S. In Fig. 5.3(b), $S^{\rm lin}(\pi/2)$ is plotted for various temperatures. We see that for $E_C \lesssim 3k_BT$ the structure is smeared out and the absolute value of spin is nearly constant due to a suppression of the Coulomb blockade.

After considering the accumulated spin, we now analyze the linear conductance $G^{\rm lin} = (\partial I/\partial V)|_{V=0}$ of the single-electron spin-valve transistor. The conductance, normalized to the conductance of a single-electron spin-valve transistor with parallel lead magnetizations $G^{\rm lin}(0) = e^2N_c\rho_I\Gamma\Delta_{N_0}/(8k_BT\sinh\frac{\Delta_{N_0}}{k_BT})$, can be expressed in terms of the rotation angle $\beta^{\rm lin}(\phi)$ as

$$\frac{G^{\rm lin}(\phi)}{G^{\rm lin}(0)} = 1 - \frac{p^2\sin^2\frac{\phi}{2}}{1+\tan^2\beta^{\rm lin}(\phi)}\,. \tag{5.5}$$

In *Fig. 5.4* (a), the conductance $G^{\rm lin}(\phi = \pi/2)$ is plotted as a function of gate voltage. Since it is an even function of charging energy Δ_{N_0}, the conductance is symmetric

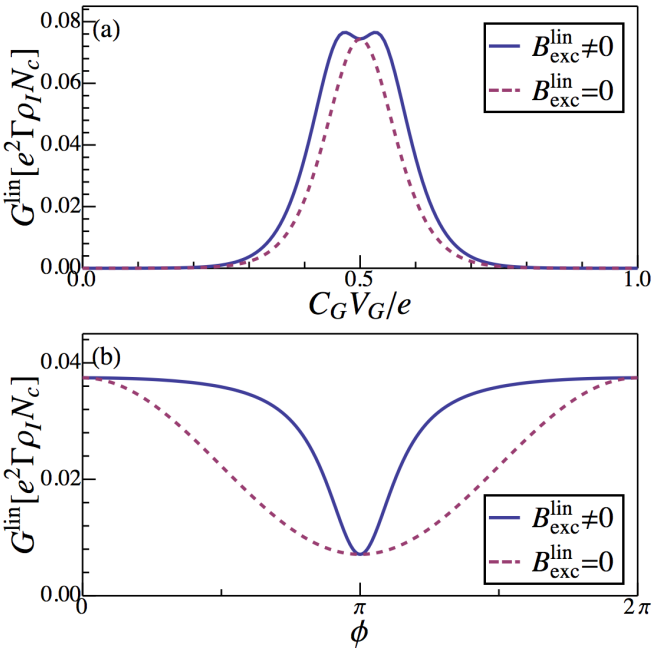

Figure 5.4: Linear conductance in units of $e^2\Gamma\rho_I N_c$ with (solid) and without (dashed) the effect of the exchange field: (a) V_G-dependence in case of $\phi = \pi/2$ and (b) ϕ-dependence with applied gate voltage $C_G V_G = 4e/10$. For both plots the parameters $p_L = p_R = 0.9$, $\Gamma_L = \Gamma_R = \Gamma/2$, and $E_C = 15 k_B T$ were chosen.

with respect to the resonance points, given by half-integer values of $C_G V_G/e$. Away from the resonances, the conductance is suppressed due to Coulomb blockade. The difference between the solid and dashed lines illustrates the influence of the exchange field. The dashed lines are obtained by manually setting $B^{\rm lin}_{\rm exc}$ to zero. The exchange field rotates the accumulated spin out of its blocking position. Hence, it increases the conductance of the single-electron spin-valve transistor except for the symmetry point at resonance. As a consequence, for high polarizations, $p \gtrsim 0.9$, the maximum at resonance can even turn into a local minimum.

Consideration of the conductance as a function of the magnetization angle ϕ, see *Fig. 5.4* (b), shows that the exchange field reduces the spin-valve effect. We emphasize that, though the solid and dashed lines coincide for $\phi \in \{0, \pi, 2\pi\}$, the exchange field does not vanish in all of these points. In fact, it points parallel to the accumulated spin and, therefore, $\mathbf{B}^{\rm lin}_{\rm exc}$ does not rotate $\mathbf{S}$ out of the ($\hat{\mathbf{n}}_L$,$\hat{\mathbf{n}}_R$)-plane.

5.1.1 Conclusion of the Results in the Linear-Response Regime

Finally, we want to conclude the main results concerning the electronic transport through the single-electron spin-valve transistor in the linear-response regime. We found that the exchange field weakens the spin-valve effect and increases the linear conductance through the system. It rotates the accumulated island spin out of the plane that is defined by the polarization directions of the two ferromagnetic leads and reduces the absolute value of $\mathbf{S}$. Furthermore, the exchange field leads to a high orientation sensitivity of the accumulated spin on variation of the applied gate voltage, which is convenient for a controlled manipulation of $\mathbf{S}$.

5.2 Nonlinear-Response Regime

We now turn to the nonlinear-response regime, $eV \gtrsim k_B T, E_C$. The transport voltage V is symmetrically applied to both leads, i.e., the chemical potentials are $\mu_L = eV/2$ and $\mu_R = -eV/2$. We start by considering metallic islands that are symmetrically tunnel coupled to the ferromagnetic leads ($\Gamma_L = \Gamma_R$). Besides the current-voltage characteristics of the single-electron spin-valve transistor, additionally, the spin dynamics and the magnetoresistance of the system are discussed. Furthermore, the second derivative of the current with respect to the bias voltage is introduced as a tool to identify different transport processes. Finally, the impact of asymmetric tunnel-coupling strengths on transport are considered with an explicit focus on the the influence of the exchange field.

5.2.1 Current-Voltage Characteristics and Island Spin

The current through the single-electron spin-valve transistor as a function of bias voltage for different polarizations p is shown in *Fig. 5.5*(a). Here, the angle between the

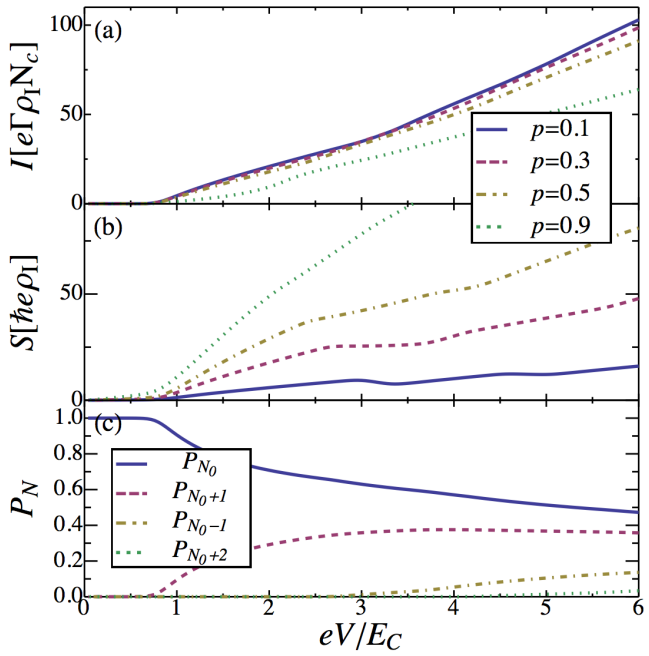

Figure 5.5: (a) Current I through single-electron spin-valve transistor in units of $e\Gamma\rho_I N_c$ for different polarizations p, (b) the corresponding island spin accumulation S, and (c) the relevant occupation probabilities P_N in the case $p = 0.3$. For all three plots, the parameters $p_L = p_R = p$, $\Gamma_L = \Gamma_R = \Gamma/2$, $\phi = \pi/2$, $C_G V_G = 3e/10$, and $E_C = 50 k_B T$ were chosen.

lead magnetizations is chosen to be $\phi = \pi/2$. Due to the larger spin accumulation for higher lead polarizations, the current reduces with increasing p. At low bias voltages, the transport through the system is blocked until eV exceeds the Coulomb blockade threshold $2\Delta_{N_0}$ and both spin reservoirs of the next charging state $(N_0 + 1)$ enter the transport window. We introduce the notation $E_{N;\sigma}$ for the excitation energy of the σ channel of charge state N. From this definition it follows that $E_{N_0+1;\sigma} = 2\Delta_{N_0}$. By further increasing of the source-drain voltage, more and more levels of the continuous spectrum contribute to transport, and the current increases continuously (in contrast

to a stepwise increase for islands with a discrete level spectrum). We note that we assumed here symmetric tunnel couplings, $\Gamma_L = \Gamma_R = \Gamma/2$. By an asymmetric choice of the tunnel couplings, the Coulomb step at $eV = 2\Delta_{N_0}$ and also the steps of the other charging states that enter for higher V can be made much more pronounced.[4,5] This effect and further implications of asymmetric tunnel couplings on transport through single-electron spin-valve transistors will be discussed in detail in subsection 5.2.4. In *Fig. 5.5*(c), the corresponding occupation probabilities of the relevant charging states ($N \in \{N_0 - 2, N_0 - 1, N_0, N_0 + 1\}$) are plotted as a function of the bias voltage (for $p = 0.3$). The probability to find the island in a given charge state N decreases for states with higher excitation energies. In general, the voltage that is necessary to excite the island state (N, σ) is determined by the equation $eV = |2\Delta_N + \sigma\Delta\mu(V)|$. Here, $\Delta\mu(V)$ is the island level splitting for the respective bias voltage and σ contributes with a factor +1 for the $\uparrow$ reservoir and -1 for the $\downarrow$ reservoir. It is proportional to the spin accumulation $S(\phi)$, which is plotted in *Fig. 5.5* (b). By means of $\Delta\mu(V)$ the transition voltages can be determined self consistently. We emphasize that due to a finite island spin accumulation, either the spin $\uparrow$- or spin $\downarrow$ reservoir enters the transport window at the transition voltages of the occupation probabilities, see *Fig. 4.1*.

An analysis of the bias-voltage dependence of the island spin, see *Fig. 5.5* (b), yields that S can be decomposed into two components, an oscillating one and a component that monotonously increases.[100,101] Since the former is suppressed for higher p, let us consider the graph of $p = 0.1$ to explain this behavior. Our theory describes sequential tunneling, hence in the Coulomb-blockade regime, spin accumulation is exponentially suppressed. For $eV > 2\Delta_{N_0}$, both spin reservoirs of the charging state N_0+1 contribute to transport and S increases with increasing V until the $\uparrow$ reservoir of charging state $N_0 - 1$ enters the transport window. Now, there is an additional channel for the $\uparrow$ electrons to leave the island and S decreases until the corresponding $\downarrow$ reservoir is reached. Subsequently, the spin accumulation increases until $\downarrow$ electrons can tunnel into charging state $N_0 + 2$. A reduction of S follows, then the state $\uparrow, N_0 + 2$ can be occupied and the spin accumulation increases again. By further increasing of V this processes of depletion and filling repeat. To understand the reduced influence of the oscillating component for higher p, we first assume antiparallely polarized leads $\phi = \pi$. In this case, the tunneling rates of the processes, which lead to a decrease of S, are proportional to $1 - p$, hence they occur less for higher p. Since there is a more complex but similar behavior of the tunneling rates for finite noncollinear angles ϕ, we can conclude that, in general, the oscillations are weaker for higher polarizations.

5.2.2 Tunnel Magnetoresistance

The finite spin accumulation on the island results in a nonzero TMR. Due to the noncollinear system we define an angular-dependent magnetoresistance:

$$\mathrm{TMR}(\phi) = \frac{I(0) - I(\phi)}{I(0)}, \tag{5.6}$$

with $I(\phi)$ being the current through the single-electron spin-valve transistor in which the magnetization directions of the leads enclose the angle ϕ. In *Fig. 5.6*, the bias-

and gate-voltage dependence of the TMR is plotted for different polarizations and an angle $\phi = \pi/2$. In both cases, the TMR shows an oscillatory behavior originating

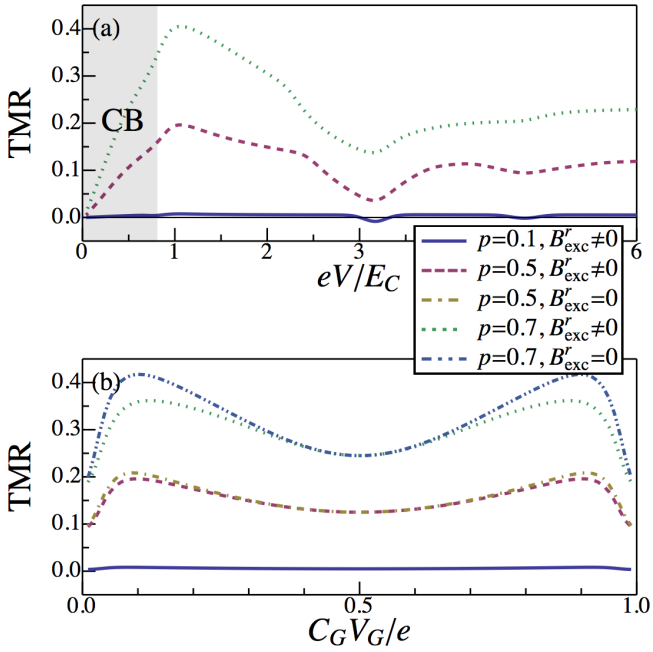

Figure 5.6: TMR of a non-collinear setup ($\phi = \pi/2$) for different polarizations p. Plot (a) shows the bias dependence for $C_GV_G = 3e/10$ and (b) the gate dependence for $eV = 2E_C$. The dashed-dotted lines represent the cases where the exchange field is manually set to $\mathbf{B}^r_{\text{exc}} = 0$. For both plots, the remaining parameters were chosen to be $p_L = p_R = p$, $\Gamma_L = \Gamma_R = \Gamma/2$, and $E_C = 50k_BT$.

from the bias/gate dependence of the spin accumulation.[102–106] Naturally, the magnetoresistance is more pronounced for higher p. For lower polarizations, we observe sign changes of TMR caused by the oscillating spin accumulation.[100] We want to emphasize that for obtaining reliable results in the Coulomb-blockade regime [marked by the grey area in *Fig. 5.6*(a)], one has to take cotunneling processes into account, which we neglect in our theory. Next, we focus on the analysis of the influence of the exchange field on the TMR, which is illustrated by the dashed-dotted lines in *Fig. 5.6*(b). To obtain the lines representing the case of an absent exchange field, we manually set $\mathbf{B}^r_{\text{exc}} = 0$ in Eq. (4.14). For gate voltages representing a vanishing exchange field ($C_GV_G/e \in \{0, 1/2, 1\}$), naturally, the two graphs coincide. Comparison of the TMR gate dependence for different polarizations shows, that the exchange field has a stronger effect for higher p. By affecting the accumulated spin the exchange field decreases the TMR.

5.2.3 Second Derivative of the Current-Voltage Characteristics

In order to identify the threshold voltages at which new transport channels open, it is convenient to study the second derivative of the current $\partial^2 I/\partial V^2$, see *Fig. 5.7*. The positions of the peaks directly represent the already discussed excitation energies of the relevant charging states. All charging states induce two peaks, one for each spin channel $(\uparrow, \downarrow)$. An exception is the first peak $(N_0 + 1)$, which does not split into two due to the exponentially suppressed spin accumulation at the relevant voltage, see *Fig. 5.5*(b). The vertical lines in the figure mark the voltages at which the charge

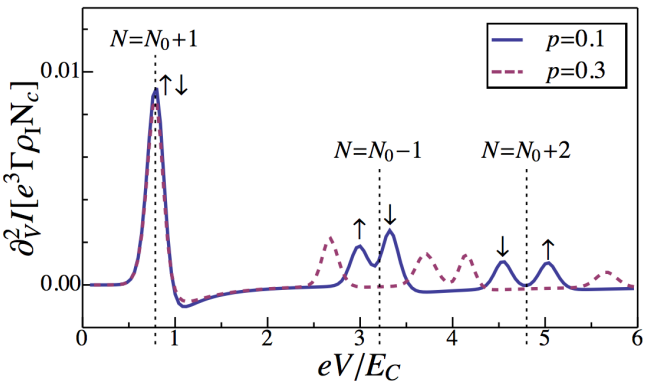

Figure 5.7: Second derivative of the current $\partial^2 I/\partial V^2$ in units of $e^3\Gamma\rho_I N_c$ for two different polarizations p and $\phi = \pi/2$. The excitation energies of the charge/spin states represented by the peaks strongly depend on the lead polarization p. Parameters $p_L = p_R = p$, $\Gamma_L = \Gamma_R = \Gamma/2$, $C_G V_G = 3e/10$, and $E_C = 50 k_B T$ were chosen.

states ($N \in \{N_0 - 1, N_0 + 1, N_0 + 2\}$) would enter the transport window if one neglects spin accumulation. Due to the fact that the accumulated island spin strongly depends on the lead polarizations, the excitation energies $E_{N;\sigma}$ are also sensitive to a variation of p, see *Fig. 5.8*. The described behavior suggests that in experiments, a measurement of $\partial^2 I/\partial V^2$ as a function of bias voltage can be used as a convenient tool to determine the spin splitting of the chemical potential on the island and, thus, the degree of polarization of the leads.

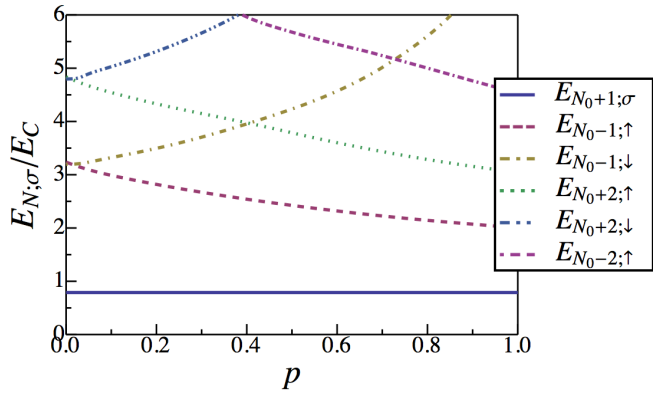

Figure 5.8: Polarization dependence of the excitation energies $E_{N;\sigma}$ normalized to E_C. The chosen parameters are $p_L = p_R = p$, $\phi = \pi/2$, $\Gamma_L = \Gamma_R = \Gamma/2$, $C_G V_G = 3e/10$, and $E_C = 50 k_B T$.

5.2.4 Asymmetric Tunnel Couplings

In the present paragraph, we explicitly want to consider the impact of asymmetric tunnel-coupling strengths on the current-voltage characteristics of a single-electron spin-valve transistor. For this purpose, we define the ratio of tunnel-coupling strength $a \equiv \Gamma_L/\Gamma_R$, which is a measure for the asymmetry of the junction resistances. In *Fig. 5.9*, the current of the antiparallel setup ($\phi = \pi$) is plotted as a function of the applied bias voltage for different asymmetries. Due to reasons of comparability

each current graph is normalized to its respective value at a fixed bias voltage that is arbitrarily chosen to be $V = 18E_C/e$, i.e., the normalized current is defined as $I_{\mathrm{norm}}(V) \equiv I(V)/I(18E_C/e)$. The solid line that represents the strongly asymmetric coupling (a=40) shows well developed Coulomb-charging steps. The characteristic staircases are suppressed for lower asymmetries, which are represented by the dashed (a=10) and dot-dashed (a=1) lines. To explain the origin of this behavior, we compare the island occupation probabilities of the strongly asymmetric system and the transistor with symmetric tunnel-coupling strengths, see *Fig. 5.10*. The symmetrically applied bias voltage drives the electrons from the left to the right lead through the system. We start by analyzing the strongly asymmetric setup (a=40), see *Fig. 5.10*(a). Due to the asymmetric coupling the resistance of the left tunnel junction is much smaller than

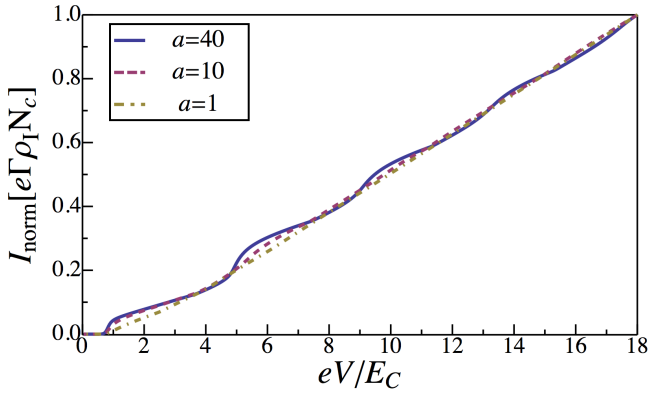

Figure 5.9: Current-voltage characteristics of the single-electron spin-valve transistor for different coupling asymmetries a. The chosen parameters are $C_G V_G = 3e/10$, $p_L = p_R = 3/10$, $\phi = \pi$, and $E_C = 50k_BT$. For clarity, the current is normalized as explained in the text.

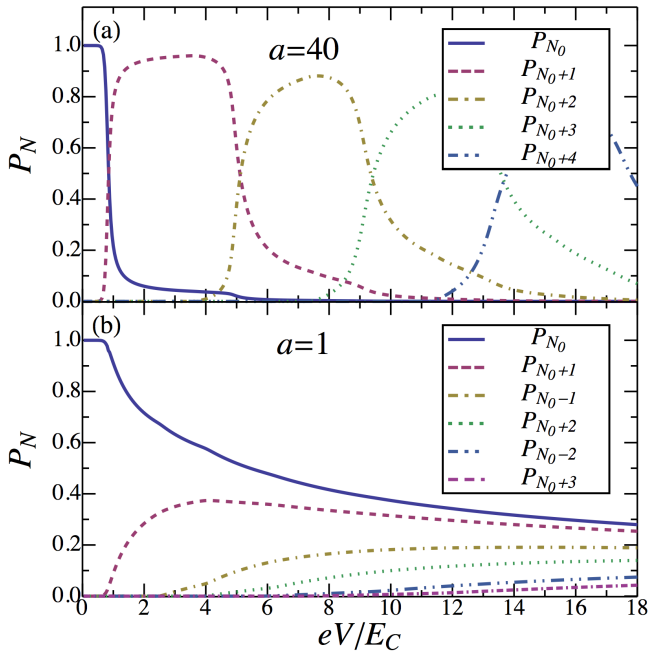

Figure 5.10: Occupation probabilities of the island charge states for (a) strongly asymmetric (a=40) and (b) symmetric (a=1) tunnel-coupling strengths. The other parameters are chosen as in *Fig. 5.9*.

that of the right junction and transport through the island is limited by Γ_R. With increasing voltage the central electrode fills up with electrons when additional charge states can be occupied. Each step in the current-voltage characteristics corresponds to one peak of the discrete excitation-energy spectrum of the island charging states, see section 2.2. Although the charge states $N_0 - 1$, $N_0 - 2$, and $N_0 - 3$ are energetically allowed in the considered bias voltage interval, the respective occupation probabilities are strongly suppressed. The system tends to occupy the highest allowed charging state. Due to the reducing amplitude of each P_N for increasing N the respective Coulomb steps are less pronounced. In contrast to the asymmetric system tunneling out of the island is not suppressed in the symmetric setup (a=1), see *Fig. 5.10*(b). In this case, the magnitude of the occupation probabilities does not increase stepwise but continuously. This results in a continuous increase of the current through the system.

In the previous discussion of the present paragraph, we considered single-electron spin-valve transistors containing leads that exhibit relatively low polarizations of 30%. By using higher polarized systems ($p > 60\%$), further transport features can be observed for systems with strongly asymmetric tunnel-coupling strengths ($a > 30$), see *Fig. 5.11*. In *Fig. 5.11*(a) the I-V curve of a noncollinear setup ($\phi = \pi/2$) is plotted. The dashed curve represents the artificial case of an absent exchange field and serves

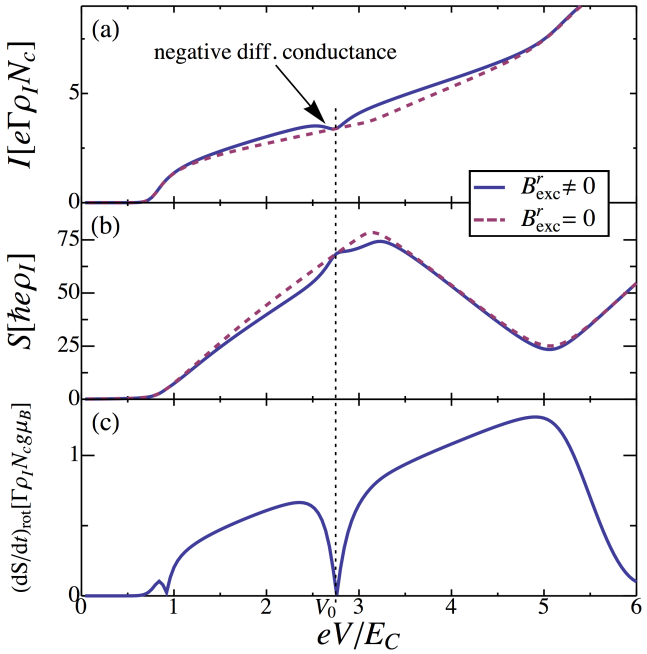

Figure 5.11: Transport characteristics of an asymmetrically coupled single-electron spin-valve transistor: (a) current and (b) island spin accumulation are plotted with (solid) and without (dashed) the effect of the exchange field. The rotation contribution of the island spins kinetic equation is shown in (c). For all three plots, the parameters are chosen to be $a = 40$, $C_G V_G = 3e/10$, $p_L = p_R = 8/10$, $\phi = \pi/2$, and $E_C = 50 k_B T$.

as a comparison to identify the effects of the field. This graph is obtained by manually setting B^r_{exc} to zero. We consider the current in a bias-voltage regime between two Coulomb steps. Analog to the linear response regime, the exchange field increases the current that is flowing through the system. However, there is a dip in the current that results in a regime of negative differential conductance. A comparison of the

solid and dashed lines yields that for a certain bias voltage V_0 the exchange field does not affect transport through the system. The two graphs coincide. In general, the enhancement of the current is accompanied by a reduction of the spin accumulation on the island, see *Fig. 5.9*(b). As the current does, also the spin accumulation graph shows an additional steplike feature and it is also unaffected by the exchange field at V_0. To understand this transport behavior of the system, we perform an analysis of the rotation contribution of the kinetic spin equation

$$\left(\frac{\mathrm{d}\langle \mathbf{S}\rangle}{\mathrm{d}t}\right)_{\mathrm{rot}} = -\frac{g\mu_B}{\hbar}\sum_r \int \mathrm{d}\omega\, \mathbf{s}(\omega)\times \mathbf{B}^r_{\mathrm{exc}}(\omega), \tag{5.7}$$

which was introduced in chapter 4. We start by considering the absolute value of this term with the above introduced parameters, see *Fig. 5.9*(c). It is an oscillating function of the bias voltage and vanishes for V_0. As a consequence, the kinetic equation of the island spin only contains an accumulation and a relaxation term that both do not depend on the exchange field. Hence it does not affect the transport through the system for bias voltage V_0. A vanishing rotation contribution means that the island spin is not precessed out of the plane defined by the lead polarization directions. But a vanishing rotation term is not equivalent to an absent exchange field $\mathbf{B}^r_{\mathrm{exc}}(\omega)$. In fact, the single exchange field contributions for a given ω are finite but cancel each other due to the integration over the level energies ω and the cross product with the spin density $\mathbf{s}(\omega)$. The bias voltage dependence of the magnitude of $\mathbf{B}^L_{\mathrm{exc}}(\omega)$ for different ω is presented in *Fig. 5.12*. Where we plotted the exchange field for energies

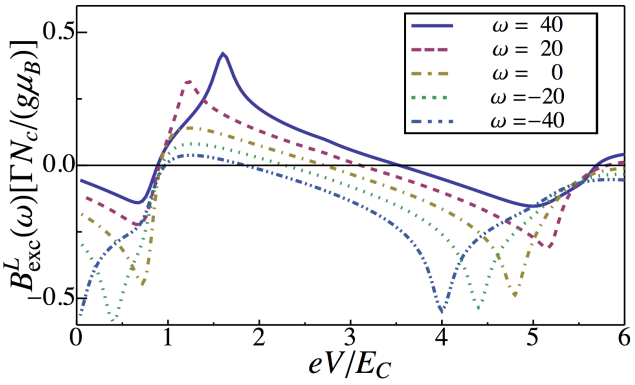

Figure 5.12: Bias voltage dependence of the left exchange field contribution for different island level energies ω. The parameters are chosen as in *Fig. 5.11*.

ω that contribute to the rotation term for voltages of about V_0. Due to the strong asymmetric coupling, the virtual tunneling processes between island and right lead are suppressed. A comparison shows that the exchange field between left lead and island is two orders in magnitudes larger than the right one. Hence the field $\mathbf{B}^L_{\mathrm{exc}}(\omega)$ governs the precession of the island spin. The spin density $\mathbf{s}(\omega)$ has a steplike structure and vanishes for $\omega \ll -\Delta\mu$ and $\omega \gg \Delta\mu$. It determines the regime of level energies ω that contribute to the integral of Eq. (5.7). Analog to the absolute value of $(\mathrm{d}\langle\mathbf{S}\rangle/\mathrm{d}t)_{\mathrm{rot}}$, the exchange field oscillates with a variation of the bias voltage. For all values of ω the position of the first sign change stays nearly constant. It corresponds to the Coulomb blockade threshold. In contrast to this, further sign changes, that correspond to larger

voltages, strongly depend on the considered level energy. Eventually, we conclude that the regimes of negative differential conductance are evoked by the oscillatory behavior of the exchange field between the source lead and the island, while the field of the drain electrode is suppressed due to asymmetric coupling strengths.

5.2.5 Conclusion of the Results in the Nonlinear-Response Regime

We have investigated the current-voltage characteristics and spin dynamics of the single-electron spin-valve transistor in the nonlinear-response regime. The origin of the island spin accumulation oscillations for low polarizations of the ferromagnetic leads was explained. Analog to the linear response regime, we, furthermore, found that the exchange field reduces the spin accumulation and increases the current through the system. This gives rise to regimes of negative differential conductance in the limit of strongly asymmetric tunnel-coupling strengths. Additionally, it was demonstrated that $\mathbf{B}_{\mathrm{exc}}^{r}$ leads to a reduction of the TMR. In the context of a detailed analysis of the different transport processes, we considered the second derivative of the current $\partial^2 I/\partial V^2$ and suggest it as a tool to determine the spin splitting of the chemical potential on the island, which, in turn, depends on the degree of spin polarization in the leads of the single-electron spin-valve transistor.

6 Current Noise

A fundamental characteristic of conductors is the time-dependent fluctuation of the electric current through the system. To explain the existence of the current noise we perform a gedankenexperiment. Let us assume that we observe the current flow through a device and detect the electrons that have passed it in a given time t_0. The experiment is performed several times. For almost all repetitions of the measurement, the detector will show a different number of transferred electrons that usually differs from the average current. This effect also appears at very low temperatures and in this case it originates from the quantization of charge of the carriers. In 1918, Schottky investigated the noise of electric conductors and called this contribution evoked by the charge quantization the *shot noise*.[107] Due to the large amount of electrons that are transferred through the most electric circuits usually shot noise compared to the current itself is negligible. For instance if a current of one Ampere is flowing through a conductor then more than 10^{18} electrons pass the system per second. However, it becomes relevant on short time scales or in very small systems. Hence it is reasonable to consider noise in the context of mesoscopic conductors.

A consideration of the mean current yields no information about its fluctuations. But their analysis is desirable due to the fact that it can reveal profound properties of the underlying quantum dynamics and transport processes. One of the pioneering works concerning shot noise in mesoscopic conductors was performed by Beenakker and Büttiker in 1992.[108] They considered electronic transport through a disordered phase-coherent conductor. A reduction of the Fano factor below the Poissonian value is described and addressed to the presence of open quantum channels and voltage fluctuations. Here, we already used the term *Fano factor*, which is defined as the current-to-noise ratio of the system:

$$F \equiv \frac{S^{II}}{2eI}, \tag{6.1}$$

with S^{II} being the current noise. It is named after Ugo Fano who introduced it to investigate the ionization fluctuations of fast charged particles.[109] An interpretation of the Fano factor F of mesoscopic conductors often relies on its comparison with the normalized noise of well known processes. In this context the Poisson distribution that describes uncorrelated transport of classical particles plays an important role. For Poisson processes the Fano factor is given by $F_{\text{Poisson}} = 1$. The different regimes of transport are called *sub-Poissonian* ($F < 1$), *Poissonian* ($F = 1$), and *super-Poissonian* ($F > 1$).

For fermionic transport processes the noise-to-current ratio is smaller than the Poissonian value. This suppression of the Fano factor is caused by the Pauli exclusion

principle which leads to an ordered transport of electrons. A basic example of systems exhibiting fermionic behavior are quantum-point contacts.[110–114] The transport through these systems is governed by an one-dimensional transverse channel between two bulk reservoirs. Hence the Pauli principle evokes that at most two electrons of different spin can simultaneously be transmitted into the other reservoir, i.e., transport processes are correlated and noise is reduced.

An example for a mesoscopic setup that exhibits super-Poissonian transport characteristics is a normal-metal-superconductor junction. The current noise of these kind of hybrid systems was first analyzed by Khlus in 1987.[115] His pioneering publication was followed by several theoretical[112,113,116–119] and experimental[120–122] works also considering the current fluctuations of normal-metal-superconductor junctions. In these systems, charge carriers are transferred through the junction via Andreev reflection. There are two different explicit forms of Andreev-reflection processes depending on the transport direction. Concerning transport from the normal region into the superconductor, two electrons with opposite spins enter the latter by forming a Cooper pair. While for transport in the opposite direction, a Cooper pair breaks in the superconductor and its constituent parts (two electrons with opposite spins) enter the normal metal. In general, the Fano factor can indicate the effectively transferred charge per transport process. In the special case of a normal-metal-superconductor junction F is equal to two, which represents the fact that in each Andreev-refection process two electrons are transported through the junction. In literature super-Poissonian transport statistics are often called bosonic. This naming is consistent for the above setup, since charge is transferred by braking or creating a Cooper pair which is a boson. However, several mesoscopic systems exhibit super-Poissonian noise although the current is exclusively carried by electrons (fermions). Among these there are devices containing electron reservoirs that are coupled to quantum wells,[123] quantum dots,[124–130] single molecules,[131–133] carbon nanotubes,[131,134] single-barrier semiconductor heterostructures,[135] and quantum rings.[136] Several of these devices represent single-electron transistors. One example for a single-electron transistor that is showing super-Poissonian current fluctuations (in fermionic transport) is the quantum-dot spin-valve, which is composed of a single-level quantum dot that is tunnel coupled to two ferromagnetic leads. In this system, the enhancement of the Fano factor originates from electron-bunching effects caused by the interplay of interaction effects and finite spin polarization.[45,48] The current noise of systems composed of two ferromagnetic leads enclosing a central electrode is discussed in more detail in the context of our results concerning the current fluctuation of the single-electron spin-valve transistor, see section 6.2.

In the previous chapters of the present work, only the average current and the spin dynamics were considered. Above, we demonstrated that an additional investigation of the current noise of mesoscopic conductors reveals extra information of underlying transport processes that are not included in the mean current. This motivates us to analyze the current fluctuations of the single-electron spin-valve transistor.

6.1 Noise Formula

We start our investigations by extending the diagrammatic technique derived in chapter 3 to calculate the frequency-dependent current noise of the single-electron spin-valve transistor. The formalism is based on the work of Braun *et al.*, where the current fluctuations of the quantum-dot spin valve are analyzed by means of the diagrammatic real-time approach.[45] Previously, Thielmann *et al.* already derived a theory (relying on the same diagrammatic technique) that enables an investigation of the zero-frequency shot noise of a mesoscopic system composed of a single-level quantum dot[131] or a single molecule[137] coupled to two electrodes. But finite-frequency noise was not considered there. Parts of the present section are published in Ref. [138].

Current fluctuations of a mesoscopic conductor are described by the current-current correlation function

$$S^{II}(t) = \langle I(t)I(0)\rangle + \langle I(0)I(t)\rangle - 2\langle I\rangle^2 . \tag{6.2}$$

We are interested in the frequency-dependent current noise that can be defined as the Fourier transform of $S^{II}(t)$:

$$\begin{aligned} S^{II}(\omega) &= \int_{-\infty}^{\infty} \mathrm{d}t\; S^{II}(t) e^{-i\omega t} \\ &= \int_{-\infty}^{\infty} \mathrm{d}t\; \left(\langle I(t)I(0)\rangle + \langle I(0)I(t)\rangle\right) e^{-i\omega t} - 4\pi \langle I\rangle^2 \delta(\omega). \end{aligned} \tag{6.3}$$

The used definitions cause $S^{II}(\omega)$ to be symmetrized in frequency, i.e., $S^{II}(\omega) = S^{II}(-\omega)$. It represents a real physical observable. To measure the symmetrized noise over a wide frequency range Aguado and Kouwenhoven proposed a double quantum dot as a detector.[139] Further detailed considerations concerning the detection of current fluctuations in quantum mechanical systems were performed by Gavish *et al.*.[140] They explicitly focus on the differences between unsymmetrized and symmetrized noise and discuss the requirements for possible detectors.

For finite frequencies, the total current flowing through the single-electron spin-valve transistor is not equal to the symmetrized current $I = (I_L - I_R)/2$ that occurs in Eq. (6.3). In general, displacement currents appear that have to be taken into account by defining the current as $I = (C_L I_L - C_R I_R)/(C_L + C_R)$.[141] However, in our model we assume symmetric junction capacitances, see section 3.1, and hence the general formula corresponds to the definition of the symmetrized current.

In the following, we demonstrate how the calculation of the noise $S^{II}(\omega)$ can be realized within the diagrammatic technique. Analog to the Laplace transform that enables the transition of the master equation from time into frequency space, see subsection 3.2.4, the Fourier transform in Eq. (6.3) evokes an additional bosonic line carrying the energy $\hbar\omega$. However, this line connects two current vertices that replace two vertices originating from the tunneling Hamiltonian. The current vertices can appear in the same kernel block $\mathbf{W}$ or they are separated by the already introduced frequency dependent propagator $\mathbf{\Pi}(\omega)$. An illustration of the diagrammatic representation is shown in *Fig. 6.1*. The position of each current vertex depends on the corresponding noise

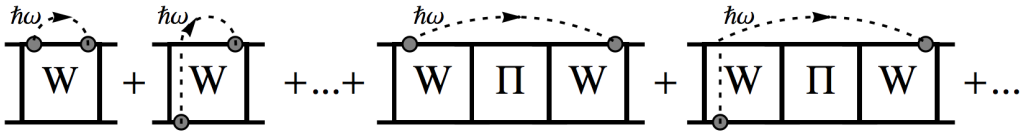

Figure 6.1: Diagrammatic representation of the finite-frequency current noise $S^{II}(\omega)$. Two current vertices that are placed on the upper or lower contour are connected by a bosonic line carrying the energy $\hbar\omega$.

contribution ($\langle I(t)I(0)\rangle$ or $\langle I(0)I(t)\rangle$) and the time of the current operator (0 or t). This different locations result in the generation of three new kinds of kernels that are depicted in *Fig. 6.2*. In $\mathbf{W}^I_<(\omega)$ and $\mathbf{W}^I_>(\omega)$ one current vertex placed on the upper or lower contour is contacted by the bosonic line that enters the diagram from the left or leaves it to the right, respectively. While in the diagrams of $\mathbf{W}^{II}(\omega)$ the additional line connects two current vertices. This new objects sum all irreducible diagrams with one ($\mathbf{W}^I_{<(>)}(\omega)$) or two ($\mathbf{W}^{II}(\omega)$) tunneling vertices replaced by current vertices in all possible topological different ways. Eventually, we can write down the formula for the frequency-dependent noise in the diagrammatic matrix notation:

$$S^{II}(\omega) = \frac{1}{2}\sum_{\gamma=\pm} \mathrm{tr}\left[\mathbf{W}^{II}(\gamma\omega)\hat{\rho}_{\mathrm{red}} + \mathbf{W}^I_<(\gamma\omega)\mathbf{\Pi}(\gamma\omega)\mathbf{W}^I_>(\gamma\omega)\hat{\rho}_{\mathrm{red}}\right] - 4\pi\langle I\rangle^2\delta(\omega). \quad (6.4)$$

At a first glance, the current noise diverges for $\omega \to 0$ due to the divergence of the propagator $\mathbf{\Pi}(\omega = 0)$. However, the full expression of $S(\omega = 0)$ remains finite since the delta function in combination with the summands with $\gamma = +$ and $\gamma = -$ cancel the divergences.

The noise formula in Eq. (6.4) represents the general expression of the current fluctuations of the single-electron spin-valve transistor. However, in the present thesis the limit of weak island-lead coupling is investigated. Therefore, only sequential-tunneling processes have to be taken into account. As a consequence, only diagrams containing one tunneling line contribute to the kernels, i.e., they are expanded up to first

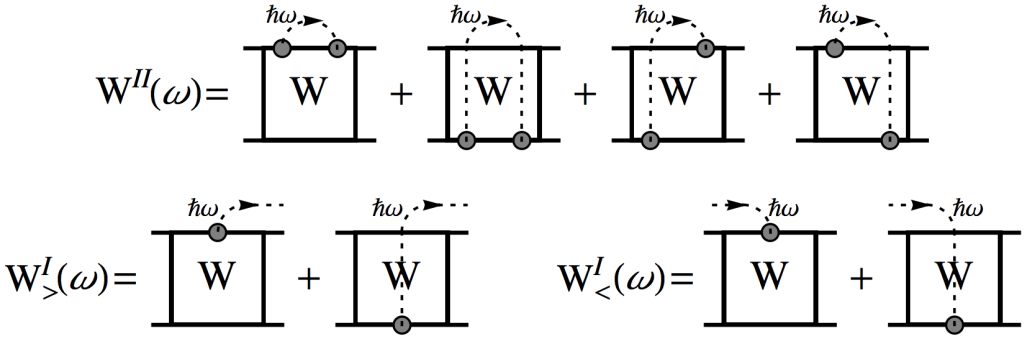

Figure 6.2: Diagrammatic representation of the frequency-dependent kernels that occur in the general expression of the current noise, see Eq. (6.4).

order in Γ, see subsection 3.2.5. But this procedure does not lead to a consistent expansion of the noise. In fact $S^{II}(\omega)$ contains additional second-order contributions. However, in the calculation of the kernels the second-order contributions (cotunneling) were neglected. We obtain the noise formula that consistently describes the sequential-tunneling by limiting the frequency to the tunnel-coupling strength ($\omega \sim \Gamma$). In this limit the frequency dependence of the kernels can be neglected since each correction in ω evokes contributions that are at least proportional to Γ^2. The only frequency dependence we keep is contained in the reduced propagator $\mathbf{\Pi}(\omega)$. By means of Eq. (3.20) we obtain $\mathbf{\Pi}(\omega) = \left(\mathbf{\Pi}^{(0)}(\omega)^{-1} - \mathbf{W}(\omega)\right)^{-1}$. This expression is treated consistently when exclusively the frequency dependence of the free propagator is taken into account. Finally, we obtain the consistent noise formula that describes sequential tunneling and low frequencies $\omega \sim \Gamma$ to be

$$S^{II}(\omega) = \frac{1}{2}\sum_{\gamma=\pm} \mathrm{tr}\left[\mathbf{W}^{II}\hat{\rho}_{\mathrm{red}} + \mathbf{W}^{I}\left(\mathbf{\Pi}^{(0)}(\gamma\omega)^{-1} - \mathbf{W}\right)^{-1}\mathbf{W}^{I}\hat{\rho}_{\mathrm{red}}\right] - 4\pi\langle I\rangle^2\,\delta(\omega), \tag{6.5}$$

with the definitions $\mathbf{W} = \mathbf{W}(\omega = 0)$, $\mathbf{W}^I = \mathbf{W}^I_<(\omega = 0) = \mathbf{W}^I_>(\omega = 0)$, and $\mathbf{W}^{II} = \mathbf{W}^{II}(\omega = 0)$. This formula for $S^{II}(\omega)$ depends on all the elements of the reduced density matrix $P^{\chi_1}_{\chi_2}$. An effective description that only contains the independent degrees of freedom of the system (the charge-state occupation probabilities P_N and the accumulated island spin $\mathbf{S}$) is obtained by executing the same procedure as in the derivation of the kinetic equations, see chapter 4. This enables to remove the coherent superpositions on the right-hand side of Eq. (6.5), i.e., only diagonal matrix elements P_χ enter. In the island-charge-state basis the frequency dependent noise is then given by

$$\begin{aligned} S^{II}(\omega) \;=\; & -4\pi\langle I\rangle^2\,\delta(\omega) + \mathbf{e}^{\mathrm{T}}\widetilde{\mathbf{W}}^{II}\mathbf{P} \\ & + \frac{1}{2}\mathbf{e}^{\mathrm{T}}\left[\sum_{\gamma=\pm}\widetilde{\mathbf{W}}^{I}(\widetilde{\mathbf{\Pi}}^{(0)}(\gamma\omega)^{-1} - \widetilde{\mathbf{W}})^{-1}\widetilde{\mathbf{W}}^{I}\right]\mathbf{P}, \end{aligned} \tag{6.6}$$

where the vector $\mathbf{e}$ is defined by $e_N = 1$ for all N and the vector of the island-occupation probabilities $\mathbf{P} = (.., P_{N-1}, P_N, P_{N+1}, ...)$ fulfills the normalization condition $\mathbf{e}^{\mathrm{T}}\mathbf{P} = 1$. The matrix elements of the kernels in charge space that have to be plugged in the formula Eq.(6.6) are defined as follows:

$$\begin{aligned} \widetilde{W}_{N\,N'} \;=\; & \pi\sum_{r\sigma}\left\{\delta_{N,N'+1}\alpha^{+}_{r\sigma}(\Delta_{N-1}) + \delta_{N+1,N'}\alpha^{-}_{r\sigma}(\Delta_N)\right. \\ & \left. -\delta_{N,N'}\left[\alpha^{+}_{r\sigma}(\Delta_N) - \alpha^{-}_{r\sigma}(\Delta_{N-1})\right]\right\}, \end{aligned} \tag{6.7}$$

$$\widetilde{W}^{I}_{N\,N'} \;=\; e\pi\sum_{r\sigma}\pm\left[\delta_{N,N'+1}\alpha^{+}_{r\sigma}(\Delta_{N-1}) - \delta_{N+1,N'}\alpha^{-}_{r\sigma}(\Delta_N)\right], \tag{6.8}$$

$$\widetilde{W}^{II}_{N\,N'} \;=\; \frac{e^2\pi}{2}\sum_{r\sigma}\left[\delta_{N,N'+1}\alpha^{+}_{r\sigma}(\Delta_{N-1}) + \delta_{N+1,N'}\alpha^{-}_{r\sigma}(\Delta_N)\right]. \tag{6.9}$$

In Eq. (6.8) the upper/lower sign has to be chosen for the kernel contributions representing the current through the left/right tunnel junction ($r = L/R$).

As mentioned above, in the considered limit the only frequency dependence that is contained in the noise is represented by the free propagator of the system. In charge space it is given by

$$\widetilde{\Pi}^{(0)\,N_1}_{\;\;N_2\,N'}(\omega) = \frac{i}{-\hbar\omega + i0^+}\delta_{N_1,N'}\delta_{N_2,N'}. \tag{6.10}$$

Hence $\widetilde{\mathbf{\Pi}}^{(0)}(\omega)$ is represented by a diagonal matrix. For finite frequencies, the $i0^+$ in Eq. (6.10) drops together with the delta function in Eq. (6.6).

In the Eqs. (6.7)-(6.9) one finds that the kernels $\widetilde{\mathbf{W}}$, $\widetilde{\mathbf{W}}^I$, and $\widetilde{\mathbf{W}}^{II}$ are proportional to the island rate functions $\alpha^{\pm}_{r\sigma}$, which makes the expression of the current noise reliable for frequencies $\omega \lesssim \alpha^{\pm}_{r\sigma}$.

6.2 Results

In literature, there are several publications dealing with current fluctuations of restricted limits of the single-electron spin-valve transistor. The complexity of the required theoretical description drastically simplifies if one considers unpolarized leads ($p = 0$). Naturally, the noise in this limit of two normal leads coupled to a central normal region with a continuous level spectrum (NNN) was theoretically investigated first. In the corresponding works zero-frequency[142–144] as well as finite-frequency[141,145–148] current fluctuations were considered and in all cases found to be sub-Poissonian. Since in experiments the shot noise is often superimposed by other sources of noise, as the noise of the used amplifiers or the $1/f$ noise that occurs due to defects in or near the junctions, there are just a few experimental works studying the current fluctuations of the NNN system. The most of them have to restrict their noise measurements to the regime of large bias voltages.[149–151] However, recently Kafanov and Delsing published a paper in which they measured the noise of the NNN system over a wide voltage range.[152] Their presented results agree very well with theoretical predictions for sequential tunneling in single-electron transistors.

An alternative simplification of the single-electron spin-valve transistor is not to allow for polarization directions enclosing an arbitrary angle ϕ, but instead to restrict the investigations to collinear setups ($p \neq 0$, $\phi \in \{0, \pi\}$). Also this limit of the system attracted much interest that was additionally stimulated by the fact that the noise-to-current ratio is crucial for expected applications in microelectronic technology.[35,153–156] The charge and the spin current noise are considered for zero frequencies as well as for finite frequencies. A few works additionally focus on the investigation of the effect of spin-flip scattering on the charge or spin current fluctuations.[154–156] It is predicted that the Fano factors strongly depend on the lead polarization, the spin-flip scattering intensity, and the contact resistances.

In the present thesis, the general single-electron spin-valve transistor is investigated, i.e., we consider finite lead polarizations and arbitrary angles between the lead polarization directions ($p \neq 0$, $\phi \in [0, 2\pi]$). Tserkovnyak and Brataas already performed an analysis of the shot-noise angle dependence concerning this setup, however, they neglected the Coulomb charging effects on the central electrode.[157] Within their theory

they find a strong dependence of the Fano factor on the relative orientation of the lead magnetizations. As explained in chapter 4, the exchange field can be interpreted as a many-body interaction effect that vanishes in the limit of noninteracting island electrons. Hence by neglecting charging effects Tserkovnyak and Brataas automatically remove the exchange field from their theory.

The influence of the exchange field on the mean current and the spin dynamics has been discussed in the previous chapters of the present thesis. We demonstrated that it strongly affects the properties of the system. Therefore, an incorporation of this effect into the theory that is used for the calculation of the current noise is important. In our results concerning the current fluctuations, that will be presented in this section, the exchange field is fully taken into account since it is an immanent part of the used theoretical framework, see chapter 4.

The following discussion of the frequency-dependent noise of the single-electron spin-valve transistor is organized as follows. We consider the zero-frequency and the low-frequency limits in two separated subsections 6.2.1 and 6.2.2, respectively. In the case of noncollinear aligned magnetization directions of the leads the exchange field is relevant and its impact on the current fluctuations will be analyzed in detail. Most of the results presented in this section are additionally published in Ref. [138].

6.2.1 Zero-Frequency Current Fluctuations

We start our discussion by considering the limit of unpolarized leads. As mentioned in the introducing part above, the current fluctuations of this special case of the single-electron spin-valve transistor were already discussed in literature. However, we want to present the basic properties of the NNN setup to enable a better understanding of the underlying physics for the finite polarized system. First, we discuss the influence of different tunnel-coupling strength asymmetries $a \equiv \Gamma_L/\Gamma_R$ on the noise. In *Fig. 6.3*(a), the Fano factor of the NNN system is plotted for different ratios a as a function of the applied bias voltage V. With increasing a the sub-Poissonian Fano factor exhibits strongly pronounced Coulomb-blockade oscillations which represent the steps in the current-voltage characteristics. Hence the maxima of these oscillations occur at the excitation energies of the relevant island charge states. In subsection 5.2.3 we explained that these are indicated by peaks in the second derivative of the current with respect to the bias voltage, see *Fig. 6.3*(b). For strong asymmetric couplings the occupation probability for charge state $N_0 - 1$ is suppressed which is represented by a reduction of the height of the $N_0 - 1$ peak. This behavior results in the fact that the first step in the Fano-factor graph, that is clearly visible for $a = 2$, smears out for higher asymmetries. We want to emphasize that for obtaining reliable results in the Coulomb-blockade regime, where sequential-tunneling transport is completely blocked (low bias voltages), cotunneling processes have to be taken into account. In *Fig. 6.3* this regime is marked by the grey area. At high bias voltages sequential-tunneling processes are dominant and the Fano factors converge to values that are given by

$$F_{V\to\infty} = \frac{\Gamma_L^2 + \Gamma_R^2}{(\Gamma_L + \Gamma_R)^2} = \frac{1 + a^2}{(1 + a)^2}. \tag{6.11}$$

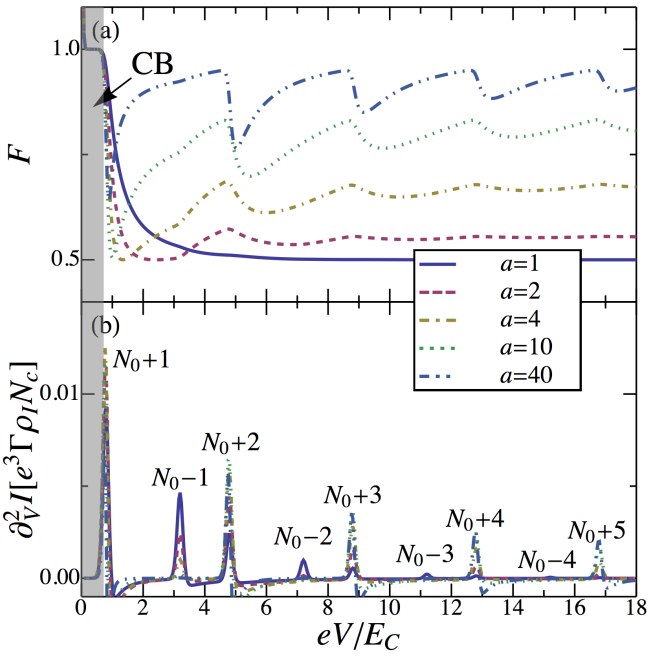

Figure 6.3: NNN system: (a) Fano factor and (b) second derivative of the current as a function of the applied bias voltage V for different asymmetry parameter a. The Coulomb-blockade regime, where transport through the device is completely blocked, is marked by the grey area. For both plots, the remaining parameters were chosen to be $C_G V_G = 3e/10$ and $E_C = 50 k_B T$.

We see that the saturation values of the noise-to-current ratio are independent of the external induced charge that is governed by the gate voltage. Additionally, a variation of temperature does not affect $F_{V\to\infty}$ but for higher T the oscillations are smeared out. For strong asymmetric junction-resistance ratios $a \gg 1$ one obtains $F_{V\to\infty} = 1$. This Poissonian behavior is expected as in the considered limit the NNN system actually acts as a single normal tunnel barrier.

A further important feature is that additional information is contained in the current noise in comparison to the average current. To illustrate this effect, we consider the mean current and the Fano factor for coupling asymmetries $a = 1/3$ and $a = 1/2$, see *Fig. 6.4*. In contrast to the rest of this thesis, the bias voltage is applied to the left lead, while the voltage on the right reservoir is set to zero, i.e., the charging states $N_0 - n$ with $n \in \mathbb{N}^+$ are always occupied. In this situation, the current-voltage characteristics for $a = 1/2$ and $a = 1/3$ are almost identical for $eV \lesssim 3E_C$. Hence by measuring the current in this regime it is not possible to determine the junction asymmetry of the used sample. However, the Fano factor curves exhibit clear differences that enable the determination of a. The above discussed results correspond to those predicted by Hershfield *et al.*[142] and Bagrets *et al.*.[143]

To proceed we turn to the situation of collinear polarized leads. Analog to the calculations in chapters 4 and 5, we assume that both leads are made of the same material, i.e., the leads are symmetrically polarized $p_L = p_R = p$. Hence for parallel aligned lead magnetization directions ($\phi = 0$) there is no spin accumulation on the central island. This results in the fact, that both the current and the noise are independent of the lead polarization. In the more general case $p_L \neq p_R$ there is a finite island spin accumulation which results in a polarization dependent Fano factor. The situation changes for the antiparallel setup ($\phi = \pi$) as in this case the spin accumulation strongly depends

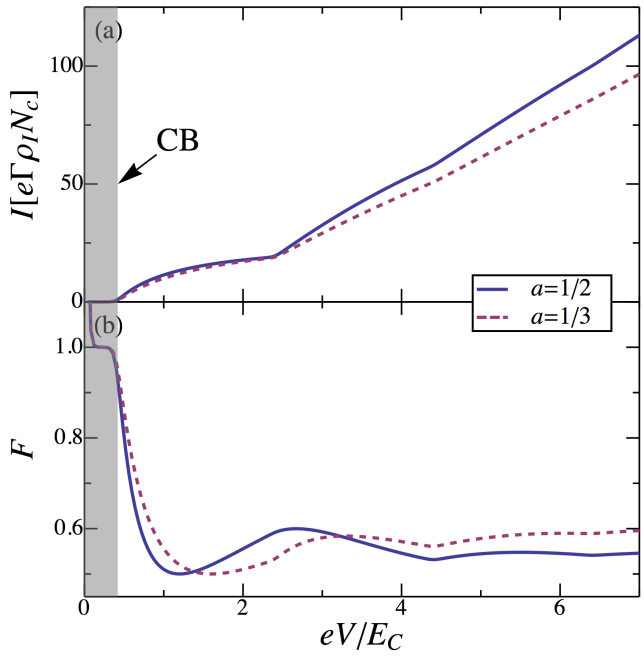

Figure 6.4: (a) Average current and (b) Fano factor of the NNN system as a function of the bias voltage V for different coupling-strength ratios a. Remaining parameters were chosen as in *Fig. 6.3*.

on p. In *Fig. 6.5*(a) we plotted the antiparallel Fano factor for different values of the lead polarization and a large asymmetry parameter ($a = 10$). The above discussed sharp structure of the $p = 0$ graph smears out for finite polarizations. Additionally, the positions of the maxima change. Both effects are caused by the finite island spin accumulation since it induces a spin dependence of the charging-state excitation energies $E_{N;\sigma}$ that results in a more complex excitation spectrum. To illustrate this behavior we plotted the second derivative of the current in *Fig. 6.5*(b) and consider the case of $p = 20\%$. The single charging-state peaks of the unpolarized situation are split up into two peaks representing the two different spin reservoirs of the island (marked by the up and down arrows). We emphasize that the first peak ($N_0 + 1$) does not split due to the exponentially suppressed island spin accumulation in the Coulomb-blockade regime. For the charging states $N_0 + n$ with $n \in \mathbb{N}^+$ the spin-down (spin-up) excitation energies are shifted towards lower (higher) bias voltages. While for $N_0 - n$ the displacements of the spin-reservoir excitations are contrariwise. However, due to the asymmetric coupling the occupation of the latter states is strongly suppressed.

Even for very large asymmetry parameters $a \gg 1$ and highly polarized materials $p > 90\%$ the obtained Fano factors remain sub-Poissonian. This is in contrast to systems consisting of two ferromagnetic leads tunnel coupled to a central region that exhibits a discrete energy spectrum.[45,48,153] In the case of a quantum-dot spin valve super-Poissonian statistics arises as a result of bunching effects that are caused by spin blockade. In the single-electron spin-valve transistor such bunching effects do not occur since its transport behavior is significantly different. To illustrate this we start by considering the quantum-dot spin valve with parallel aligned lead magnetization directions in the regime where the single level of the dot is predominant occupied by one electron. Finite polarizations evoke that mainly majority spins enter the dot.

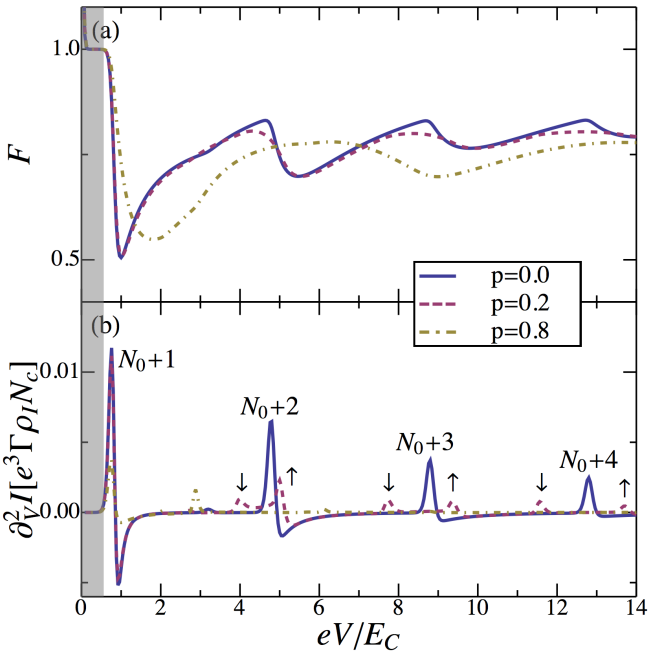

Figure 6.5: Antiparallel setup ($\phi = \pi$) of the single-electron spin-valve transistor: (a) Fano factor and (b) second derivative of the current as a function of the applied bias voltage V for different lead polarizations p. For both plots, the remaining parameters were chosen to be $C_G V_G = 3e/10$, $E_C = 50 k_B T$, and $a = 10$.

These can easily leave into the drain lead due to the parallel lead magnetizations. However, if a minority spin occupies the single level then its large dwell time (few minority states in the drain electrode) leads to a temporary blockade of the current through the system since there are no further charging states in the transport window. Hence the rare event of a minority charge carrier tunneling onto the dot bunches the flow of majority electrons. This behavior leads to super-Poissonian noise. In contrast to this, the continuous level structure of the single-electron spin-valve transistor prevents bunching caused by minority electrons. This is due to the fact that there are two different processes that change the charging state of the system after a minority electron tunneled onto the island. On the one hand the same electron or another minority charge carrier can leave the central electrode into the drain with a small probability (as for the quantum-dot spin valve). But on the other hand, contrary to the single-level system, it is additionally possible that also majority electrons can tunnel into the drain, see *Fig. 4.1*. Even for higher polarizations the latter process is not suppressed. It transfers the system into the lower island charging state and enables the subsequent repetition of island filling and depletion processes. Therefore, the transport through the system is not blocked by minority electrons as in the case of single-level quantum dots.

For completeness, we show in *Fig. 6.6* the second derivative of the Fano factor with respect to the applied bias voltage V. As the second derivative of the mean current with respect to V also this quantity reflects the threshold voltages of the relevant charging states. These are indicated by a peak-trough structure (two peaks with opposite sign). However, a more precise consideration of the plot reveals that the information about the splitting of the island chemical-potential, which is contained in $\partial^2 I/\partial V^2$, is lost in the second derivative of F. Hence its measurement does not allow for a determination of the degree of polarization of the ferromagnetic leads. Furthermore, the peaks are

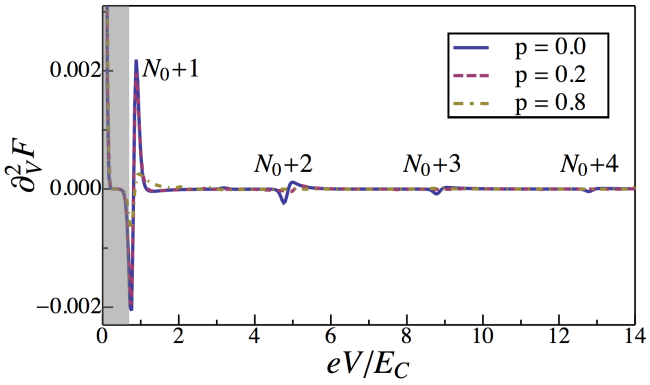

Figure 6.6: Second derivative of the Fano factor with respect to the applied bias voltage as a function of bias for different lead polarizations in the antiparallel setup $\phi = \pi$. The threshold voltages of different charging states are indicated by a peak-trough structure. The remaining parameters were chosen as in *Fig. 6.5*.

less pronounced in comparison to the peaks of the current derivative.

Having discussed the limit of unpolarized leads as well as the case of parallel and antiparallel magnetization directions we now turn to the noncollinear single-electron spin-valve transistor. If one neglects the Coulomb interaction of electrons on the central island and additionally assumes that the leads are held at zero temperature then the following analytic expression of the Fano factor is obtained:[157]

$$F = \frac{1}{2}\left(1 + p^2 \sin^2 \frac{\phi}{2}\right). \tag{6.12}$$

In this limit, the Fano factor exclusively depends on the polarization of the leads and on the angle ϕ between the p-vectors. The formula represents a monotonically increasing F from its minimum $F(0) = 1/2$ to its maximal value $F(\pi) = (1 + p^2)/2$. However, by neglecting the Coulomb-repulsion energy crucial single-charging effects that govern the transport characteristics of the system are not taken into account, see chapter 2. Hence Eq. (6.12) is an insufficient description of the noise in a single-electron spin-valve transistor.

In our formalism the electron-electron interaction on the central island is taken into account nonperturbatively. Its interplay with the finite spin polarization gives rise to the exchange field that acts on the accumulated spin on the central island. In the following the impact of the field on the current fluctuations of the system is discussed in detail. The exchange field is an immanent part of the used theoretical framework and occurs in the kinetic equation of the island spin, see Eqs. (4.14) and (4.18). As already introduced in chapter 4, the expression of the exchange field contribution that is induced between island and lead r is given by

$$\mathbf{B}^r_{\mathrm{exc}}(\omega) = \frac{p_r \Gamma_r N_c}{2\pi g \mu_B}\, \hat{\mathbf{n}}_r \sum_N P_N \int' \mathrm{d}\omega' \left[\frac{f_r^-(\omega')}{\omega' - \omega - \Delta_N} + \frac{f_r^+(\omega')}{\omega' - \omega - \Delta_{N-1}}\right]. \tag{6.13}$$

Due to the lead Fermi functions that appear in the integral the exchange field depends on the applied bias voltage. Therefore, to investigate how the exchange field affects the

current noise we have to identify a voltage regime where the field noticeably influences the transport. To this end, we consider the current through the system as a function of the bias voltage for a noncollinear angle $\phi = \pi/2$, see *Fig. 6.7*. In the presented

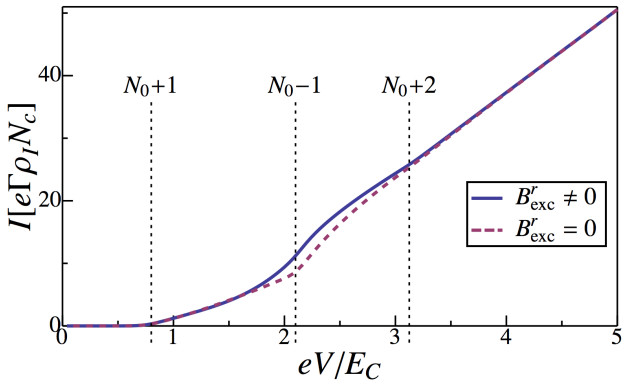

Figure 6.7: Current through the noncollinear ($\phi = \pi/2$) single-electron spin-valve transistor with (solid) and without (dashed) the effect of the exchange field. The dashed vertical lines indicate the threshold voltages of different charging states. The remaining parameters were chosen to be $p = 9/10$, $C_G V_G = 3e/10$, $E_C = 50 k_B T$, and $a = 1$.

figure the influence of the exchange field is illustrated by the difference of the two shown graphs. Here, the dashed line represents the current of an artificial situation where both exchange-field kinetic-equation contributions $\mathbf{B}^r_{\rm exc}$ were manually set to zero. While for the calculation of the solid line the field is fully taken into account. A comparison of the two graphs yields that in the vicinity of the threshold voltage, that enables the occupation of the charging state $N_0 - 1$, the field strongly affects the current-voltage characteristics. Here, we point out that to observe a significant effect of the exchange field highly polarized leads with $p \gtrsim 0.7$ have to be considered.

After identifying a voltage regime where the exchange field is pronounced we now describe its influence on the current fluctuations of the single-electron spin-valve transistor. In *Fig. 6.8* the charge current, the zero-frequency noise, and the Fano factor are plotted as a function of the angle between the lead polarization directions ϕ. All three plots are calculated for symmetric tunnel-coupling strengths ($a = 1$) and a bias voltage of $V = 2E_C/e$ that lies in the voltage window exhibiting pronounced exchange fields. The precession of the island spin caused by the field leads to an increase of current and noise. However, the enhancement of the latter is weaker for all angles ϕ and therefore the spin precession results in an decreased sub-Poissonian Fano factor. This behavior is also present in systems with asymmetry parameters a being unequal to one. The plotted Fano factors exhibit a monotonic behavior between the two collinear situations. We emphasize that this is caused by the special choice of the parameters, i.e., there are parameter sets for which the maxima (minima) of F do not occur at the collinear angles. In Fig. 6.8(c), we additionally plotted the graph of the Fano factor of the noninteracting situation ($E_C = 0$) given by Eq. (6.12). A comparison shows that a consideration of the noninteracting limit is insufficient to obtain reliable results of

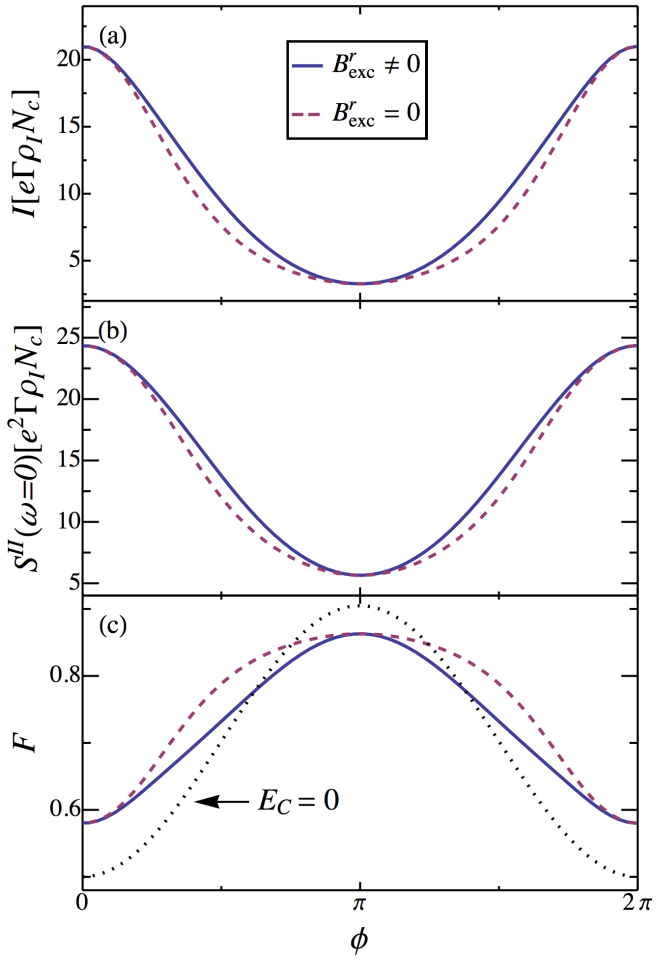

Figure 6.8: Noncollinear single-electron spin-valve transistor: (a) charge current, (b) zero-frequency noise and (c) Fano factor as a function of the angle between the lead polarization directions ϕ with (solid) and without (dashed) the effect of the exchange field. The parameters were chosen to be $p = 9/10$, $eV = 2E_C$, $C_G V_G = 3e/10$, $E_C = 50 k_B T$, and $a = 1$.

the current fluctuations of the single-electron spin-valve transistor. Even for collinear setups the interacting Fano factor strongly deviates from the noninteracting one.

Conclusion of the Zero-Frequency Noise Results

We have investigated the zero-frequency current fluctuations of the single-electron spin-valve transistor. The considerations were split into three parts where the NNN system (for completeness), the case of collinear aligned lead polarization directions, and the general noncollinear situation were discussed. In every three limits sub-Poissonian transport statistics were observed. We found that finite lead polarizations smear out the characteristic Coulomb-blockade oscillations of the Fano factor as a function of the bias voltage. The origin of this behavior was addressed to the splitting of the charging-state excitation energies caused by the non-vanishing spin accumulation on the metallic island. Furthermore, we identified the voltage regime in which the effect of the exchange field is pronounced and demonstrated that $\mathbf{B}^r_{\rm exc}$ leads to a reduction of the Fano factor.

6.2.2 Finite-Frequency Current Fluctuations

In subsection 6.2.1 we found that the zero-frequency Fano factor of the single-electron spin-valve transistor exhibits oscillations evoked by the electron-electron interaction on the central island. The amplitude of these oscillations vanishes in the case of symmetric tunnel couplings ($a = 1$) and increases for higher asymmetry parameters a. To analyze the frequency dependence of the current noise we consider $F(\omega)$ in different regimes of these oscillations, see *Fig. 6.9*. We restrict our investigations to

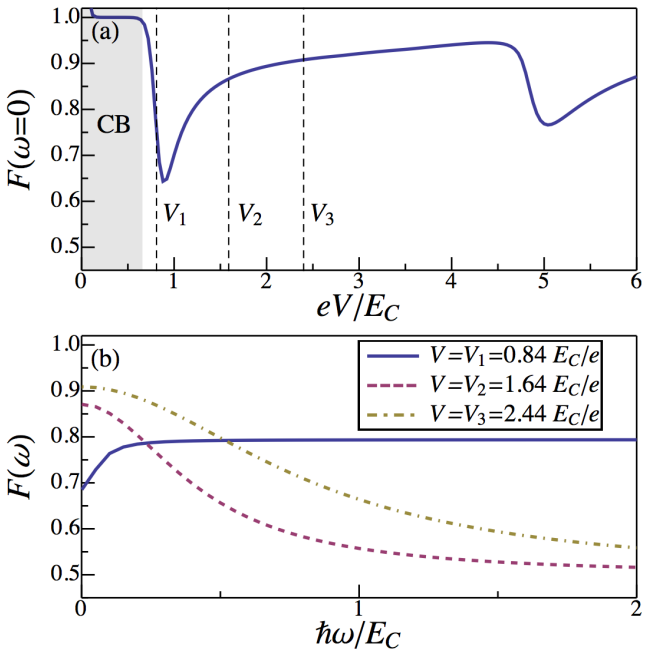

Figure 6.9: Current fluctuations of the noncollinear ($\phi = \pi/2$) single-electron spin-valve transistor: (a) Zero-frequency Fano factor as a function of bias voltage V. (b) Frequency-dependent Fano factor as a function of ω for different V. For both plots the parameters were chosen to be $p = 2/10$, $C_G V_G = 3e/10$, $E_C = 50 k_B T$, and $a = 40$.

a bias voltage range where the island is exclusively occupied by N_0 or by $N_0 + 1$ electrons. In the upper plot the zero-frequency Fano factor is shown and the different voltages V_i with $i = 1, 2, 3$ for which we will study the current noise are marked by the dashed black lines in *Fig. 6.9*(a). The energy $eV_1 = 0.84E_C$ is slightly larger than the excitation energy of the charging state $N_0 + 1$, i.e., it represents a Coulomb step in the current-voltage characteristics. While the other two voltages are lying in between two charging steps and the condition $P_{N_0} + P_{N_0+1} = 1$ is fulfilled. The respective frequency-dependent Fano factors (fixed V_i) are plotted as a function of the frequency ω in *Fig. 6.9*(b). For all voltages the Fano factors are composed of a dynamical frequency-dependent contribution reflecting correlations (V_2, V_3) and anticorrelations (V_1) as well as a constant contribution. The explicit value of the latter is given by $S^{II}(\omega \gg E_C/\hbar)$. A comparison shows that for larger voltages the noise spectra are broadened and the constant term is shifted below the value of the zero-frequency noise to current ratio.

All three graphs in *Fig. 6.9*(b) indicate that the structure in the noise is destroyed for large enough frequencies. Hence we consider the half width $\omega_{F_{1/2}}$ of the frequency dependent Fano factor as a function of the applied bias voltage to determine the scale on which the system looses its correlation information, see *Fig. 6.10*. In the considered

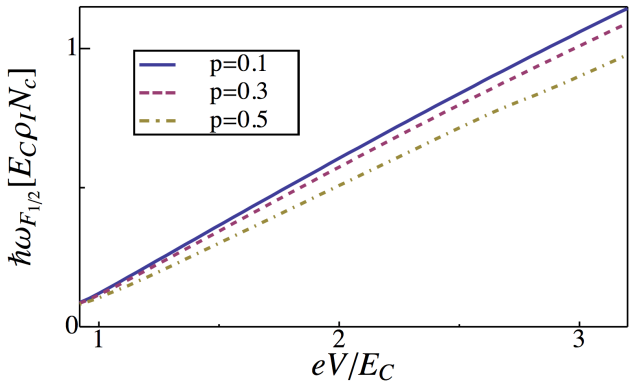

Figure 6.10: Half width of the frequency-dependent Fano factor as a function of V for different polarizations p. The frequency is measured in units $E_C\rho_I N_c$ and the remaining parameters were chosen to be $\phi = \pi/2$, $C_G V_G = 3e/10$, $E_C = 50k_BT$, and $a = 40$.

voltage regime where only two charging states are allowed the half width is linear in V. The slope of the obtained straight line is proportional to $\pi\alpha_0$, with the used definition $\alpha_0 \equiv \sum_{r\sigma} \alpha^0_{r\sigma}$. It is maximal for $p = 0$ and decreases with increasing degree of lead polarization. Here, we emphasize that as soon as the voltage is large enough to bring additional higher charging states into the transport window this simple behavior of $\omega_{F_{1/2}}$ is not valid anymore.

Conclusion of the Finite-Frequency Noise Results

We analyzed the frequency dependence of the current noise and found that $F(\omega)$ reflects correlations and anticorrelations. However, the noise structure is lost for high enough frequencies. In this context we identified the frequency scale that represents the loss of information.

7 Conclusions

The single-electron spin-valve transistor is a convenient model system to study the interplay of single-charging phenomena and spintronic effects. It exhibits typical electronic-transport features of ferromagnet/normal-metal hybrid structures as a finite spin accumulation on the central electrode as well as a tunnel magnetoresistance. Additionally, due to the small size of the mesoscopic metallic island single-charging effects as Coulomb blockade or Coulomb oscillations appear. Furthermore, evoked by the finite spin polarization and the electron-electron interaction an exchange field arises that acts on the accumulated spin.

The challenge of the present thesis was to derive a theory that describes the electronic transport through the single-electron spin-valve transistor for *noncollinear* lead-magnetization directions. To treat the collinear ferromagnetic system a simple generalization of the all-normal-metal theory can be performed by separately taking into account the two spin species. However, for arbitrary angles between the magnetizations the situation drastically complicates since the direction of the accumulated island spin is in general not parallel aligned to the lead magnetizations, i.e., there is no canonical choice for the spin-quantization axis on the island. Hence the used tunneling Hamiltonian contains an SU(2) rotation that connects the different lead and island quantization axes. As a result coherent superpositions of different microscopic island states appear. By means of a diagrammatic real-time approach we developed an adequate theoretical formalism simultaneously incorporating the noncollinearity and the strong Coulomb interaction on the central island, see chapter 3. Within the theory a generalized master equation was derived that describes the time evolution of the reduced density matrix, in which the lead degrees of freedom were integrated out. Starting from this master equation kinetic equations for the island charge and spin that effectively describe the electronic transport through the system were calculated in chapter 4.

In chapter 5 we analyzed in detail the spin dynamics and the electric current of the single-electron spin-valve transistor. For a conservation of the electron-spin information after tunneling on the central island it is necessary that the typical dwell time of electrons is much shorter than the spin-flip relaxation time of the normal metal. In this case, there is an effective spin accumulation on the metallic island as soon as a finite bias voltage is applied to the ferromagnetic leads. We found that the accumulated macroscopic spin is strongly affected by the interaction-induced exchange field. Namely, it is rotated out of the plane defined by the magnetization directions of the two ferromagnets which leads to interesting transport properties. We started by considering the linear-response regime, where the bias voltage is small compared to the temperature and the charging-energy scale. Here, we found a high sensitivity of the island spin on the variation of the applied gate voltage. This behavior is a consequence of the exchange field and allows for a manipulation of the macroscopic spin by a pre-

cise electrical control. Furthermore, the field increases the linear conductance of the single-electron spin-valve transistor and additionally weakens the spin-valve effect.

Analog to the linear regime, we found that for higher bias voltages the exchange field also leads to an increase of the current accompanied by a reduction of the accumulated island spin. This gives rise to regimes of negative differential conductance in the limit of strongly asymmetric tunnel couplings to the ferromagnets. Furthermore, we discussed the basic spintronic effects of the device, i.e., the spin accumulation and the tunnel magnetoresistance. In the nonlinear-response regime the spin accumulation as a function of bias voltage can be decomposed into two components, an oscillating one and a component that monotonously increases. This behavior was addressed to the complex spin dependent level structure of the system. The TMR was found to exhibit a nontrivial dependence on the applied voltages. It oscillates with bias and gate voltages which enables an electrical control of the magnetoresistance intensity. Naturally, analog to the current also the TMR is affected by the exchange field resulting in a small reduction of the resistance effect.

In a following analysis of the electric current flowing through the device, we demonstrated that the consideration of the second derivative of the current with respect to the bias voltage can be useful to identify the different charging states that contribute to transport. In this context, we suggested the second derivative as a tool to determine the spin splitting of the electrochemical potential on the central island. The latter strongly depends on the degree of spin polarization in the leads. Hence the measurement of the second derivative of the current enables to determine the polarization of the used lead material.

But not only the spin dynamics and the average current were considered. Motivated by the fact that current fluctuations can reveal additional information of electronic transport processes in mesoscopic systems we also investigated the frequency-dependent current noise of the single-electron spin-valve transistor, see chapter 6. The current-to-noise ratio represented by the Fano factor was found to remain sub-Poissonian in the zero-frequency limit as well as for finite frequencies. This means that in the considered system electron correlations reduce the Fano factor below its classical value. This is in contrast to ferromagnetic SETs that contain a central part exhibiting a discrete level spectrum. In these setups electron bunching effects caused by the finite spin polarization lead to super-Poissonian current fluctuations. Furthermore, we found that the exchange field leads to a further reduction of the noise of the single-electron spin-valve transistor. Additionally, it was demonstrated that the observed oscillations of the current-to-noise ratio as a function of the applied bias voltage smear out with increasing degree of lead polarization.

The derived formalism also allows for the investigation of the finite-frequency current fluctuations. Current-current correlations and anticorrelations are reflected by the frequency-dependent Fano factor. However, the structure in the noise is lost for high enough frequencies and we identified the corresponding frequency scale corresponding to the loss of information.

A Kernel elements of the kinetic equations

In the calculation of the matrix elements of the kernel $\mathbf{W}$ to first order in the tunnel coupling only one island level l and channel number ν is involved. Its value depends on the energy and the occupation of this level as well as on the total island charge. As discussed in chapter 4, we need matrix elements that describe transitions from a state that is diagonal in the occupation of the considered island level to a state that may be diagonal (for the kinetic equations of P_N and S_z) or off-diagonal (for the kinetic equations of $S^{\pm}$). Explicit calculation yields

$$W^{\sigma\,0}_{\sigma\,0}(l,\nu,N) = \frac{1}{\hbar}\sum_{rs}\Gamma^r_{s\sigma} f_r^+(\epsilon_l+\Delta_N)\,, \tag{A.1}$$

$$W^{0\,\sigma}_{0\,\sigma}(l,\nu,N) = \frac{1}{\hbar}\sum_{rs}\Gamma^r_{s\sigma} f_r^-(\epsilon_l+\Delta_{N-1})\,, \tag{A.2}$$

$$W^{d\,\sigma}_{d\,\sigma}(l,\nu,N) = \frac{1}{\hbar}\sum_{rs}\Gamma^r_{s\bar{\sigma}} f_r^+(\epsilon_l+\Delta_N)\,, \tag{A.3}$$

$$W^{\sigma\,d}_{\sigma\,d}(l,\nu,N) = \frac{1}{\hbar}\sum_{rs}\Gamma^r_{s\bar{\sigma}} f_r^-(\epsilon_l+\Delta_{N-1})\,, \tag{A.4}$$

where $f_r^+(E) = f_r(E)$ describes tunneling of electrons from lead r into the island and $f_r^-(E) = 1 - f_r(E)$ tunneling out of the island into lead r. Hence the elements above describe processes that change the occupation of the central electrode. These parts of the kernel are related to the diagonal matrix elements where the total island charge remains constant via

$$W^{0\,0}_{0\,0}(l,\nu,N) = -\sum_{\sigma} W^{\sigma\,0}_{\sigma\,0}(l,\nu,N), \tag{A.5}$$

$$W^{\sigma\,\sigma}_{\sigma\,\sigma}(l,\nu,N) = -W^{0\,\sigma}_{0\,\sigma}(l,\nu,N) - W^{d\,\sigma}_{d\,\sigma}(l,\nu,N), \tag{A.6}$$

$$W^{d\,d}_{d\,d}(l,\nu,N) = -\sum_{\sigma} W^{\sigma\,d}_{\sigma\,d}(l,\nu,N). \tag{A.7}$$

The matrix elements with off-diagonal final states can also be divided into those where the total island charge changes during the transition,

$$W^{\sigma\,0}_{\bar{\sigma}\,0}(l,\nu,N) = \frac{2\pi}{\hbar}\sum_{rs}\rho^r_s V^{r^*}_{s\sigma} V^r_{s\bar{\sigma}} f_r^+(\epsilon_l+\Delta_N), \tag{A.8}$$

$$W^{\sigma\,d}_{\bar{\sigma}\,d}(l,\nu,N) = -\frac{2\pi}{\hbar}\sum_{rs}\rho^r_s V^{r^*}_{s\sigma} V^r_{s\bar{\sigma}} f_r^-(\epsilon_l+\Delta_{N-1}), \tag{A.9}$$

and those where the total island charge remains constant,

$$W^{\sigma\uparrow}_{\bar{\sigma}\uparrow}(l,\nu,N) = -\frac{2\pi i}{\hbar}\sum_{rs}\rho^r_s V^{r^*}_{s\sigma}V^r_{s\bar{\sigma}}I(N), \tag{A.10}$$

$$W^{\sigma\downarrow}_{\bar{\sigma}\downarrow}(l,\nu,N) = \frac{2\pi i}{\hbar}\sum_{rs}\rho^r_s V^{r^*}_{s\sigma}V^r_{s\bar{\sigma}}I^*(N)\,, \tag{A.11}$$

with the integral expression

$$I(N) = \int\frac{\mathrm{d}\omega}{2\pi}\left[\frac{f^-_r(\omega)}{\epsilon_l+\Delta_{N-1}-\omega+i0^+} + \frac{f^+_r(\omega)}{\epsilon_l+\Delta_N-\omega-i0^+}\right], \tag{A.12}$$

which represents transition processes of island-charge states, while $\mathrm{Re}\,I(N)$ exclusively describes virtual charge transfer.

Bibliography

[1] S. Lindebaum and J. König, Phys. Rev. B **84**, 235409 (2011).

[2] J. Bardeen and W. H. Brattain, Phys. Rev. **74**, 230-231 (1948).

[3] M. H. Devoret and H. Grabert, *Single Charge Tunneling* (Plenum, New York, 1992)

[4] M. Amman, R. Wilkins, E. Ben-Jacob,P. D. Maker, and R. C. Jaklevic, Phys. Rev. B **43**, 1146 (1991).

[5] D. V. Averin, A. N. Korotkov, and K. K. Likharev, Phys. Rev. B **44**, 6199 (1991).

[6] S. Datta and B. Das, Appl. Phys. Lett. **56**, 665 (1990).

[7] S. A. Wolf, D. D. Awschalom, R. A. Buhrman, J. M. Daughton, S. von Molnár, M. L. Roukes, A. Y. Chtchelkanova, and D. M. Treger, Science **294**, 1488 (2001).

[8] J. F. Gregg, I. Petej, E. Jouguelet, and C. Dennis, J. Phys. D: Appl. Phys. **35**, R121 (2002)

[9] I. Žutić, J. Fabian, and S. Das Sarma, Rev. Mod. Phys. **76**, 323 (2004).

[10] G. Binasch, P. Grünberg, F. Saurenbach and W. Zinn, Phys. Rev. B **39**, 4828 (1989).

[11] M. N. Baibich, J. M. Broto, A. Fert, F. Nguyen Van Dau, F. Petroff, P. Etienne, G. Creuzet, A. Friederich, and J. Chazelas, Phys. Rev. Lett. **61**, 2472 (1988).

[12] M. Jullière, Phys. Lett. A **54**, 225 (1975).

[13] S. Maekawa and U. Gäfvert, IEEE Trans. Magn. **18**, 707 (1982).

[14] J. C. Slonczewski, Phys. Rev. B **39**, 6995 (1989).

[15] T. Miyazaki and N. Tezuka, J. Magn. Magn. Mater. **139**, L231 (1995).

[16] J. S. Moodera, L. R. Kinder, T. M. Wong und R. Meservey, Phys. Rev. Lett. **74**, 16 (1995).

[17] H. Jaffrès, D. Lacour, F. Nguyen Van Dau, J. Briatico, F. Petroff and A. Vaurès, Phys. Rev. B **64**, 64427 (2001).

[18] M. Johnson and R. H. Silsbee, Phys. Rev. Lett. **55**, 1790 (1985).

[19] M. Johnson and R. H. Silsbee, Phys. Rev. B. **37**, 5326 (1988).

[20] M. Zaffalon and B. J. van Wees, Phys. Rev. Lett. **91**, 186601 (2003).

[21] M. Zaffalon and B. J. van Wees, Phys. Rev. B **71**, 125401 (2005).

[22] F. J. Jedema, A. T. Filip, and B. J. van Wees, Nature **410**, 345 (2001).

[23] F. J. Jedema, H. B. Heersche, A. T. Filip, J. J. A. Baselmans, and B. J. van Wees, Nature **416**, 713 (2002).

[24] F. J. Jedema, M. S. Nijboer, A. T. Filip, and B. J. van Wees, Phys. Rev. B **67**, 085319 (2003).

[25] T. Kimura and Y. Otani, Phys. Rev. Lett. **99**, 196604 (2007).

[26] N. Tombros, C. Jozsa, M. Popinciuc, H. T. Jonkman, and B. J. van Wees, Nature **448**, 571 (2007).

[27] N. Tombros, S. Tanabe, A. Veligura, C. Jozsa, M. Popinciuc, H. T. Jonkman, and B. J. van Wees, Phys. Rev. Lett. **101**, 046601 (2008).

[28] C. Jozsa, M. Popinciuc, N. Tombros, H. T. Jonkman, and B. J. van Wees, Phys. Rev. Lett. **100**, 236603 (2008).

[29] W. Han, W. H. Wang, K. Pi, K. M. McCreary, W. Bao, Y. Li, F. Miao, C. N. Lau, and R. K. Kawakami, Phys. Rev. Lett. **102**, 137205 (2009).

[30] M. Popinciuc, C. Jozsa, P. J. Zomer, N. Tombros, A. Veligura, H. T. Jonkman, and B. J. van Wees, Phys. Rev. B **80**, 214427 (2009).

[31] M. Braun, *Transport durch ein Quantenpunkt-Spinventil* (PhD thesis), Ruhr-Universität Bochum (2006).

[32] B. R. Bułka, Phys. Rev. B **62**, 1186 (2000).

[33] J. König and J. Martinek, Phys. Rev. Lett. **90**, 166602 (2003).

[34] M. Braun, J. König, and J. Martinek, Phys. Rev. B **70**, 195345 (2004).

[35] J. Martinek, Y. Utsumi, H. Imamura, J. Barnaś, S. Maekawa, J. König, and G. Schön, Phys. Rev. Lett. **91**, 127203 (2003).

[36] J. Martinek, M. Sindel, L. Borda, J. Barnaś, J. König, G. Schön, and J. von Delft Phys. Rev. Lett. **91**, 247202 (2003).

[37] A. Cottet, W. Belzig, and C. Bruder, Phys. Rev. Lett. **92**, 206801 (2004).

[38] A. Cottet, W. Belzig, and C. Bruder, Phys. Rev. B **70**, 115315 (2004).

[39] I. Weymann, J. Barnaś, J. König, J. Martinek, and G. Schön, Phys. Rev. B **72**, 113301 (2005).

[40] I. Weymann, J. König, J. Martinek, J. Barnaś, and G. Schön, Phys. Rev. B **72**, 115334 (2005).

[41] J. Fransson, Europhys. Lett. **70**, 796 (2005).

[42] J. Fransson, Phys. Rev. B **72**, 045415 (2005).

[43] W. Rudziński, J. Barnaś, R. Świrkowicz, and M. Wilczyński, Phys. Rev. B **71**, 205307 (2005).

[44] I. Weymann, Europhys. Lett. **76**, 1200 (2006).

[45] M. Braun, J. König, and J. Martinek, Phys. Rev. B **74**, 075328 (2006).

[46] P. Simon, P. S. Cornaglia, D. Feinberg, and C. A. Balseiro, Phys. Rev. B **75**, 045310 (2007).

[47] J. Splettstoesser, M. Governale, and J. König, Phys. Rev. B **77**, 195320 (2008).

[48] S. Lindebaum, D. Urban, and J. König, Phys. Rev. B **79**, 245303 (2009).

[49] B. Sothmann, D. Futterer, M. Governale, and J. König, Phys. Rev. B **82**, 094514 (2010).

[50] B. Sothmann and J. König, Phys. Rev. B **82**, 245319 (2010).

[51] M. Baumgärtel, M. Hell, S. Das, and M. R. Wegewijs, Phys. Rev. Lett. **107**, 087202 (2011) .

[52] K. Yakushiji, S. Mitani, K. Takanashi, S. Takahashi, S. Maekawa, H. Imamura, and H. Fujimori, Appl. Phys. Lett. **78**, 515 (2001).

[53] M. M. Deshmukh and D. C. Ralph, Phys. Rev. Lett. **89**, 266803 (2002).

[54] A. N. Pasupathy, R. C. Bialczak, J. Martinek, J. E. Grose, L. A. K. Donev, P. L. McEuen, and D. C. Ralph, Science **306**, 86 (2004).

[55] L. Y. Zhang, C. Y. Wang, Y. G. Wei, X. Y. Liu, and D. Davidovic, Phys. Rev. B **72**, 155445 (2005).

[56] S. Sahoo, T. Kontos, J. Furer, C. Hoffmann, M. Gräber, A. Cottet, and C. Schönenberger, Nat. Phys. **1**, 99 (2005).

[57] K. Hamaya, M. Kitabatake, K. Shibata, M. Jung, M. Kawamura, K. Hirakawa, T. Machida, S. Ishida, Y. Arakawa, Appl. Phys. Lett. **91**, 022107 (2007).

[58] J. R. Hauptmann, J. Paaske, and P. E. Lindelof, Nat. Phys. **4**, 373 (2008).

[59] C. A. Merchant and N. Marković, J. Appl. Phys. **105**, 07C711 (2009).

[60] L. Hofstetter, A. Geresdi, M. Aagesen, J. Nygard, C. Schönenberger, and S. Csonka, Phys. Rev. Lett. **104**, 246804 (2010).

[61] J. V. Holm, H. I. Jorgensen, K. Grove-Rasmussen, J. Paaske, K. Flensberg, and P. E. Lindelof, Phys. Rev. B **77**, 161406(R) (2008).

[62] D. Darau, G. Begemann, A. Donarini, and M. Grifoni, Phys. Rev. B **79**, 235404 (2009).

[63] W. Wetzels, G. E. W. Bauer, and M. Grifoni, Phys. Rev. B **72**, 020407(R) (2005).

[64] W. Wetzels, G. E. W. Bauer, and M. Grifoni, Phys. Rev. B **74**, 224406 (2006).

[65] T. A. Fulton and G. J. Dolan, Phys. Rev. Lett. **59**, 109 (1987).

[66] T. L. Ho, Phys. Rev. Lett. **51**, 2060 (1983).

[67] E. Ben-Jacob and Y. Gefen, Phys. Lett. **108A**, 289 (1985).

[68] D. V. Averin and K. K. Likharev, J. Low Temp. Phys. **62**, 345 (1986).

[69] M. Büttiker, Phys. Scri. **T14**, 82 (1986).

[70] J. B. Barner and S. T. Ruggiero, Phys. Rev. Lett. **59**, 807 (1987).

[71] P. J. M. van Bentum, R. T. M. Smokers, and H. van Kempen, Phys. Rev. Lett. **60**, 2543 (1988).

[72] R. Wilkins, E. Ben-Jacob, and R. C. Jaklevic, Phys. Rev. Lett. **63**, 801 (1989).

[73] R. Wilkins, M. Amman, E. Ben-Jacob, and R. C. Jaklevic, Phys. Rev. B **42**, 8698 (1990).

[74] V. Chandrasekhar, Z. Ovadyahu, and R. A. Webb, Phys. Rev. Lett. **67**, 2862 (1991).

[75] H. Birk, M. J. M. de Jong, and C. Schönenberger, Phys. Rev. Lett. **75**, 1610 (1995).

[76] U. Meirav, M. A. Kastner, and S. J. Wind, Phys. Rev. Lett. **65**, 771 (1990).

[77] L. P. Kouwenhoven, N. C. van der Vaart, A. T. Johnson, W. Kool, C. J. P. M. Harmans, J. G. Williamson, A. A. M. Staring, and C. T. Foxon, Z. Phys. B **85**, 367 (1991).

[78] Y. Ootuka, K. Ono, H. Shimada, and S. Kobayashi, Physica B **227**, 307 (1996).

[79] K. Ono, H. Shimada, and Y. Ootuka, J. Phys. Soc. Jpn **66**, 1261 (1997).

[80] H. Shimada, K. Ono, and Y. Ootuka, J. Phys. Soc. Jpn **67**, 1359 (1998).

[81] K. Ono, H. Shimada, and Y. Ootuka, J. Phys. Soc. Jpn **67**, 2852 (1998).

[82] H. Brückl, G. Reiss, H. Vinzelberg, M. Bertram, I. Mönch, and J. Schumann, Phys. Rev. B **58**, R8893 (1998).

[83] Y. Takemura and J. Shirakashi, Jpn. J. Appl. Phys. **40**, 128 (2001).

[84] H. Shimada, K. Ono, and Y. Ootuka, J. Appl. Phys. **93**, 8259 (2003).

[85] R. Matsuda, A. Kanda, and Y. Ootuka, Physica B **329**, 1304 (2003).

[86] T. Niizeki, H. Kubota, Y. Ando, and T. Miyazaki J. Magn. Magn. Mat. **272-276**, 1947 (2004).

[87] J. Wunderlich, T. Jungwirth, B. Kaestner, A. C. Irvine, A. B. Shick, N. Stone, K.-Y. Wang, U. Rana, A. D. Giddings, C. T. Foxon, R. P. Campion, D. A. Williams, and B. L. Gallagher, Phys. Rev. Lett. **97**, 077201 (2006).

[88] A. Bernand-Mantel, P. Seneor, N. Lidgi, M. Muñoz, V. Cros, S. Fusil, K. Bouzehouane, C. Deranlot, A. Vaures, F. Petroff, and A. Fert, Appl. Phys. Lett. **89**, 062502 (2006).

[89] P. Seneor, A. Bernand-Mantel, and F. Petroff, J. Phys.: Condens. Matter **19**, 165222 (2007).

[90] R. S. Liu, D. Suyatin, H. Pettersson, and L. Samuelson, Nanotechnology **18**, 055302 (2007).

[91] A. Bernand-Mantel, P. Seneor, K. Bouzehouane, S. Fusil, C. Deranlot, F. Petroff, and A. Fert, Nat. Phys. **5**, 920 (2009).

[92] T. Junno, S.-B. Carlsson, H. Q Xu, L. Montelius, and L. Samuelson, Appl. Phys. Lett. **72**, 548 (1998).

[93] L. V. Keldysh, JETP **20**, 1018 (1965).

[94] J. König, H. Schoeller, and G. Schön, Phys. Rev. Lett. **76**, 1715 (1996).

[95] J. König, J. Schmid, H. Schoeller, and G. Schön, Phys. Rev. B **54**, 16820 (1996).

[96] H. Schoeller, in *Mesoscopic Electron Transport*, edited by L. L. Sohn, L. P. Kouwenhoven, and G. Schön (Kluwer, Dordrecht, 1997).

[97] J. König, *Quantum Fluctuations in the Single-Electron Transistor* (Shaker, Aachen, 1999).

[98] C. W. J. Beenakker, Phys. Rev. B **44**, 1646 (1991).

[99] J. Barnaś, J. Martinek, G. Michałek, B. R. Bułka, and A. Fert, Phys. Rev. B **62**, 12363 (2000).

[100] F. Ernult, K. Yakushiji, S. Mitani, and S. Takahashi, J. Phys.: Condens. Matter **19**, 165214 (2007).

[101] J. Barnas and I. Weymann, J. Phys.: Condens. Matter **20**, 423202 (2008).

[102] K. Majumdar and S. Hershfield, Phys. Rev. B **57**, 11521 (1998).

[103] A. N. Korotkov and V. I. Safarov, Phys. Rev. B **59**, 89 (1999).

[104] A. Brataas, Y. V. Nazarov, J. Inoue, and G. E. W. Bauer, Phys. Rev. B **59**, 93 (1999).

[105] A. Brataas, Yu. V. Nazarov, J. Inoue, and G. E. W. Bauer, Eur. Phys. J. B **9**, 421 (1999).

[106] I. Weymann and J. Barnas, Phys. Status Solidi B **236**, 651 (2003).

[107] W. Schottky, Ann. der Phys. **57**, 541 (1918).

[108] C. W. J. Beenakker and M. Büttiker, Phys. Rev. B **46**, 1889 (1992).

[109] U. Fano, Phys. Rev. **72**, 26 (1947).

[110] L. S. Levitov and G. B. Lesovik, JETP Lett. **58**, 230 (1993).

[111] G. B. Lesovik and L. S. Levitov, Phys. Rev. Lett. **72**, 538 (1994).

[112] B. A. Muzykantskii and D. E. Khmelnitskii, Phys. Rev. B **50**, 3982 (1994).

[113] W. Belzig, Physik Journal **Nr. 8/9**, 75 (2005).

[114] M. Vanević, Y. V. Nazarov, and W. Belzig, Phys. Rev. Lett. **99**, 76601 (2007.)

[115] V. A. Khlus, Zh. Exp. Theor. Fiz. **93**, 2179 (1987) [Sov. Phys. JETP **66**, 1243 (1987)].

[116] A. L. Fauchère, G. B. Lesovik, and G. Blatter, Phys. Rev. B **58**, 11177 (1998).

[117] G. B. Lesovik, T. Martin and J. Torrès, Phys. Rev. B **60**, 11935 (1999).

[118] J. Torrès, T. Martin, and G. B. Lesovik, Phys. Rev. B **63**, 134517 (2001).

[119] M. J. M. de Jong and C. W. J. Beenakker, Phys. Rev. B **49**, 16070 (1994).

[120] X. Jehl and M. Sanquer, Phys. Rev. B **63**, 052511 (2001).

[121] C. Hoffmann, F. Lefloch, M. Sanquer, and B. Pannetier, Phys. Rev. B **70**, 180503(R) (2004).

[122] B. Kaviraj, O. Coupiac, H. Courtois, and F. Lefloch, Phys. Rev. Lett. **107**, 077005 (2011).

[123] Ya. M. Blanter and M. Büttiker, Phys. Rev. B **59**, 10217 (1999).

[124] E. V. Sukhorukov, G. Burkard, and D. Loss, Phys. Rev. B **63**, 125315 (2001).

[125] G. Kießlich, A. Wacker, and E. Schöll, Phys. Rev. B **68**, 125320 (2003).

[126] W. Belzig, Phys. Rev. B **71**, 161301(R) (2005).

[127] V. H. Nguyen and V. L. Nguyen, Phys. Rev. B **73**, 165327 (2006).

[128] B. R. Bułka, Phys. Rev. B **77**, 165401 (2008).

[129] G. Michałek and B. R. Bułka, Phys. Rev. B **80**, 035320 (2009).

[130] R.-Q. Wang, L. Sheng, L.-B. Hu, B. Wang, and D. Y. Xing Phys. Rev. B **84**, 115304 (2011).

[131] A. Thielmann, M. H. Hettler, J. König, and G. Schön, Phys. Rev. B **71**, 045341 (2005).

[132] F. Elste and C. Timm, Phys. Rev. B **73**, 235305 (2006).

[133] L. D. Contreras-Pulido and R. Aguado, Phys. Rev. B **81**, 161309(R) (2010).

[134] I. Weymann, J. Barnaś, and S. Krompiewski, Phys. Rev. B **78**, 035422 (2008).

[135] A. Reklaitis and L. Reggiani, Phys. Rev. B **62**, 16773 (2000).

[136] F. Cavaliere, F. Haupt, R. Fazio, and M. Sassetti, Phys. Rev. B **71**, 235325 (2005).

[137] A. Thielmann, M. H. Hettler, J. König, and G. Schön, Phys. Rev. B **68**, 115105 (2003).

[138] S. Lindebaum and J. König, arXiv:1206.0954 (2012).

[139] R. Aguado and L. P. Kouwenhoven, Phys. Rev. Lett. **84**, 1986 (2000)

[140] U. Gavish, Y. Levison, and Y. Imry, Phys. Rev. B **62**, R10637 (2000).

[141] A. N. Korotkov, Phys. Rev. B **49**, 10381 (1994).

[142] S. Hershfield, J. H. Davies, P. Hyldgaard, C. J. Stanton, and J. W. Wilkins, Phys. Rev. B **47**, 1967 (1993).

[143] D. A. Bagrets and Yu. V. Nazarov, Phys. Rev. B **67**, 085316 (2003).

[144] A. Braggio, J. König, and R. Fazio, Phys. Rev. Lett. **96**, 026805 (2006).

[145] U. Hanke, Yu. M. Galperin, K. A. Chao, and N. Zou, Phys. Rev. B **48**, 17209 (1993).

[146] U. Hanke, Yu. M. Galperin, and K. A. Chao, Phys. Rev. B **50**, 17209 (1994).

[147] G. Johansson, A. Käck, and G. Wendin, Phys. Rev. Lett. **88**, 046802 (2002).

[148] A. Käck, G. Wendin, and G. Johansson, Phys. Rev. B **67**, 035301 (2003).

[149] A. Aassime, G. Johansson, G. Wendin, R. J. Schoelkopf, and P. Delsing, Phys. Rev. Lett. **86**, 3376 (2001).

[150] A. Aassime, D. Gunnarsson, K. Baldh, and P. Delsing, Appl. Phys. Lett. **79**, 4031 (2001).

[151] L. Roschier, P. Hakonen, K. Bladh, P. Delsing, K. W. Lehnert, L. Spietz, and R. J. Schoelkopf, J. Appl. Phys. **95**, 1274 (2004).

[152] S. Kafanov and P. Delsing, Phys. Rev. B **80**, 155320 (2009).

[153] B. R. Bułka, Phys. Rev. B **60**, 12246 (1999).

[154] E. G. Mishchenko, Phys. Rev. B **68**, 100409(R) (2003).

[155] L. Lamacraft, Phys. Rev. B **69**, 081301 (2004).

[156] M. Zareyan and W. Belzig, Europhys. Lett. **70**, 817 (2005).

[157] Y. Tserkovnyak and A. Braatas, Phys. Rev. B **64**, 214402 (2001).

List of Publications

(A) *Spin-induced charge correlations in transport through interacting quantum dots with ferromagnetic leads*,
S. Lindebaum, Daniel Urban, and J. König, Phys. Rev. B **79**, 245303 (2009).

(B) *Theory of transport through noncollinear single-electron spin-valve transistors*,
S. Lindebaum and J. König, Phys. Rev. B **84**, 235409 (2011).

(C) *Current fluctuations of noncollinear single-electron spin-valve transistors*,
S. Lindebaum and J. König, arXiv:1206.0954.

Parts of this thesis have already been published. In particular, the chapter 2-5 contain parts of reference **(B)** and chapter 6 comprises parts of reference **(C)**.

Acknowledgements

Finally, I would like to thank all the people without whom this thesis would have never been produced like it is.

Prof. Dr. Jürgen König for giving me the opportunity to work in his group. I am grateful that he was always open for physical discussions and that he supported me in improving my presentation skills.

David Futterer and **Bastian Hiltscher** for helping me to overcome an uncountable number of physical and numerical problems. Without these guys I probably would have been lost. I am extremely lucky to have two of the best friends one can imagine. Of course, I explicitly apologize for my attacks of rage that they had to suffer :-).

Stephan Rojek for fruitful discussions concerning physics as well as for spending the lunch break with us.

Dr. Alfred Hucht for helping me to deal with minor and major computer problems.

Dr. Björn Sothmann and **Nina Winkler** for answering my physical questions and for related support.

All the other members of the AG König and AG Entel for the nice working atmosphere in our group.

Kay Thust for bringing forward my understanding of physics during our diploma studies in Bochum and for being a great friend.

Katrin Sonntag and my lovely family for their love, sympathy and motivation during my PhD studies. Thank you Katrin for brighten up my mood when I was down. I assure you all that I am aware of your uniqueness.